Bringing Cyclopropenium to Life

Spencer D. Brucks

Submitted in partial fulfillment of the
requirements for the degree of
Doctor of Philosophy
in the Graduate School of Arts and Sciences

COLUMBIA UNIVERSITY

2018

ABSTRACT

Bringing Cyclopropenium to Life

Spencer D. Brucks

Burgeoning fields of nanomedicine and theranostics are propelled forward by the creative and systematic design of synthetic polymers. Cationic polyelectrolytes, comprising covalently-linked cations within each repeat unit, have drawn particular interest for their ability to bind nucleic acids and permeate cell membranes. Expanding the design space of these systems, we introduced a new family of polyelectrolytes based on the carbon-centered cyclopropenium cation. Cyclopropenium is a modular, aromatic building block with unique structural and electronic properties and, when coupled with modern living polymerization techniques, can be incorporated into macromolecules with precise size, shape, and composition. This thesis describes the translation of cationic polyelectrolytes based on cyclopropenium to biomedical applications and is structured into three parts. The first part evaluates cyclopropenium polymers as candidate non-viral vectors for gene therapy and demonstrates that some derivatives are both biocompatible and efficacious transfection agents. In the second part, nanoparticles comprising cyclopropenium are exploited as live-cell image contrast agents and evolved into potentially theranostic tools. The final part describes a facile route to a novel class of cyclopropenium-based polymers. Together, this thesis illustrates that cyclopropenium is a versatile component of polyelectrolytes, poised to address leading biological challenges.

TABLE OF CONTENTS

LIST OF FIGURES

Introduction

Part One

Part Two

Part Three

ACKNOWLEDGMENTS

At the end of this five-year process there are a great many people whom I am most thankful for. First, I would like to thank my advisor, Prof. Luis M. Campos. I came to Columbia exclusively to work for Luis and am so grateful that I did. Luis has served as both a research and teaching mentor for me, and as I continue pursuing my own independent teaching-research career, I consider myself very lucky to have him as a resource. In the lab, I was grateful Luis gave me the freedom to pursue projects as I saw most fit, even as we pushed into research areas out of both our comfort zones. The independence and creativity Luis cultivated is something I will hopefully take with me for the rest of my career.

Beyond Luis, I have been lucky to have a fantastic thesis committee whose ideas, feedback, and support are most appreciated. I met Profs. Colin Nuckolls and Shalom Wind when I took their courses in my first year at Columbia and they have served on my committee ever since. They are kind, intelligent, and thoughtful – all traits that I try to emulate as a young researcher. I have worked in close collaboration with both Prof. Wei Min and Prof. Brent Stockwell throughout my PhD and I can't imagine "bringing cyclopropenium to life" without them. I have learned countless technical and problem-solving skills from them that I never would have otherwise. Lastly, in the final year of my PhD I began attending Prof. Allie Obermeyer's group meetings in order to learn more about protein-polymer conjugates and what questions engineers are asking of highly-charged polymer systems. More than just appreciative for the opportunity and the conversations, I am in awe of Allie's skills as a PI. If I am ever fortunate enough to manage my own research group, I will do my best to channel Allie's ability to manage, lead, and motivate a young group.

Before Columbia, I received my first research training in the laboratory of Prof. William

Dichtel under the supervision of now Dr. David Bunck. I have the upmost gratitude that they both continue to serve as mentors for me taking an interest in all aspects of my career. During my first years at Columbia, I was fortunate to work with other fantastic scientists and they too continue to serve as role models and advisors. Much thanks to Drs. Helen Tran and Mike Inkpen.

Of course, I need to thank my first mentors and first teachers: my parents. They instilled a love of discovery and experimentation and knowledge. From my dad who would google "cyclopropenium" to my mom who would listen to me ramble about that day's experiment, none of this would be possible without you. My younger sister Emily, being a younger sibling, was my first student; but, I am not sure she realizes how much I have learned from her.

In terms of research specifically, I have worked with a diverse array of terrific collaborators. Among them, there is no one I worked more closely with, or for longer than Dr. Jessica Freyer. And while no one drove me more insane than Jess, no one single person was more instrumental in my PhD. Also on our cyclopropenium polyelectrolyte team: Sebastian Russell, who has led efforts into understanding the self-assembly of our materials, and whose joining really made it feel like a team; Rachel Starr, who I have had the deep privilege of mentoring and working alongside for two years and who is the future of these projects; Dr. Ramya Raghunathan who is an extremely talented synthetic chemist and an overall delight to be around; and Prof. Avi Domb, who worked as a visiting scientist in our lab for six months and whose vitality and creativity are inspirational. From Wei's group, I had an ideal collaboration with Dr. Fanghao Hu that I enjoyed tremendously. Fanghao is smart, assiduous, well-read and I always looked forward to experiments together. From Brent's group, I worked closely with Dr. Carrie Capps (née Yozwiak) who trained me to be an independent cell culturist and has become a close friend. I worked with a handful of undergrads and a rotation student and I am appreciative

of their energy and ideas: Maria Escamilla, Alexa Abdelaziz, Graham Gobieski, and Yivan Jiang. I've greatly enjoyed conversations with Prof. Valerio Dorrello who has been instrumental in getting the targeted nanoparticles project off the ground. Finally, Yan Zhang (Stockwell lab) and I worked on a drug delivery project and Trévon Gordon (Obermeyer lab) and I coated and imaged nanoparticles, neither of which is described herein. Viewed together, I consider myself very fortunate to have been at a school like Columbia and work for a boss like Luis that so supports and encourages diversity. Exploiting the creative talent, ideas, and background of all people is undoubtedly the best way to tackle the hardest challenges in front of us.

Finally, nearly four years ago I registered the twitter handle @SomosCampos as a derivative joke to Luis's @SoyLuisCampos. In that time, the moniker somoscampos (translation: We are Campos) has taken on an entire meaning of its own. I have no doubt that I have been a part of one of the best research teams in the world. Group members are some of my closest friends, confidantes, and just overall some of the nicest, smartest people you will ever meet. I will always be grateful to have had the opportunity to work alongside them. Their names, in order of when I started working with them, are: Jianlong Xia, Liangliang Zhu, Helen Tran, Jessica L. Freyer, Sam N. Sanders, Jonathan Z. Low, Sebastian T. Russell, Andrew B. Pun, Anastasia A. Voevodin, Elango Kumarasamy, Lauren M. Yablon, Xiaodong Yin, Rachel L. Starr, Ramya Raghunathan, Kaia R. Parenti, and Emily M. Churchill.

This work was funded by a National Science Foundation Graduate Research Fellowship (No. DGE 16-44869)

INTRODUCTION:

BRINGING CYCLOPROPENIUM TO POLYMERS

[This introduction is based in part on the following publications: *Nat. Commun.* **2015**, *6*, 5950; *Angew. Chem. Int. Ed.* **2016**, *55*, 40, 12382; *Macromolecules* **2015**, *48*, 8, 2519]

Natural polymers are essential to all forms of life. DNA, composed of only four nucleotide monomers, is the universal genetic code across all three domains of life: Bacteria, Archaea, and Eukarya. Sugars are the most abundant biomolecules on earth and they are all built from covalently linked monosaccharide monomers.[1] And, just twenty canonical amino acids, when connected through amide bonds, serve as the building blocks for all proteins. Collectively, it is polymeric structures that are responsible for the defining features of life: from the assembly of membranes and cytoskeletons to communication, motility, metabolism, and replication. Nature is able to accomplish this immense array of functions by assembling its polymers with unrivaled precision.[2]

By contrast, synthetic polymers have historically been derided as crude, impure, and not worthy of academic study. Polymers were chiefly synthesized through vulcanization, an uncontrolled process involving extensive heating in the presence of sulfur, until a stiff gel formed. Synthetic polymers were the domain of rubbers and resins, understood as colloidal clusters of small molecules, with unknown molecular weights. Less than a century ago, Staudinger was mocked for suggesting that a covalently bonded polymer could even exist. Relegated to the realm of industrial process, synthetic polymers were considered greasy and anything but precise.[3,4]

The development of living polymerization techniques over the past half-century has begun to erode this notion. Whereas traditional polymerizations are chaotic processes with growth, termination, and chain-transfer all happening simultaneously, living polymerizations are characterized by equivalent growth across all chains in the absence of irreversible termination or chain transfer processes. This produces polymers where the degree of polymerization increases linearly with conversion of monomers permitting molecular weights to be both controlled and

predicted. These strategies, including Ziegler-Natta olefin polymerization, ring-opening metathesis polymerization, and reversible-deactivation radical polymerizations, have enabled the design of macromolecules with precise size, shape, and composition.[2,5–7]

Ready access to well-defined macromolecules has inspired researchers to imagine what synthetic polymers can offer biology. With the development of robust and modular polymerization techniques suddenly synthetic polymers are no longer crude aggregates but are predictably tunable with immense chemical diversity.[8] While nature's palette of monomers is fairly limited in scope, synthetic chemists are predominantly limited by their imaginations. As Grubbs and Grubbs recently wrote, now "allow almost any sentient creature with access to a fume hood and an inert gas tank [can] make a vast range of polymers".[5] This accessibility and chemical diversity have led scientists to appreciate the role synthetic polymers can serve in biological systems. Burgeoning fields of nanomedicine and theranostics are propelled forward by the creative and rational design of synthetic polymers with varied composition, architecture, and functionality.[6,9–12]

An emergent class of polymers that has drawn particular interest is cationic polyelectrolytes. Comprising a covalently-linked cation with an electrostatically associated anion at each repeat unit, cationic polyelectrolytes introduce a novel design element into the polymer scaffold. Rational engineering of these systems has been exploited in a range of biomedical applications. The embedded positive charge can rapidly complex and package anionic nucleic acids through entropic displacement of its counterion, motivating study of these materials as gene delivery vectors. Additionally, the cationic unit promotes cell adhesion and uptake affording a platform to enter, diagnose, and treat live cells.[13–16]

Heretofore, most functional units investigated for cationic polyelectrolytes have been heteroatom based, with polymers containing phosphonium,[17] ammonium,[18] or imidazolium[19]

being particularly common (**Figure 1**). Polymers such as poly(L-lysine), poly(ethylenimine), and chitosan are also regularly employed but possess pH-dependent cations.[20,21] While valuable, all of these systems are limited in their ability to tune physical properties. The principal strategies to modulate functionality are varying alkyl substituent chain length and spacer chemistry from the polymer backbone. Thus, the identification of new cationic polyelectrolytes with unique pathways to tune function is of high import.

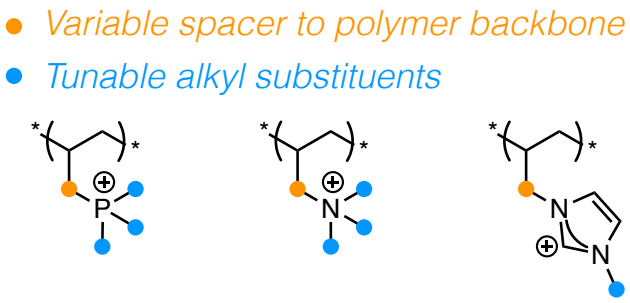

Figure 1. Structures of leading cationic polyelectrolytes. Common handles to modify chemical structure (blue) and tether to polymer backbone (orange) can be used to tune functionality.

We envisaged incorporating the carbon-centered cyclopropenium cation into polyelectrolytes as a non-conventional polymer building block. As the smallest Hückel aromatic, cyclopropenium possesses an unusually high degree of stability for a carbocation,[22] which can be further enhanced via incorporation of amino substituents onto the ring (i.e. trisaminocyclopropenium).[23,24] Consequently, trisaminocyclopropenium is uniquely both carbon-centered and electron-rich with tunable amino substituents. These novel structural and electronic properties have already motivated the development of cyclopropenium ions as metal ligands,[25] organocatalysts,[26] and fuel cell membranes[27,28] and we hypothesized they could meaningfully expand the design space of available cationic polyelectrolytes as well.

Our vision for a cyclopropenium-based monomer included a polymerizable unit, a spectator group (which could potentially also serve as a functional handle), and four additional

modular handles to tune physical properties (**Figure 2A**). We elected to study styrenic derivatives as they are amenable to a wide range of reversible-deactivation radical polymerization strategies. Thus, we designed a styrene-based monomer and subsequently used reversible-addition fragmentation chain-transfer polymerization (RAFT) to assemble homopolymers, statistical copolymers, and diblock copolymers of varying composition (**Figure 2B**). The specific details of the synthesis have been described elsewhere,[29] but this route importantly furnished a library of linear cyclopropenium polymers of varying composition and hydrophilicity. We further recognized that our monomer was amphiphilic and thus could serve as a polymerizable surfactant in an emulsion polymerization to form nanoparticles (*vide infra)*.

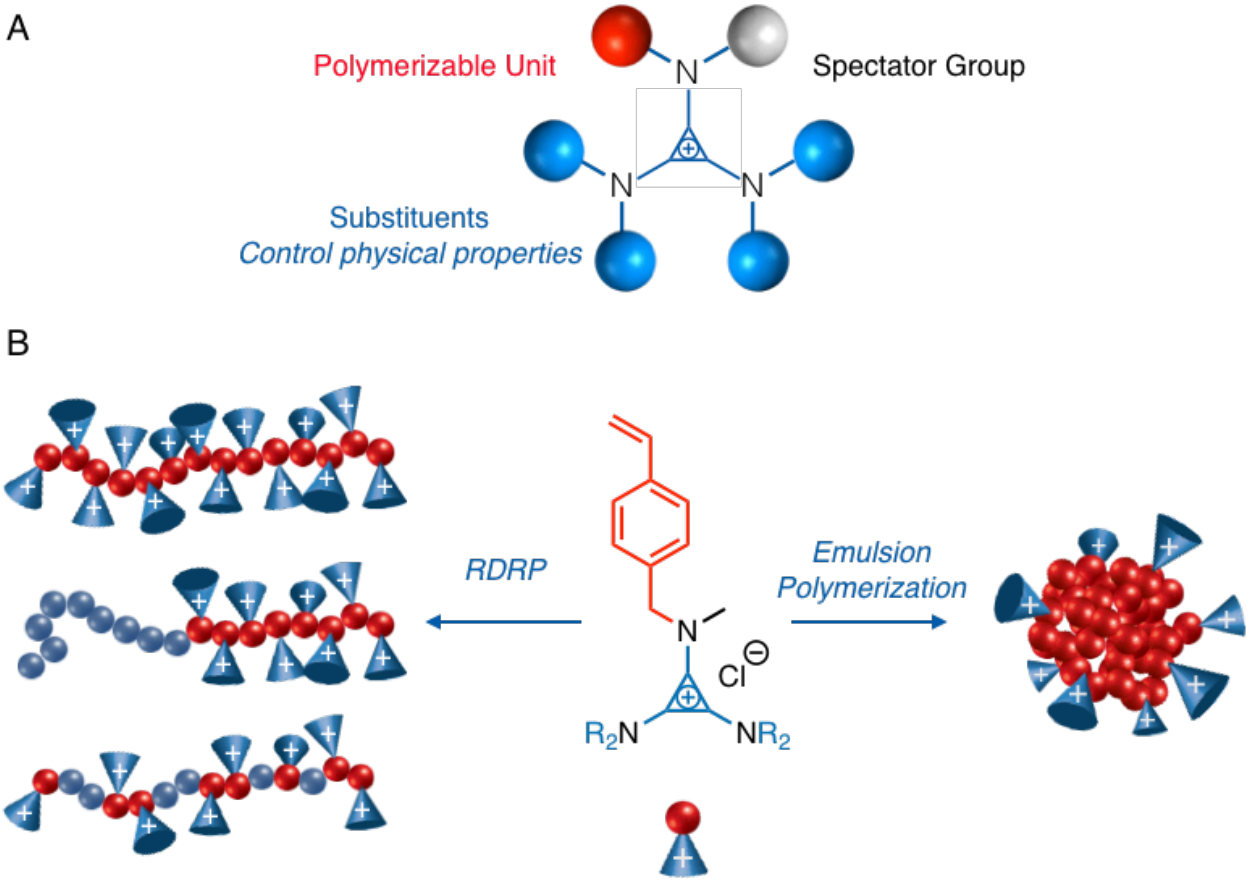

Figure 2. The cyclopropenium cation as a non-conventional polymer building block. (a) Schematic design of polymerizable cyclopropenium-based monomer. (b) The styrenic cyclopropenium monomer can be employed in reversible-deactivation radical polymerization (RDRP) to yield homopolymers, block copolymers, and statistical copolymers, or in emulsion polymerization to yield nanoparticles.

What truly unlocked the chemistry of linear cyclopropenium polymers however, was the development of a post-polymerization functionalization strategy. Due to the cationic nature of the cyclopropenium groups, our first library of synthesized polymers could not be characterized by size exclusion chromatography. This limitation on our understanding of molecular weight and dispersity hampered our ability to make direct comparisons between different polymers. Thus, we developed a route to cyclopropenium-based polymers from a well-characterized neutral precursor polymer (**Figure 3**). A one-step post-polymerization click reaction quantitatively converted either pendent or main-chain secondary amines to trisaminocyclopropenium rings. With the specific details of the reaction described elsewhere,[29] this robust transformation enabled precise structure-property relationship studies across a family of cyclopropenium-based polymers while holding effects of dispersity and degree of polymerization constant.

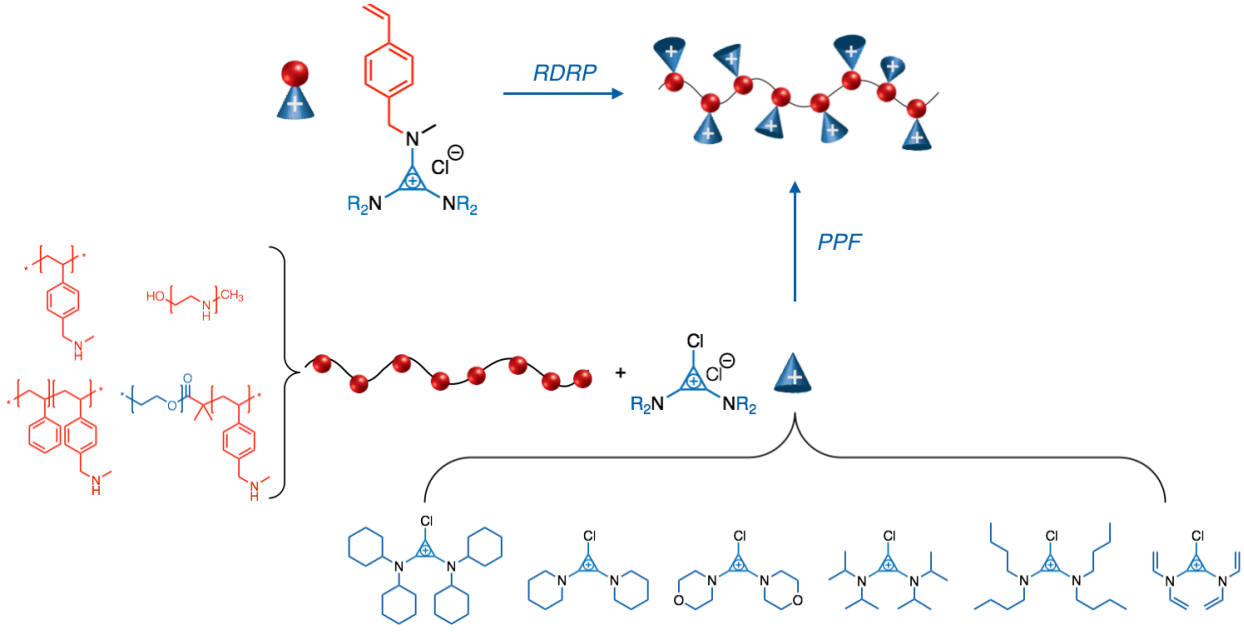

Figure 3. Synthesis of cyclopropenium-based polymers can be accomplished either through reversible-deactivation radical polymerization (RDRP) of a cyclopropenium-based monomer or through a post-polymerization functionalization (PPF) coupling a cyclopropenium chloride to a neutral parent polymer. The neutral polymer can be composed of either main-chain or pendent secondary amines in either a homopolymer or block copolymer. The cyclopropenium salt tolerates a variety of amino substituents.

Concomitantly, we investigated synthetic strategies to develop cationic surface-charged nanoparticles using cyclopropenium monomers and block copolymers via surfactant-free emulsion

polymerization. Both monomers and block copolymers were found to stabilize oil-in-water emulsions as functional surfactants where the diameter of the resultant nanoparticle could be reliably tuned from 30-100 nm with narrow dispersity (**Figure 4**). Simply increasing the percent loading of surfactant increased the surface-to-volume ratio and decreased particle size. Additionally, as cyclopropenium is a remarkably stably cation,[23] these nanoparticles were found to retain their highly positive surface charge for the pH range of 1.4 to 12.6. The ability of cyclopropenium-containing molecules to stabilize a nanoparticle interface eliminates the need for additional surfactants, solvents, or multi-step protocols, highlighting their potential in biological, imaging, and industrial applications.

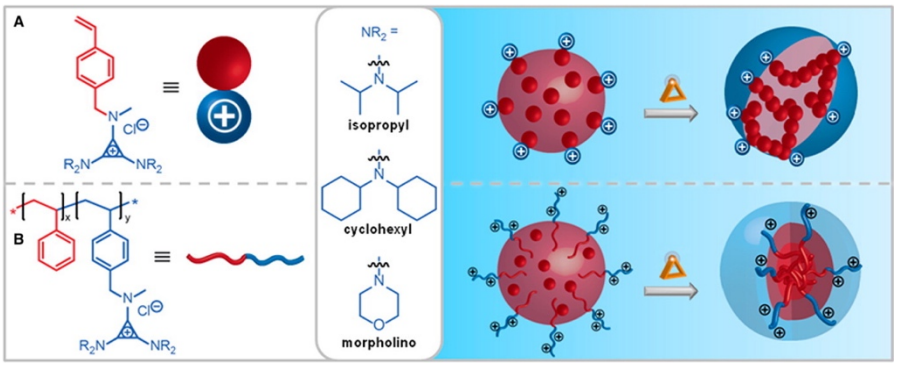

Figure 4. Illustrated representation of the surfactant-free emulsion polymerization of (a) cyclopropenium-based monomers and (b) cyclopropenium-containing block copolymers to form surface-charged polymer nanoparticles.

This thesis describes our first studies of this family of cyclopropenium-based polymers and nanoparticles for biomedical applications. The first part describes our efforts evaluating cyclopropenium-based polymers as candidate non-viral vectors for gene delivery. In the second part, we show how the nanoparticles can be exploited as live-cell image contrast agents and potentially theranostic tools. In the final part, we briefly describe a new project developing a novel class of cyclopropenium-based polymers. Collectively, this thesis illustrates the different avenues through which we have brought cyclopropenium-centered cationic polyelectrolytes to life.

REFERENCES

(1) Wang, L.-X.; Davis, B. G. *Chem. Sci.* **2013**, *4*, 3381–3394.
(2) Lutz, J.-F.; Lehn, J.-M.; Meijer, E. W.; Matyjaszewski, K. *Nat. Rev. Mater.* **2016**, No. 16024, 16024.
(3) Stahl, G. A. In *Polymer Science Overview*; 1981; pp 25–44.
(4) Society, A. C. *The Foundation of Polymer Science by Hermann Staudinger (1881-1965)*; 1999.
(5) Grubbs, R. B.; Grubbs, R. H. *Macromolecules* **2017**, *50* (18), 6979–6997.
(6) Hawker, C. J.; Wooley, K. L. *Science* **2005**, *309* (5738), 1200–1205.
(7) Blasco, E.; Sims, M. B.; Goldmann, A. S.; Sumerlin, B. S.; Barner-Kowollik, C. *Macromolecules* **2017**, *50* (14), 5215–5252.
(8) Langer, R.; Tirrell, D. A. *Nature* **2004**, *428*, 487–492.
(9) Yin, H.; Kanasty, R. L.; Eltoukhy, A. A.; Vegas, A. J.; Dorkin, J. R.; Anderson, D. G. *Nat. Rev. Genet.* **2014**, *15* (8), 541–555.
(10) Vauthier, C.; Ponchel, G. *Polymer Nanoparticles for Nanomedicines: A Guide for their Design, Preparation and Development*; 2016.
(11) Peppas, N. A.; Khademhosseini, A. *Nature* **2016**, *540*, 335–336.
(12) Elsabahy, M.; Heo, G. S.; Lim, S.-M.; Sun, G.; Wooley, K. L. *Chem. Rev.* **2015**, *115* (19), 10967–11011.
(13) Ramos, J.; Forcada, J.; Hidalgo-Alvarez, R. *Chem. Rev.* **2014**, *114* (1), 367–428.
(14) Xu, F. J.; Yang, W. T. *Prog. Polym. Sci.* **2011**, *36* (9), 1099–1131.
(15) Merdan, T.; Kopeček, J.; Kissel, T. *Adv. Drug Deliv. Rev.* **2002**, *54*, 715–758.
(16) Samal, S. K.; Dash, M.; Van Vlierberghe, S.; Kaplan, D. L.; Chiellini, E.; van Blitterswijk, C.; Moroni, L.; Dubruel, P. *Chem. Soc. Rev.* **2012**, *41* (21), 7147–7194.
(17) Jangu, C.; Long, T. E. *Polymer* **2014**, *55* (16), 3298–3304.
(18) Jaeger, W.; Bohrisch, J.; Laschewsky, A. *Prog. Polym. Sci.* **2010**, *35* (5), 511–577.
(19) Nishimura, N.; Ohno, H. *Polymer* **2014**, *55* (16), 3289–3297.
(20) Morille, M.; Passirani, C.; Vonarbourg, A.; Clavreul, A.; Benoit, J. P. *Biomaterials* **2008**, *29*, 3477–3496.
(21) Mintzer, M. A.; Simanek, E. E. *Chem. Rev.* **2009**, *109* (979), 259–302.
(22) Breslow, R. *J. Am. Chem. Soc.* **1957**, *79* (1), 5318.
(23) Yoshida, Z.; Tawara, Y. *J. Am. Chem. Soc.* **1971**, *93* (1962), 2573–2574.
(24) Bandar, J.; Lambert, T. *Synth.* **2013**, *45*, 2485–2498.
(25) Bruns, H.; Patil, M.; Carreras, J.; Vázquez, A.; Thiel, W.; Goddard, R.; Alcarazo, M. *Angew. Chem. Int. Ed.* **2010**, *49* (I), 3680–3683.
(26) Bandar, J. S.; Lambert, T. H. *J. Am. Chem. Soc.* **2012**, *134*, 5552–5555.
(27) Hendriks, K. H.; Robinson, S. G.; Braten, M. N.; Sevov, C. S.; Helms, B. A.; Sigman, M. S.; Minteer, S. D.; Sanford, M. S. *ACS Cent. Sci.* **2018**, *4* (2), 189–196.
(28) Sevov, C. S.; Samaroo, S. K.; Sanford, M. S. *Adv. Energy Mater.* **2017**, *7* (1602027).
(29) Freyer, J. L. The Design and Synthesis of Aromatic Ion-Based Polyelectrolytes for Divergent Applications, 2018.

PART ONE:

BRINGING CYCLOPROPENIUM TO LIFE

CYCLOPROPENIUM POLYMERS FOR GENE DELIVERY

[This section is based on the following publications: *Angew. Chem. Int. Ed.* **2016**, *55*, 40, 12382; *Polymers* **2017**, *9*, 79; *J. Polym. Sci. A Polym. Chem.* **2017**, *55*, 19, 3167]

Gene therapy, the process by which exogenous genetic information is brought into cells by a delivery vector to impart a therapeutic effect, has captivated generations of scientists for its potential to treat genetic diseases and cancers.[1] The tantalizing vision of a single outpatient treatment to cure hemophilia, blood cancers, or hereditary blindness amongst many other disorders has motivated research for decades. After a tragic setback in the late 1990s gene therapy appeared to be on the brink of failure, but sustained efforts have driven significant progress in the past several years.[2,3] Over 2000 of clinical trials have been conducted in the last decade and just this year the US Food and Drug Administration approved Luxturna as the first gene therapy for an inherited genetic disorder.[4,5] However, the full potential of gene therapy remains unrealized.

Today, the fundamental challenge of gene therapy is the design of efficient, biocompatible delivery vectors.[4,6,7] Since the concept of gene delivery was first introduced, both viral and non-viral options have been explored, with each presenting their own benefits and drawbacks.[8] Though viruses have evolved over billions of years to efficiently deliver their DNA, the clinical translation of modified viral technologies has been limited by immunogenicity, lack of selectivity, and production difficulties.[6,9] On the contrary, synthetic non-viral vectors elicit a reduced immunogenic response and are generally much more facile to produce, but thus far have yielded lower delivery efficiencies. The development of an optimized non-viral vector, balancing clinical safety with high efficiency, thus remains the critical goal to the realization of gene therapy.[10]

Cationic polymers are one of the most commonly studied non-viral vectors due to their high stability and capacity to tune macromolecular composition and structure via robust

chemistry.[11,12] Crucially, the positive charge embedded in each monomer unit promotes rapid complexation with the negatively charged phosphate backbone of nucleic acids into a polyplex, which can mediate cell adhesion and uptake. To yield efficient cellular transfection, polyplexes must overcome a host of obstacles and barriers both outside and inside the cell. An ideal gene delivery vector must be engineered to localize at the cells of interest, permeate cell membranes, and escape the endosome by either membrane lysing or the proton sponge effect, while shielding their nucleic acid cargo from degradation and not provoking an immunogenic response (**Figure 1**).[13,14] Linear poly(ethylenimine) (PEI) was the first cationic polymer observed to rapidly bind nucleic acids into polyplexes via electrostatic interactions and has since become an industry standard non-viral vector.[15] In the subsequent years, there has been a great proliferation of cationic structures shown to bind and transfect nucleic acids.[16–18] In addition to increasing the library of cationic polymers available, these research efforts have begun to uncover some design principles towards optimizing polymeric structure for transfection. In general, it has been shown that transfection efficiency and cytotoxicity trend with molecular weight and the degree of polymer chain branching.[19–22] With the advent of reversible-deactivation radical polymerization techniques, the challenge has now become fine-tuning polymer composition and architecture to probe detailed structure-property relationships among the various polymers accessible.[23]

Our report detailing the functionalization of polymers with an array of bis(dialkylamino)cyclopropenium chloride (BACCl) derivatives affords an ideal modular platform from which to study polymers for gene delivery. In the efficient post-polymerization click reaction,

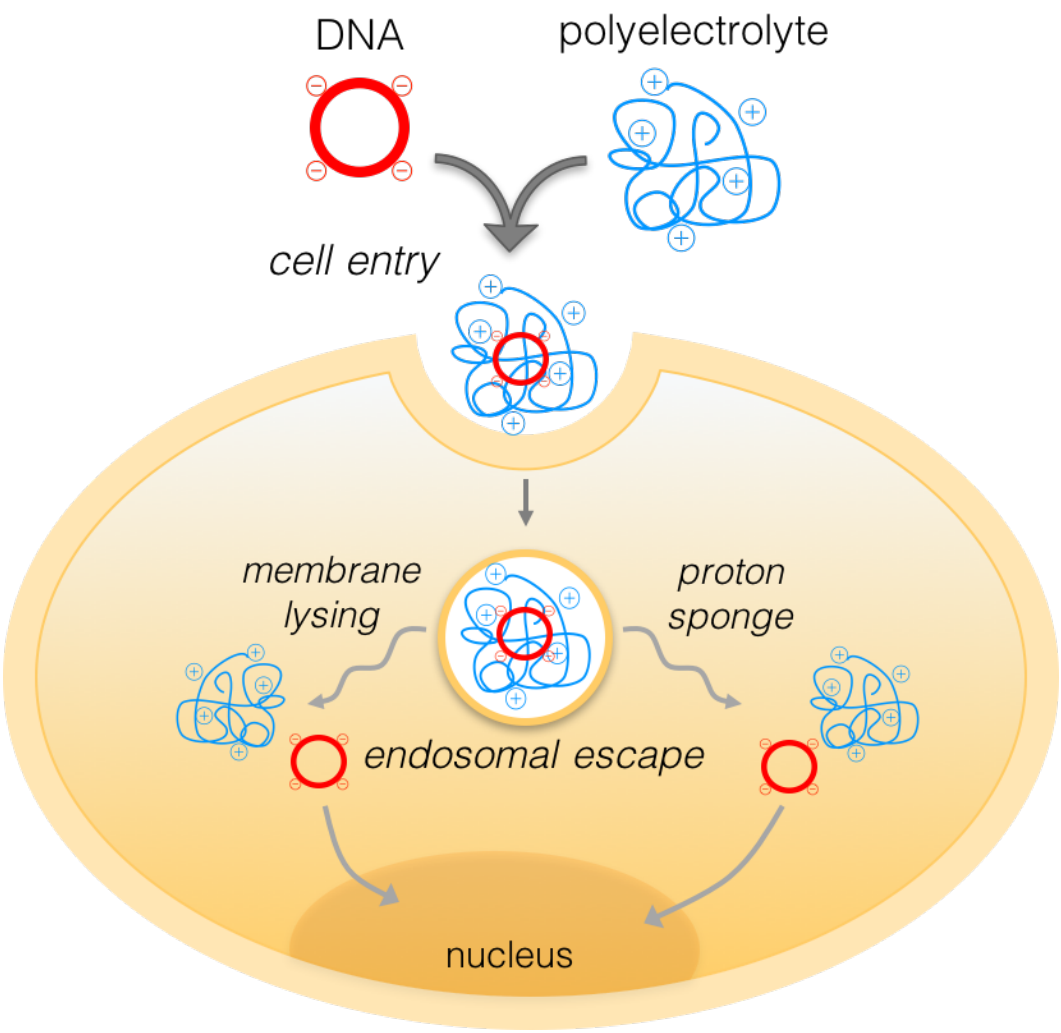

Figure 1. Transfection via a non-viral gene delivery vector. Polyplexes comprising nucleic acids (e.g. DNA) and a polyelectrolyte non-viral vector must enter the cell (typically through endocytosis), escape the endosome via either lysing of the endosomal membrane or the proton sponge effect, and release its genetic cargo for nuclear uptake.

polymers bearing either pendent or main-chain secondary amines were quantitatively transformed into the aromatic trisaminocyclopropenium (TAC) ion. This rapid reaction furnishes well-defined polyelectrolytes, where effects of dispersity and degree of polymerization are held constant, enabling precise structure-property relationship studies.

To determine whether this transformation was relevant for gene delivery we focused on the TAC homopolymers that were highly water-soluble. Furthermore, to streamline comparisons between materials we elected to change only subtle elements of the TAC structure, functionalizing

with either a morpholine (Mo) or piperidine (Pep) substituent, on two different polymer backbones, PEI and poly(methylaminostyrene) (PMAS) (**SI Figure 1**). Cytotoxicity assays and luciferase transfection experiments in HEK-293T cells revealed a significant dependence on the chemical structure of the pendent TAC ion, namely on its amino substituents, and on the identity of the polymer backbones. All four TAC polymers showed a similar toxicity profile to linear PEI (25 kg mol^{-1}) at low dosages. However, at high loadings, polyTACs were found to be more biocompatible, especially those bearing a styrene backbone (**Figure 2**). Functionalizing PEI with TAC(Mo) endowed the polymer with low toxicity, affording a cell viability of approximately 50% at both 50 and 100 μg mL^{-1} loadings.

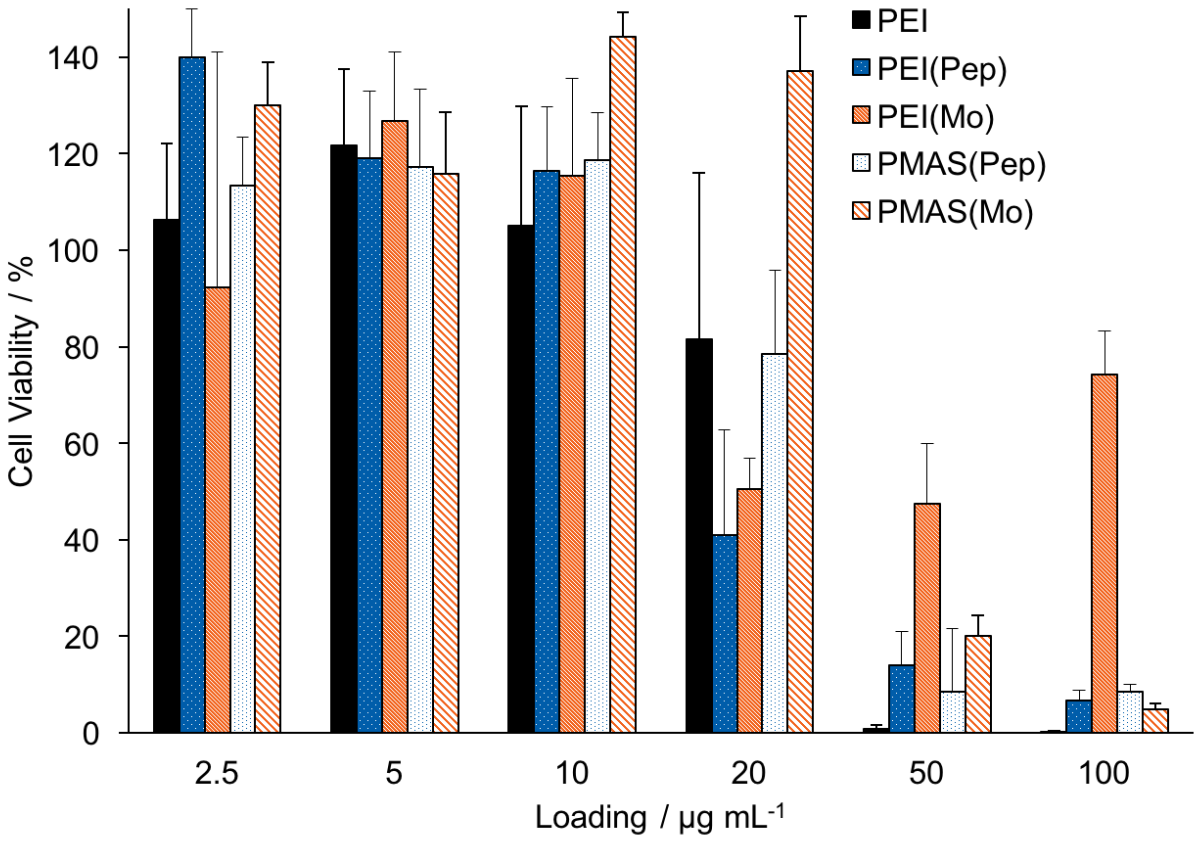

Figure 2. Biocompatibility of TAC-functionalized polymers at various doses in HEK-293T cells following 48 h incubation. Viability is measured by trypan blue dye exclusion and normalized to untreated cells. Error bars show the standard deviation of triplicate measurement.

While structural modification of PEI with TAC ions led to a lower transfection efficacy compared to the parent polymer (**Figure 3**), comparing the two modified PEI materials bearing TAC(Pep) and TAC(Mo) showed notable differences in transfection efficiency. These two materials exclusively differ in the chemistry at the 4-position of the six-membered ring: a simple variation between a methylene group and an ether oxygen. The PEI(Pep) polyplexes transfected cells almost as well as the PEI parent polymer, but polyplexes of PEI(Mo) exhibited poor transfection efficiency. Potentially, this difference may be attributed to the increased hydrophobicity of PEI(Pep) over PEI(Mo), a property that has been shown to play a key role in non-viral vectors.[24–28] Polyplexes of PEI and TAC polymers with plasmid DNA (pDNA), at their most efficient loadings (noted in Figure 3), were further characterized by dynamic light scattering for hydrodynamic diameter (D_H) and zeta potential (ζ; **SI Table 1**). Since the D_H and surface charge values are similar for PEI(Pep), PEI(Mo), and unfunctionalized PEI polyplexes, the observed discrepancy in transfection efficacy may be due to fine structural variations between each agent. As cyclopropenium is a permanent positive charge and contains no basic amines to protonate, polyplexes likely escape the endosome via membrane lysing rather than a proton sponge mechanism,[29] further suggesting that subtle changes in hydrophobicity have an enormous impact on efficacy.

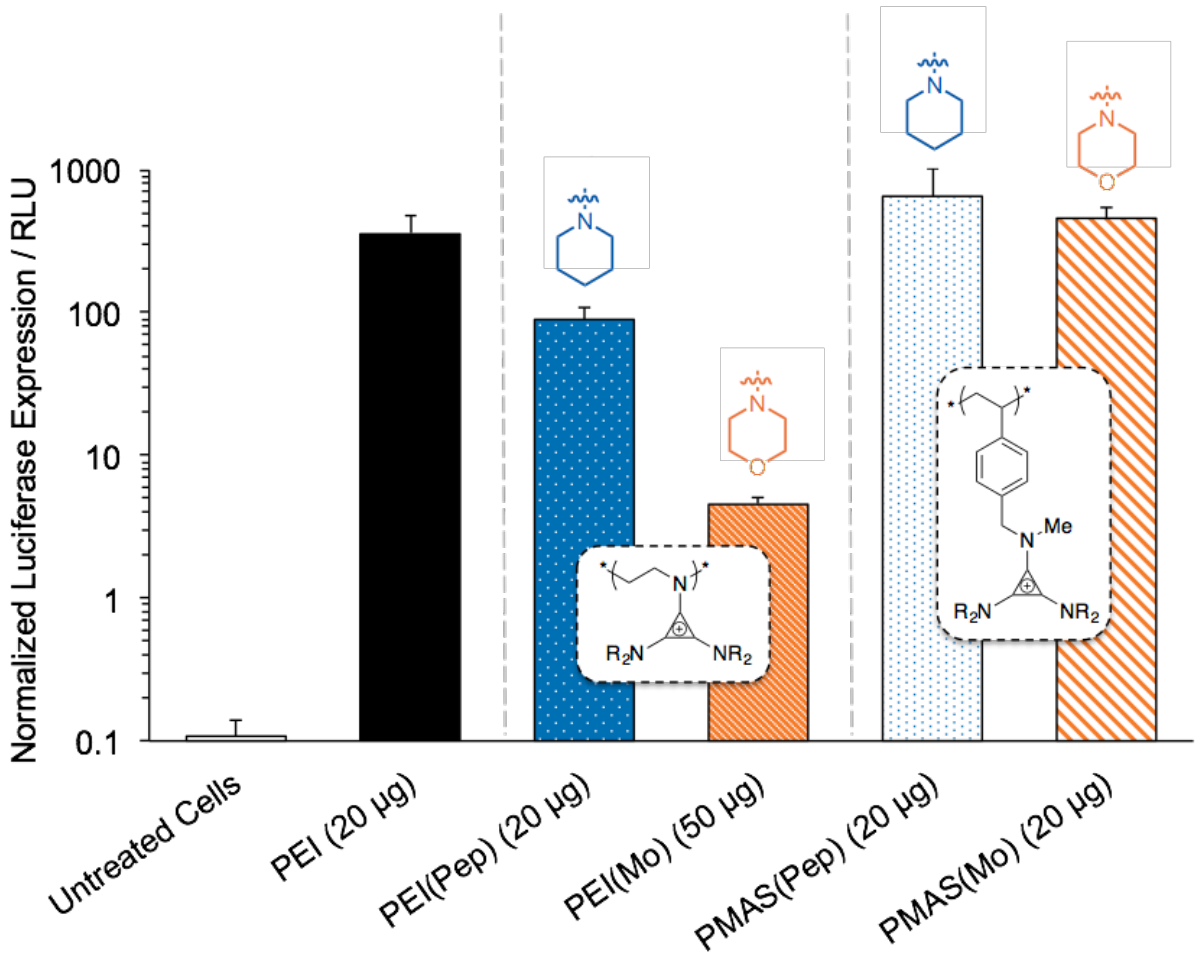

Figure 3. Luciferase expression in HEK-293T cells transfected with pDNA containing the firefly luciferase reporter gene using TAC polymers and 25 k linear PEI. Polymer backbones are noted in white boxes with amino substituents pictured above the respective bars. Luciferase expression is measured after 48 h incubation with specified polymer loadings (all with pDNA loading of 3 µg mL^{-1}) and normalized by cell count. Error bars show the standard deviation of triplicate measurement.

Changing the polymer backbone from PEI to PMAS resulted in smaller polyplexes that were also viable, efficacious transfection agents [**Figure 3 and SI Figure 2**, PMAS(Pep) and PMAS(Mo)]. All of our most effective formulations are within the size regime that Zhou and coworkers outlined for high-efficiency transfection reagents, that is, less than 500 nm.[30] Furthermore, the PMAS-based materials exhibited optimal pDNA transfection at lower charge ratios than PEI and PEI(R) polymers indicating a more efficient electrostatic binding (**SI Table 1**). Within the range of the error bars, the more hydrophobic PMAS(Pep) derivative and the

PMAS(Mo) derivative show similar efficacy, unlike in the PEI systems. These results suggest that our post-polymerization functionalization reaction with BACCl groups has great potential as a platform to tune the chemical composition of TAC-based polyelectrolytes, build detailed structure-property relationships, and inform design principles for the optimization of transfection agents.

We next extended these results by probing the effect of the substituted alkylamino chain's degree of branching on cytotoxicity and transfection efficacy. Pendent moieties have been shown to modify the structure and stability of polymer-DNA polyplexes to facilitate cellular release, with several reports exploring the effects of fine tuning a substituent alkyl chain length.[31–33] However, comparably few studies have investigated the nature of branching within an alkyl group and its effect on transfection efficacy. As our cyclopropenium platform is amenable to a wide variety of BACCl derivatives, we synthesized two more to directly compare the branching of the alkyl chain: *n*-butyl (Bu; BACBu) and isopropyl (iP; BACiP). These two BACCl structures differ in the degree of branching, and thereby "floppiness", as well as hydrophobicity, as the Bu derivative has one additional carbon. We again functionalized these derivatives on both PEI and PMAS polymer backbones furnishing a total of four additional candidate non-viral vectors.

All four homopolymers were highly water-soluble, permitting their condensation with an aqueous solution of pDNA containing the firefly luciferase reporter gene. Combining the polymers at varied loadings with a fixed amount of pDNA, and subsequently incubating in HEK-293T cells for 48 h, revealed the polymers' biocompatibility as a function of loading. We found that PEI(iP) and PMAS(Bu) were the most biocompatible with high cell viabilities through loadings of 20 μg mL^{-1} (**Figure 4**). Surprisingly, their counterparts, PEI(Bu) and PMAS(iP), exhibited notable toxicity at all loadings tested. All TAC-derived polymers in this study were highly toxic at loadings of 50 μg mL^{-1} and greater, similar to linear PEI. This stands in contrast to the work described

earlier with the more rigid piperidine or morpholine substituents which were still viable in this regime. Thus, rigidity or flexibility of substituent chains stands as an important parameter to understand optimal gene transfection. Taken together, our results suggest there is a complex interaction between a polymer backbone and its substituent in the design of biocompatible gene delivery vectors.

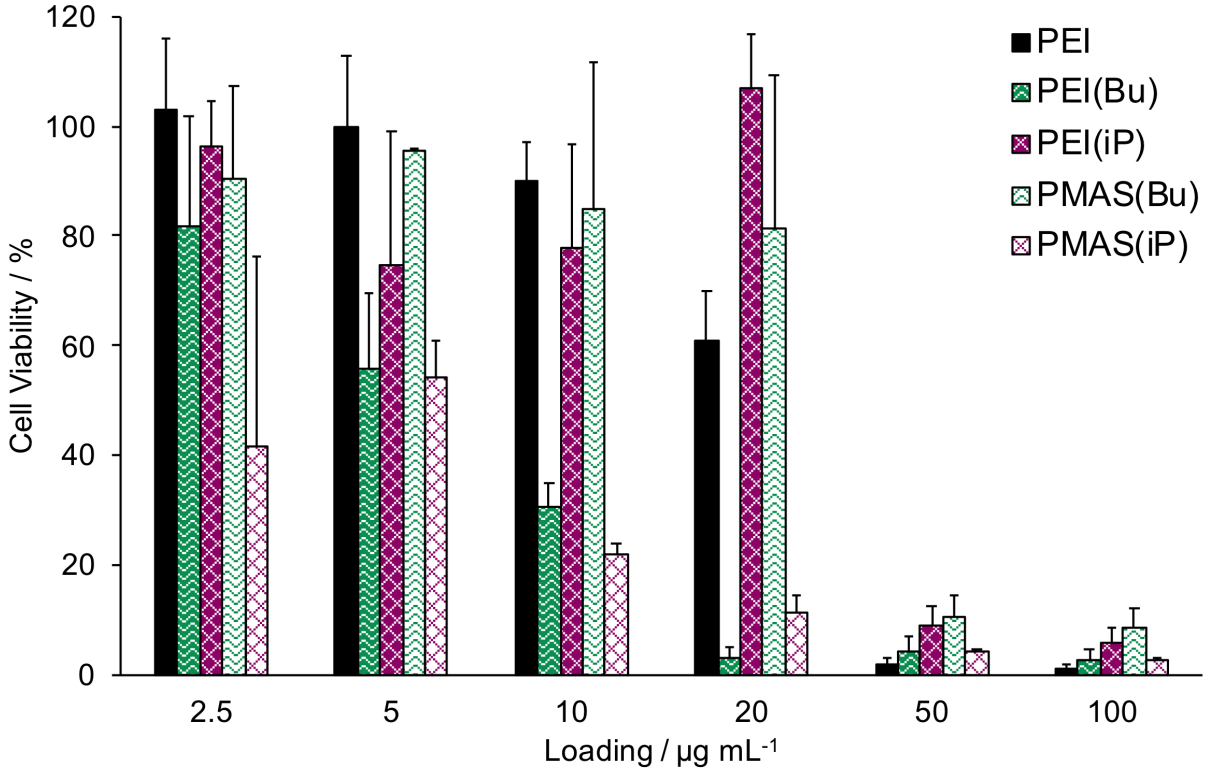

Figure 4. Biocompatibility of TAC-based polymers at various doses in HEK-293T cells following 48 h incubation. Viability is measured by trypan blue dye exclusion and normalized to untreated cells. Error bars show the standard deviation of triplicate measurement.

We further found that this fine tuning of the substituent chain branching had a dramatic influence on delivery efficacy. In order to assess the amount of polymer necessary to completely condense pDNA into a polyplex gel electrophoresis shift assays were performed (**SI Figures 3-6**). While all polymers were able to fully bind the pDNA by a weight ratio of 3.33 polymer : 1 pDNA, PEI(iP) was the most efficient, binding at a weight ratio of only 0.83 polymer : 1 pDNA. This corresponds to the lowest polymer loading tested for either biocompatibility or transfection and

less than 1 TAC unit per phosphate anion of pDNA (**SI Tables 2-3**). However, binding efficiency is not a clear indicator of delivery efficiency, as too favorable an interaction can be detrimental for eventual release of the genetic material.[34–36]

Luciferase expression assays revealed a significant dependence on the nature of the amino substituent and polymer backbone for successful gene delivery. While all TAC-based polymers transfected pDNA significantly better than the untreated controls, PMAS(iP) demonstrated the highest transfection efficacy (**Figure 5**). As is the case with unmodified linear PEI, successful delivery of intact pDNA to cells comes at the cost of significant cytotoxicity. By contrast, the nontoxic PEI(iP) demonstrated a much lower luciferase activity. Interestingly, PEI(iP) was the most efficient at compacting pDNA into a polyplex, suggesting that it binds nucleic acids too strongly and never releases its payload. Transforming either of the polymer backbones with TAC(Bu) seemed to yield successful non-viral vectors capable of both binding and slowly releasing pDNA. This could potentially be attributed to critical destabilization of the cell and endosomal membranes due to the long, flexible alkyl substituents. At their optimal loadings, both PEI(Bu) and PMAS(Bu) demonstrated two orders-of-magnitude transfection improvement over untreated control cells. Combined with the cytotoxicity and pDNA-binding data, we conclude that amongst this set of TAC polymers, PMAS(Bu) is the most potent non-viral vector.

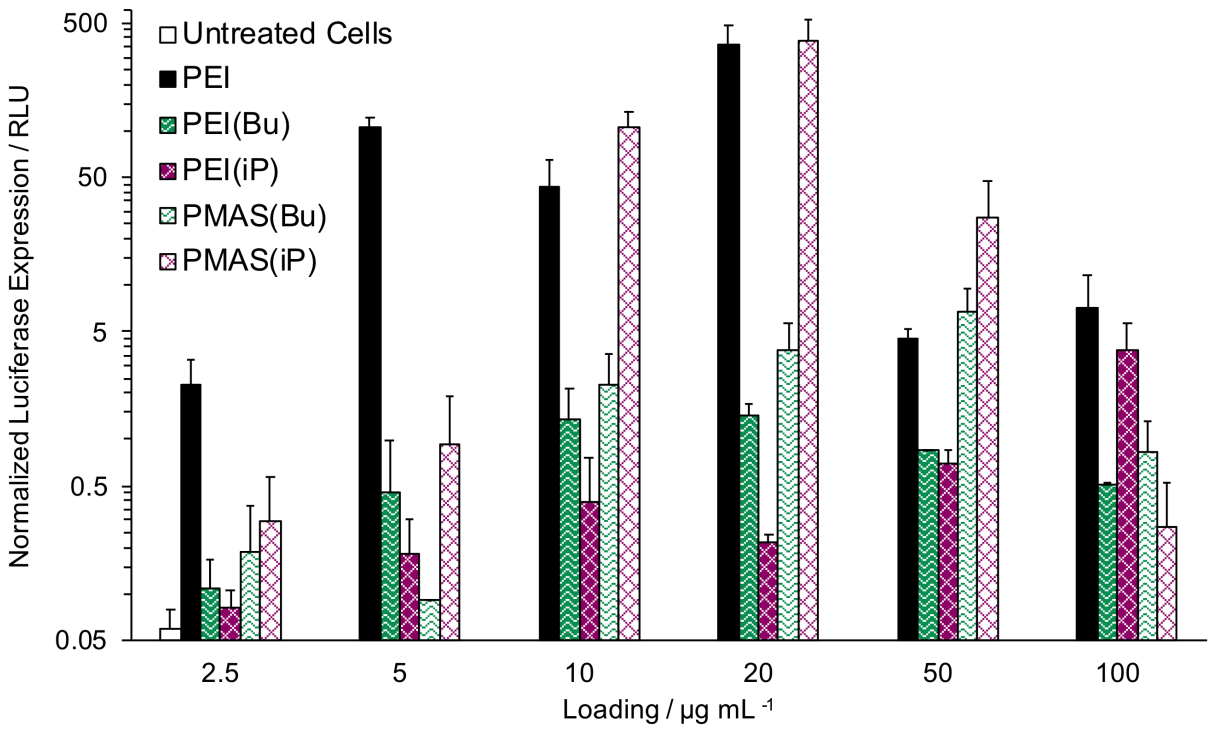

Figure 5. Luciferase expression in HEK-293T cells transfected with pDNA containing the firefly luciferase reporter gene using TAC polymers and 25 k linear PEI. Luciferase expression is measured after 48 h incubation with specified polymer loadings (all with pDNA loadings of 3 µg mL^{-1}) and normalized by cell count. Error bars show the standard deviation of triplicate measurement.

Our results demonstrate that there is an important interplay between polymer backbone and substituent structure, and that both must be carefully considered in the design of non-viral vectors. While hydrophobic modifications of non-viral vectors are frequently reported to promote transfection, our data indicate that a careful balance of hydrophobicity and substituent flexibility must be achieved for optimal gene delivery. The drastic differences in transfection efficiency deriving from minor structural variations showcases the need for synthetic strategies to modularly access a wide variety of structures. Importantly, our work exemplifies that design of transfection reagents demands precise control over all aspects of polymer structure and highlights the necessity of a robust, modular platform from which to study them.

MODULATING POLYMER ARCHITECTURE FOR ENHANCED TRANSFECTION

The singular challenge in the design of gene delivery vectors is understanding how tunable elements of polymer composition and architecture affect macroscopic properties, including biocompatibility and transfection efficacy. Equipped with a modular platform to synthesize cyclopropenium-based polymers, the question for us became which structural features to tune. Having already explored how the chemistry of the monomer and atom-level manipulations therein could affect transfection, we were inspired to study the role three-dimensional arrangement of the same monomers would play. Specifically, we were interested in how multivalent presentation of cyclopropenium units may affect their gene delivery capabilities, and thus designed both brush and star polymers.

Brush and star polymers have a three-dimensional architecture with multiple terminal groups that has motivated their recent syntheses and applications as non-viral gene delivery vectors.[37,38] Wang and co-workers have led efforts demonstrating the superior efficacy of polymers with such multivalencies, reporting over 8000-fold enhancements in transfection efficiency compared to linear analogues.[39,40] These enhancements are attributed to multiple sources: an improved interaction of polymers with DNA to form a polyplex; increased cellular uptake due to higher likelihood of electrostatic interactions with cell membrane; and, enhanced protection of DNA from enzymatic degradation.[39,41] While with linear polymers it is generally understood that increasing molecular weight increases both transfection efficiency and cytotoxicity, this effect is lessened in brush polymers where it has been shown that distributing mass across multiple side-chains attenuates the cytotoxicity.[38]

Though it has only been 15 years since the first star-shaped polymer was investigated for transfection, they have also emerged as one of the most promising classes of non-viral gene

delivery vectors.[42] Star polymers, with multiple chains, or arms, functionalized onto a single core, show a higher degree of flexibility than dendritic or other branched polymers, that may be important in the condensation of DNA. Though star polymers have demonstrated a similar trend to their linear analogues, where increasing the molecular weight of the arms increases cytotoxicity, this effect can be mitigated by increasing the number of arms.[38,43,44] Keeping the molecular weight constant and increasing the number of arms has been shown to decrease cytotoxicity across a number of different functionalities.[42,43,45] Thus, we were motivated to study if these same architecturally-based transfection enhancements would be borne out in second-generation cyclopropenium polymers.

For these studies, it is essential that the synthesized polymers have well-defined structures and narrow dispersities. Considering brushes first, we designed a synthetic route that exploited two orthogonal living polymerization techniques, atom-transfer radical polymerization (ATRP) and ring-opening metathesis polymerization (ROMP), to provide robust control over degree of polymerization in two dimensions (**Figure 6**). ATRP was employed to synthesize the side chain, ultimately dictating the number of cyclopropenium units per branch, while ROMP was used to polymerize the backbone, controlling the number of side chains.

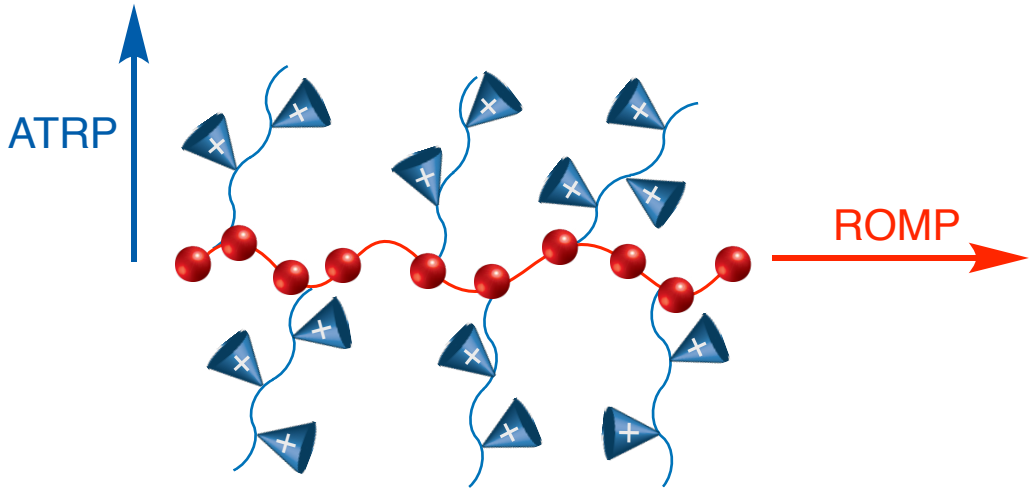

Figure 6. Orthogonal polymerization strategies, ATRP and ROMP, were employed to controllably synthesize brush side chains and backbone, respectively.

Furthermore, brush polymers can be stitched together by one of three methods, "grafting from", "grafting onto", and "grafting through", which each present advantages and disadvantages.[46,47] Easily the most common, the "grafting from" approach involves the straightforward polymerization of side-chains from a synthesized backbone but is limited by the density of initiation sites. In the "grafting onto" approach, side chains and backbone are synthesized separately and then coupled, but are restricted from high grafting densities due to steric hindrance. We decided to synthesize our brushes in a "grafting through" approach, which involves the design of functional side-chains (i.e. macromonomers) which can be subsequently polymerized into a brush. This approach guarantees complete backbone functionalization but can be difficult to achieve high degrees of backbone polymerization.[46] There is an additional choice in macromonomer design regarding the incorporation of the polymerizable handle that Xia recently demonstrated as non-trivial. The authors found that growing the macromonomer and then subsequently coupling the polymerizable handle onto it led to lower polymer dispersities and reduced chain end coupling.[48] Taking these insights into account, we designed a full synthesis for cyclopropenium-based brush polymers (**Figure 7 and SI Figures 7-12**).

Our synthetic route begins with a prototypical ATRP of *tert*-butyl methyl(4-vinylbenyzl)carbamate where the initiator contains an azide handle. This reaction proceeds rapidly and is performed at low monomer equivalents to afford short polymers (DP 15-25) of low dispersity (Đ < 1.10). These homopolymers are covalently linked with a norbornene handle via copper-catalyzed click chemistry (CuAAC) to yield the functional macromonomer. CuAAC optimization resulted in up to 90% of chain ends being functionalized as determined by ^{1}H NMR (**SI Figure 8**). We found that the efficiency of this reaction decreased as molecular weight increased, which is corroborated by other reports that generate macromonomers weighing no more than 5 kDa.[49,50] These macromonomers were then subjected to ROMP with Grubbs' 3rd generation catalyst providing the desired brush architecture. As expected for a "graft through" approach, this reaction did not go to completion with small quantities of macromonomer still remaining (**SI Figure 10**). We have been attempting to purify these materials by extensive dialysis but are in the process of developing other purification strategies. These brushes are then fully deprotected and functionalized with cyclopropenium following a modified post-polymerization functionalization strategy. For complete deprotection to the secondary amine, we found it necessary to react with trifluoroacetic acid rather than trimethylsilyl chloride and quench with a weak base. The functionalization reaction with any BACCl proceeds rapidly at low molar equivalents as confirmed by ^{1}H NMR, as previously described. Thus, in five sequential steps from monomers, we were able to synthesize cyclopropenium-based brush polymers.

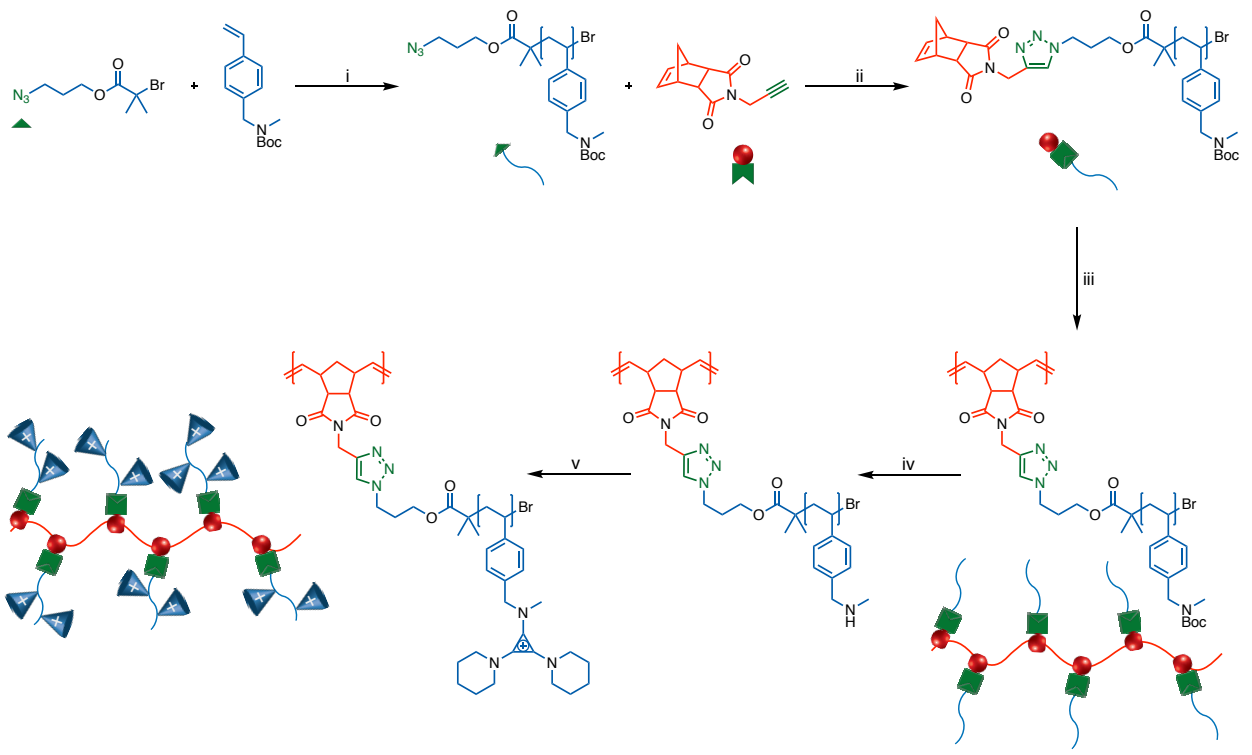

Figure 7. Synthetic scheme for cyclopropenium brush polymers. (i) CuBr, PMDETA, Anisole, 90 °C, 1-2 h; (ii) CuBr, PMDETA, dry THF, 50 °C, 24 h; (iii) Grubbs 3rd cat., dry DMF, 35 °C, 12-18 h; (iv) 1. TFA, dry DCM, rt, 2 h 2. TEA; (v) BAC(Pep)Cl, $CHCl_3$, DIPEA, 65 °C, 18 h.

Functionalized star polymers can be synthesized in fewer steps by either an "arm-first" or "core-first" approach.[42] The "arm-first" strategy allows control over arm length but can retain linear precursors after conjugation to a central core. Additionally, synthesizing the arms of the star first lacks a robust route to control the number of arms ultimately attached. On the contrary, synthesizing star polymers "core-first" enables control over arm number and simplifies purification, but requires a multifunctional initiator. This poses a significant drawback because if multiple sites are simultaneously initiated they can radically couple leading to undesirable termination.[51,52] Having been plagued by linear precursor contamination for brushes (i.e. unreacted macromonomers), we chose to synthesize cyclopropenium-based stars via a "core-first" approach.

Starting from a commercially available tetra-functional ATRP initiator we synthesized star polymers following our well-established post-polymerization functionalization route (**Figure 8**

and SI Figures 13-15). In order to eschew undesirable chain end coupling, we significantly lowered the loading of both Cu^{I} and the ligand to limit the number of sites initiated. Tuning the polymerization in this fashion furnished polymers with monomodal and narrow dispersities. From here, our modified deprotection and reported functionalization reactions were employed to unveil the secondary amine and subsequently conjugate a cyclopropenium salt. This modular approach to cyclopropenium-based star polymers is amenable to other valencies, such that the synthesis of 3-arm and 6-arm should directly follow from the commercially available reagents.[53]

As of this writing, biocompatibility and transfection experiments with these

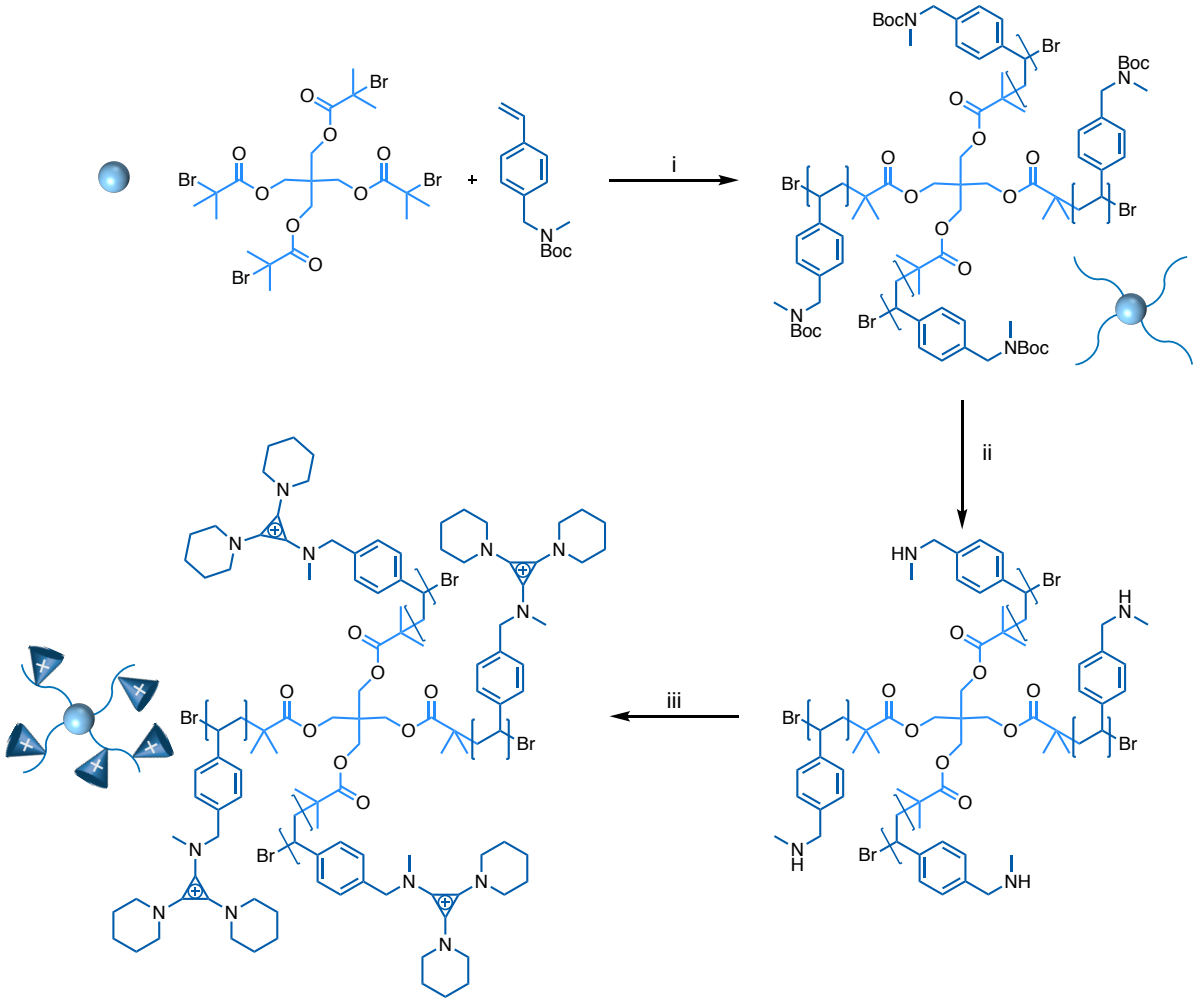

Figure 8. Synthetic scheme for cyclopropenium star polymers. (i) CuBr, PMDETA, Anisole, 90 °C, 12 h; (ii) 1. TFA, dry DCM, rt, 2 h 2. TEA; (iii) BAC(Pep)Cl, $CHCl_3$, DIPEA, 65 °C, 6 h.

cyclopropenium-based brush and star polymers are ongoing. Based on literature results, we believe that the multivalent presentation of cyclopropenium units will improve upon our previously reported transfection results, but this has not yet been experimentally demonstrated. However, these modular synthetic routes meaningfully expand the landscape of cyclopropenium polymers and will allow divergent approaches in future application-driven studies. The capacity to synthesize brushes and stars in addition to linear polymers and nanoparticles can help launch cyclopropenium into of the most accessible and widely recognized cationic polymer systems.

REFERENCES

(1) Friedmann, T.; Roblin, R. *Science* **1972**, *175* (4025), 949–955.
(2) Orkin, S. H.; Reilly, P. *Science* **2016**, *352* (6289), 1059–1061.
(3) Bender, E. *Nature* **2016**, *537* (7619), S57–S59.
(4) Yin, H.; Kanasty, R. L.; Eltoukhy, A. A.; Vegas, A. J.; Dorkin, J. R.; Anderson, D. G. *Nat. Rev. Genet.* **2014**, *15* (8), 541–555.
(5) Sheridan, C. *Nat. Biotechnol.* **2011**, *29* (2), 121–129.
(6) Mintzer, M. A.; Simanek, E. E. *Chem. Rev.* **2009**, *109* (979), 259–302.
(7) Morille, M.; Passirani, C.; Vonarbourg, A.; Clavreul, A.; Benoit, J. P. *Biomaterials* **2008**, *29*, 3477–3496.
(8) Li, S.-D.; Huang, L. *J. Control. Release* **2007**, *123* (3), 181–183.
(9) Kay, M. A. *Nat. Rev. Genet.* **2011**, *12* (5), 316–328.
(10) Kostarelos, K.; Miller, A. D. *Chem. Soc. Rev.* **2005**, *34*, 970–994.
(11) Merdan, T.; Kopeček, J.; Kissel, T. *Adv. Drug Deliv. Rev.* **2002**, *54*, 715–758.
(12) Samal, S. K.; Dash, M.; Van Vlierberghe, S.; Kaplan, D. L.; Chiellini, E.; van Blitterswijk, C.; Moroni, L.; Dubruel, P. *Chem. Soc. Rev.* **2012**, *41* (21), 7147–7194.
(13) Pack, D. W.; Hoffman, A. S.; Pun, S.; Stayton, P. S. *Nat. Rev. Drug Discov.* **2005**, *4* (7), 581–593.
(14) Lächelt, U.; Wagner, E. *Chem. Rev.* **2015**, *115* (19), 11043–11078.
(15) Boussif, O.; Lezoualc'h, F.; Zanta, M. A.; Mergny, M. D.; Scherman, D.; Demeneix, B.; Behr, J.-P. *Proc. Natl. Acad. Sci. U. S. A.* **1995**, *92*, 7297–7301.
(16) Jangu, C.; Long, T. E. *Polymer* **2014**, *55* (16), 3298–3304.
(17) Ornelas-Megiatto, C.; Wich, P. R.; Fréchet, J. M. J. *J. Am. Chem. Soc.* **2012**, *134* (4), 1902–1905.
(18) Priegue, J. M.; Lostalé-Seijo, I.; Crisan, D.; Granja, J. R.; Fernández-Trillo, F.; Montenegro, J. *Biomacromolecules* **2018**, *ASAP*.
(19) Godbey, W. T.; Wu, K. K.; Mikos, A. G. *J. Biomed. Mater. Res.* **1998**, *45* (3), 268–275.
(20) Fischer, D.; Bieber, T.; Li, Y.; Elsässer, H.-P.; Kissel, T. *Pharm. Res.* **1999**, *16* (8), 1273–1279.
(21) Layman, J. M.; Ramirez, S. M.; Green, M. D.; Long, T. E. *Biomacromolecules* **2009**, *10*, 1244–1252.
(22) Bishop, C. J.; Abubaker-Sharif, B.; Guiriba, T.; Tzeng, S. Y.; Green, J. J. *Chem. Commun.* **2015**, *51*, 12134–12137.
(23) Putnam, D. *Nat. Mater.* **2006**, *5* (6), 439–451.
(24) Buerkli, C.; Lee, S. H.; Moroz, E.; Stuparu, M. C.; Leroux, J. C.; Khan, A. *Biomacromolecules* **2014**, *15* (5), 1707–1715.
(25) Sadman, K.; Wang, Q.; Chen, Y.; Keshavarz, B.; Jiang, Z.; Shull, K. R. *Macromolecules* **2017**, *50* (23), 9417–9426.
(26) Santos, J. L.; Oliveira, H.; Pandita, D.; Rodrigues, J.; Pêgo, A. P.; Granja, P. L.; Tomás, H. *J. Control. Release* **2010**, *144* (1), 55–64.
(27) Thomas, M.; Klibanov, A. M. *Proc. Natl. Acad. Sci. U. S. A.* **2002**, *99* (23), 14640–14645.
(28) Thomas, M.; Lu, J. J.; Ge, Q.; Zhang, C.; Chen, J.; Klibanov, A. M. *Proc. Natl. Acad. Sci. U. S. A.* **2005**, *102* (16), 5679–5684.
(29) Vaidyanathan, S.; Orr, B. G.; Banaszak Holl, M. M. *Acc. Chem. Res.* **2016**, *49* (8), 1486–1493.
(30) Zhou, J.; Liu, J.; Cheng, C. J.; Patel, T. R.; Weller, C. E.; Piepmeier, J. M.; Jiang, Z.; Saltzman, W. M. *Nat. Mater.* **2012**, *11*, 82–90.
(31) Gao, Y.; Chen, L.; Zhang, Z.; Gu, W.; Li, Y. *Biomacromolecules* **2010**, *11* (11), 3102–3111.
(32) Hemp, S. T.; Smith, A. E.; Bryson, J. M.; Allen, M. H.; Long, T. E. *Biomacromolecules* **2012**, *13* (8), 2439–2445.
(33) Jarzębińska, A.; Pasewald, T.; Lambrecht, J.; Mykhaylyk, O.; Kümmerling, L.; Beck, P.; Hasenpusch, G.; Rudolph, C.; Plank, C.; Dohmen, C. *Angew. Chem. Int. Ed.* **2016**, *55* (33), 9591–9595.
(34) Yudovin-Farber, I.; Yanay, C.; Azzam, T.; Linial, M.; Domb, A. J. *Bioconjug. Chem.* **2005**, *16* (5),

1196–1203.
(35) Li, M.; Schlesiger, S.; Knauer, S. K.; Schmuck, C. *Angew. Chem. Int. Ed.* **2015**, *54* (10), 2941–2944.
(36) MacLaughlin, F. C.; Mumper, R. J.; Wang, J.; Tagliaferri, J. M.; Gill, I.; Hinchcliffe, M.; Rolland, A. P. *J. Control. Release* **1998**, *56* (1–3), 259–272.
(37) Xu, F. J.; Yang, W. T. *Prog. Polym. Sci.* **2011**, *36* (9), 1099–1131.
(38) Rinkenauer, A. C.; Schubert, S.; Traeger, A.; Schubert, U. S. *J. Mater. Chem. B* **2015**, *3* (38), 7477–7493.
(39) Zhou, D.; Cutlar, L.; Gao, Y.; Wang, W.; O'Keeffe-Ahern, J.; McMahon, S.; Duarte, B.; Larcher, F.; Rodriguez, B. J.; Greiser, U.; Wang, W. *Sci. Adv.* **2016**, *2* (6), 1–15.
(40) Liu, S.; Gao, Y.; A, S.; Zhou, D.; Greiser, U.; Guo, T.; Wang, W. *Acs Biomater. Sci. Eng.* **2017**, *3* (7), 1283–1286.
(41) Wightman, L.; Kircheis, R.; Rössler, V.; Garotta, S.; Ruzicka, R.; Kursa, M.; Wagner, E. *J. Gene Med.* **2001**, *3*, 362–372.
(42) Georgiou, T. K. *Polym. Int.* **2014**, *63* (7), 1130–1133.
(43) Synatschke, C. V.; Schallon, A.; Jérôme, V.; Freitag, R.; Müller, A. H. E. *Biomacromolecules* **2011**, *12* (12), 4247–4255.
(44) Raup, A.; Stahlschmidt, U.; Jérôme, V.; Synatschke, C. V.; Müller, A. H. E.; Freitag, R. *Polymers* **2016**, *8* (224).
(45) Byrne, M.; Victory, D.; Hibbitts, A.; Lanigan, M.; Heise, A.; Cryan, S.-A. *Biomater. Sci.* **2013**, *1* (12), 1223–1234.
(46) Verduzco, R.; Li, X.; Pesek, S. L.; Stein, G. E. *Chem. Soc. Rev.* **2015**, *44*, 2405–2420.
(47) Xia, Y.; Kornfield, J. A.; Grubbs, R. H. *Macromolecules* **2009**, *42* (11), 3761–3766.
(48) Teo, Y. C.; Xia, Y. *Macromolecules* **2015**, *48* (16), 5656–5662.
(49) Bates, C. M.; Chang, A. B.; Momčilović, N.; Jones, S. C.; Grubbs, R. H. *Macromolecules* **2015**, *48* (14), 4967–4973.
(50) Chang, A. B.; Lin, T.-P.; Thompson, N. B.; Luo, S.-X.; Liberman-Martin, A. L.; Chen, H.-Y.; Lee, B.; Grubbs, R. H. *J. Am. Chem. Soc.* **2017**, *139* (48), 17683–17693.
(51) Mendrek, B.; Sieroń, L.; Libera, M.; Smet, M.; Trzebicka, B.; Sieroń, A. L.; Dworak, A.; Kowalczuk, A. *Polymer* **2014**, *55* (18), 4551–4562.
(52) Nakayama, Y. *Acc. Chem. Res.* **2012**, *45* (7), 994–1004.
(53) Aldrich, S. *Material Matters*. 2010, pp 1–32.

SUPPORTING INFORMATION

Materials

All materials were purchased from Sigma-Aldrich and used without further purification, except as noted below. Methylene chloride (CH_2Cl_2) and *N,N*-dimethylformamide (DMF) were dried using a J.C. Meyer solvent purification system. Eluents for column chromatography were HPLC grade and purchased from Fisher Scientific. Deuterated solvents used for NMR spectroscopy were purchased from Thermo Fisher Scientific. Organic solutions were concentrated with a Buchi rotary evaporator. Dulbecco's Modified Eagle Medium (DMEM), fetal bovine serum (FBS), and penicillin/streptomycin were purchased from Invitrogen. Spectrum Labs dialysis bags were purchased from VWR.

NMR Spectroscopy

^{1}H NMR spectra were recorded on a Bruker Avance III 400 MHz spectrometer. Standard abbreviations indicating multiplicity were used as follows: s (singlet), d (doublet), t (triplet), q (quartet), m (multiplet), b (broad).

Cell culture

HEK-293T cells (American Type Culture Collection) were grown in DMEM culture medium with L-glutamine supplemented with 10% *v/v* FBS (Atlanta Biologicals) and 1% *v/v* penicillin/streptomycin (Gibco). Cultures were incubated in humidified tissue incubators (Thermo Scientific) at 37°C and 5% CO_2.

Dynamic light scattering

Polyplex size and zeta potential were measured on a Malvern Zetasizer Nano ZS (Malvern, United Kingdom). For all measurements, polyplexes were diluted 1:100 in Milli-Q water at neutral pH. The reported diameters are the average of three measurements, where each measurement comprises at least 10 acquisitions. The zeta potential was calculated according to the Smoluchowski approximation.

Cell viability

Trypan blue dye exclusion cell counting was performed in triplicate with an automated cell counter (ViCell, Beckman-Coulter). Cell viability under experimental conditions is the viable cell count reported as a percentage relative to untreated cells.

Polyplex formation

Solutions of polymer in RNase-free water were added to 3 μg of pDNA (gWiz-Luciferase; Aldevron, Fargo, ND) at specified loadings. The solutions were then vortexed at 1500 rpm for 3 min at room temperature.

Cell Transfection and Luciferase Expression

HEK-293T cells were seeded on 12-well plates at a density of 50,000 cells per well 24 hours prior to transfection. The media was then evacuated, replaced with fresh media, and supplemented with the polymer-DNA polyplexes. After 48 hours of incubation, cell viability was measured, and cells were re-plated on 96-well plates at a density of 10,000 cells per well and analyzed for luciferase activity according to the manufacturer's protocol. Briefly, 24 hours after seeding, cells were rinsed with PBS and lysed with 20 µL/well 1X Cell Lysis Buffer (Promega, Madison, WI). To the cell lysates was added 100 µL/well of Luciferase Assay Reagent (Promega) and the light produced was quickly read on a plate reader (PerkinElmer, Waltham, MA) for 10 sec per well. Results were expressed as relative light units (RLU) normalized to cell counts, with error bars representing the standard deviation from the triplicate measurement.

Gel Electrophoresis Shift Assay

Polyplexes were prepared at different weight ratios by adding 10 µL of polymer in Milli-Q H_2O to 10 µL of pDNA (5 ng/µL), and vortexing at 1500 rpm for 3 min at room temperature. To the polyplex solution was then added 2 µL of loading dye, for a total volume of 22 µL, which was subsequently added to the well. Agarose gels were prepared as 1 wt% in tris-acetate EDTA (TAE) buffer with 2 µL ethidium bromide and run at 100 V for 20 min. Gels were visualized under UV illumination at 365 nm.

Charge Ratio Calculation:

$$\frac{(3\ \mu g\ pDNA)*(MW\ per\ polymer\ repeat\ unit)}{330\ g\ per\ pDNA\ nucleotide} = Polymer\ mass\ for\ 1{:}1\ charge\ ratio\ with\ pDNA$$

Synthesis

Procedures for the synthesis of 1,2-Bis(dibutylamino)-3-chlorocyclopropenium chloride (BACBu), 2

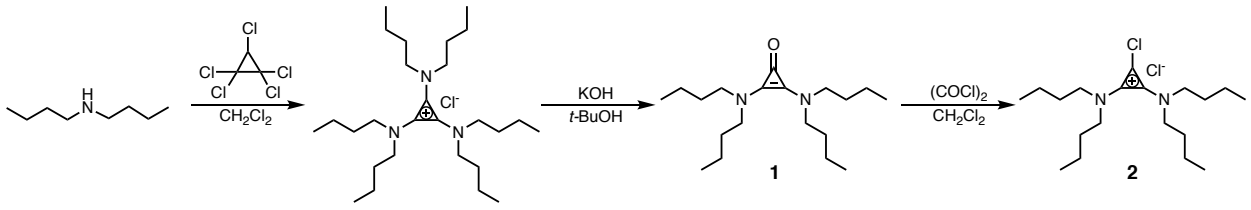

Synthesis of 2,3-Bis(dibutylamino)-1-cyclopropenone, **1**

This procedure was performed at ambient conditions. Dibutylamine (8 equiv) was slowly added to a solution of pentachlorocyclopropane (1 equiv) in CH_2Cl_2 in a round-bottom flask at 0 °C.

The solution turned orange, and was allowed to warm to room temperature with stirring overnight. The reaction mixture was washed 3 x 1 M HCl, 1 x deionized water, and 1 x brine before being dried over magnesium sulfate and concentrated under vacuum to yield a crude orange solid. The solid was dissolved in *tert*-butanol and to this was added 4M potassium hydroxide (aq). The solution was heated at 70 °C for 2 h, and then water was removed by rotary evaporation. The resulting solid was dissolved in CH_2Cl_2 and filtered to remove salt. The organic solution was dried with magnesium sulfate and re-concentrated under vacuum. The crude material was purified by column chromatography (100% EtOAc to 5% MeOH in CH_2Cl_2) to yield the title product as an orange solid (30% two-step yield). ^{1}H NMR (400 MHz, $CDCl_3$): δ 3.16 (t, 8H), 1.59 (m, 8H), 1.34 (m, 8H), 0.94 (t, 12H).

Synthesis of 1,2-Bis(dibutylamino)-3-chlorocyclopropenium chloride (BACBu), **2**
Oxalyl chloride (2 equiv) was slowly added to a solution of **1** (1 equiv) in dry CH_2Cl_2 at 0 °C under argon. The solution was allowed to warm to room temperature as the reaction proceeded for 1 h. The solution was then concentrated under vacuum to yield the title product as a brown liquid in quantitative yield. ^{1}H NMR (400 MHz, $CDCl_3$): δ 3.64 (t, 4H), 3.50 (t, 4H), 1.76 (m, 4H), 1.66 (m, 4H), 1.40 (m, 8H), 0.99 (t, 12H).

Synthesis of PMAS(Bu)

This procedure was performed open to the atmosphere. Poly(methylaminostyrene) (PMAS; DP ~50, 1 equiv amine monomer) was dissolved in $CHCl_3$ in a scintillation vial equipped with a stir bar. To the vial was added *N,N*-diisopropylethylamine (3 equiv) and **2** (1.5 equiv) dissolved in $CHCl_3$. The reaction was stirred at 65 °C for 3 h. The resulting solution was concentrated under vacuum, dissolved in minimal acetone and precipitated once into ethyl acetate at -78 °C. The precipitated powder was dissolved in methanol and transferred to a 3.5k MWCO Spectrum Labs dialysis bag and dialyzed against methanol followed by concentration under vacuum to yield a pale brown powder. ^{1}H NMR (400 MHz, $CDCl_3$): δ 7.18-6.07 (b, 200H), 4.99-4.39 (b, 100H), 3.78-2.91 (b, 575H), 1.98-1.58 (b, 400H), 1.39-1.08 (b, 650H), 1.02-0.63 (b, 600H).

Synthesis of PEI(Bu)

This procedure was performed open to the atmosphere. Linear 25 k poly(ethylenimine) (DP ~581, 1 equiv) was dissolved in $CHCl_3$ in a scintillation vial equipped with a stir bar. To the vial was added *N,N*-diisopropylethylamine (3 equiv) and **2** (1.5 equiv) dissolved in $CHCl_3$. The reaction was stirred at 65 °C for 3 h. The resulting solution was concentrated under vacuum, dissolved in minimal acetone and precipitated once into ethyl acetate at -78 °C. The precipitated powder was dissolved in methanol and transferred to a 3.5k MWCO Spectrum Labs dialysis bag and dialyzed against methanol followed by concentration under vacuum to yield a yellow-brown powder. ^{1}H

NMR (400 MHz, $CDCl_3$): δ 4.45-3.15 (b, 7000H), 1.71-1.55 (b, 3500H), 1.43-1.22 (b, 5400H), 1.00-0.90 (b, 6200H).

Procedures for the synthesis of cyclopropenium brush polymers

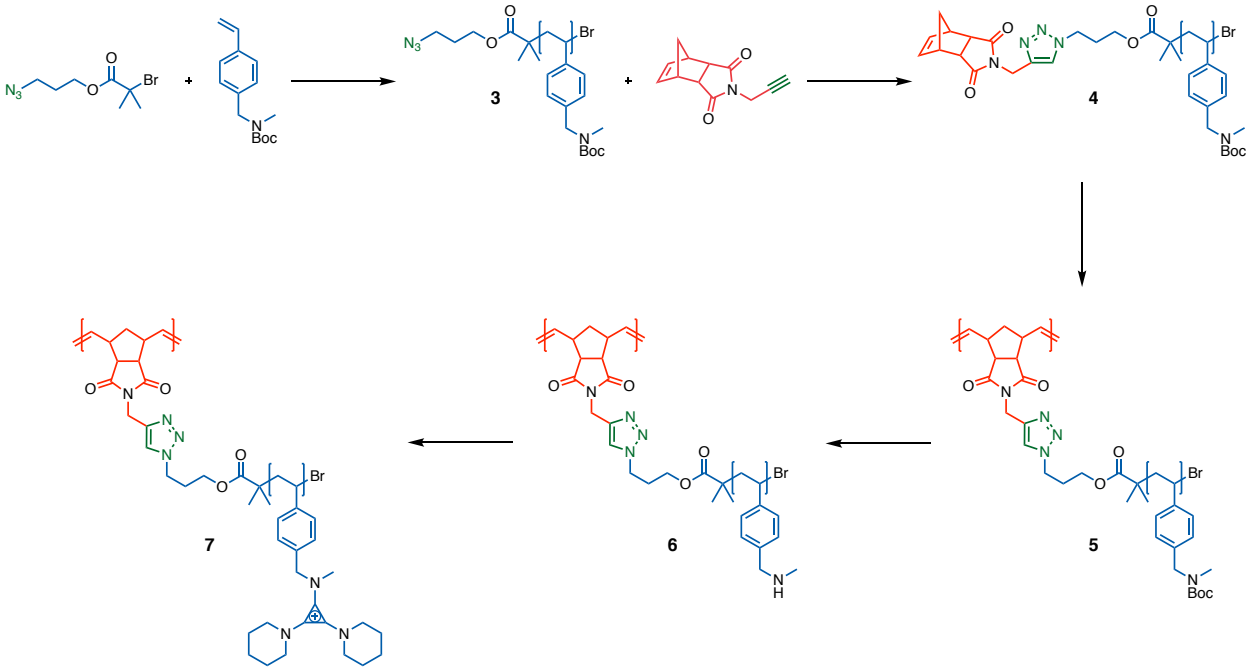

Synthesis of N_3-PBoc, **3**

Copper (I) bromide (0.5 equiv) was added to a dry Schlenk flask equipped with a stir bar and deoxygenated via three vacuum-argon cycles. Degassed *tert*-butyl methyl(4-vinylbenzyl)carbamate (40 equiv) and degassed *N,N,N',N'',N''*-pentamethyldiethylenetriamine (PMDETA; 0.5 equiv) were then added and allowed to stir for ten minutes to form copper complex. The mixture was then subjected to three freeze-pump-thaw cycles. The Schlenk flask was closed under argon and a degassed solution of 3-azidopropyl 2-bromo-2-methylpropanoate (1 equiv) dissolved in anisole was injected. The reaction mixture was heated to 90 °C and allowed to react for 1-2 h before turning viscous. The resulting gel was diluted with THF, purified from copper via an alumina plug and transferred to a 1.0 k MWCO Spectrum Labs dialysis bag and dialyzed against methanol. The purified solution was concentrated under vacuum to yield a white powder. From GPC: M_n = 5,500 $gmol^{-1}$, degree of polymerization ~ 20, Đ ~ 1.06. ^1H NMR (400 MHz, $CDCl_3$): δ 7.18-6.14 (b, 80H), 4.60-4.07 (b, 40H), 3.08-2.49 (b, 60H), 2.04-0.99 (b, 260H). (Figure S7)

Synthesis of NB-PBoc, **4**

Copper (I) bromide (0.5 equiv), **3** (1 equiv), and norbornene propargyl imide (7.5 equiv) and were added to a dry three-neck round bottom flask equipped with a stir bar and reflux condenser. The setup was subjected to three vacuum-argon cycles. Degassed *N,N,N',N'',N''*-pentamethyldiethylenetriamine (PMDETA; 0.5 equiv) in a 0.1 M solution of dry THF was then

transferred to the 3-neck flask under Argon. The reaction mixture was heated to 50 °C and stirred for 24 h. The resulting gel was diluted with THF, purified from copper via an alumina plug and transferred to a 1.0 k MWCO Spectrum Labs dialysis bag and dialyzed against methanol. The purified solution was concentrated under vacuum and dried to yield an off-white powder. ^{1}H NMR (400 MHz, $CDCl_3$): δ 7.50-7.46 (b s, 0.9H), 7.15-6.18 (b, 80H), 6.27 (s, 2H), 4.72 (broad s, 1.8zH), 4.55-4.02 (b, 40H), 3.25 (broad s, 1.8H), 3.00-2.39 (b, 60H), 2.17 (s, 2H), 2.01-1.15 (b, 270H). (Figure S8)

Synthesis of PBoc Brush, **5**

Polymer **4** (50 equiv) was dissolved in dry DMF to a concentration of 0.1 M and degassed with Argon in a reaction vial equipped with a stir bar. A degassed solution of Grubbs' third-generation catalyst (1 equiv) in dry DMF was added to the vial and then stirred at 35 °C for 12-18 h. The crude solution was then transferred to a 10 k MWCO Spectrum Labs dialysis bag and dialyzed against methanol, with 10 solvent exchanges. The purified solution was concentrated under vacuum to yield an off-white powder. From GPC: M_n = 45,000 gmol^{-1} and 5,800 gmol^{-1}, degree of polymerization ~ 8, Đ ~ 1.10. ^{1}H NMR (400 MHz, $CDCl_3$): δ 7.50-7.46 (b s, 0.9H), 7.15-6.18 (b, 80H), 6.27 (s, 2H), 5.75 (d, 0.5H), 5.23 (d, 0.5H), 4.72 (broad s, 1.8zH), 4.55-4.02 (b, 40H), 3.25 (broad s, 1.8H), 3.00-2.39 (b, 60H), 2.17 (s, 2H), 2.01-1.15 (b, 260H). (Figure S9 and S10)

Synthesis of PMAS Brush, **6**

5 (1 equiv boc monomer) was dissolved in a 1:1 mixture of trifluoroacetic acid (1.5 equiv) and dry CH_2Cl_2 and stirred at room temperature for 2 h. The reaction mixture was then concentrated under vacuum and neutralized by slowly adding triethylamine (TEA; 3 equiv) and then stirring for 10 min. This solution was dissolved in CH_2Cl_2 and washed 1 x deionized water and 1 x brine before being dried over magnesium sulfate and concentrated under vacuum to yield a pale brown powder. The NMR has residual TEA. ^{1}H NMR (400 MHz, $CDCl_3$): δ 7.50-7.46 (b s, 0.9H), 7.15-6.18 (b, 80H), 6.27 (s, 2H), 5.62 (broad s, 0.5H), 4.72 (broad s, 1.8zH), 3.92-3.34 (b, 40H), 2.55-2.30 (b, 60H), 2.17 (s, 2H), 1.60-1.16 (b, 55H). (Figure S11)

Synthesis of PMAS(Pep) Brush, **7**

This procedure was performed open to the atmosphere. **6** (1 equiv amine monomer) was dissolved in $CHCl_3$ in a scintillation vial charged with a stir bar. To the vial was added *N,N*-diisopropylethylamine (DIPEA) (3 equiv) followed by a solution of bis-1,2-(piperidino)-3-chlorocyclopropenium chloride (1.5 equiv) in chloroform. The reaction mixture was stirred at 65 °C for 18 h. The resulting solution was concentrated under vacuum, diluted with methanol, and transferred to a 3.5k MWCO Spectrum Labs dialysis bag and dialyzed against methanol. The dialyzed solution was finally concentrated under vacuum to yield a brown powder. The NMR has residual MeOH. ^{1}H NMR (400 MHz, $CDCl_3$): δ 7.22-6.04 (b, 80H), 4.90-4.39 (b, 40H), 3.29-2.96 (b, 60H), 1.96-1.00 (b, 450H). (Figure S12)

Procedures for the synthesis of cyclopropenium star polymers

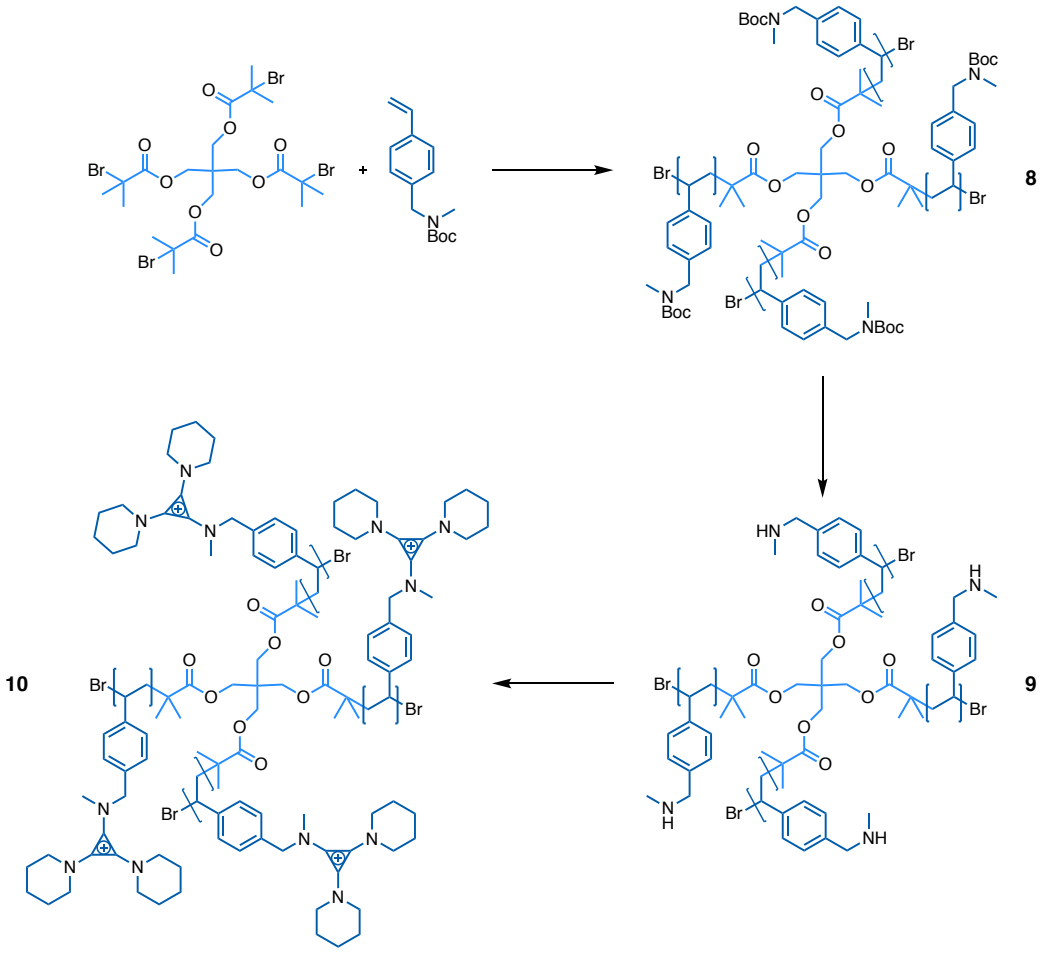

Synthesis of PBoc 4-arm Star, **8**

Copper (I) bromide (0.2 equiv) was added to a dry Schlenk flask equipped with a stir bar and deoxygenated via three vacuum-argon cycles. Degassed *tert*-butyl methyl(4-vinylbenzyl)carbamate (100 equiv) and degassed *N,N,N',N'',N''*-pentamethyldiethylenetriamine (PMDETA; 0.2 equiv) were then added and allowed to stir for ten minutes to form copper complex. The mixture was then subjected to three freeze-pump-thaw cycles. The Schlenk flask was closed under argon and a degassed solution of pentaerythritol tetrakis(2-bromoisobutyrate) (1 equiv) dissolved in anisole was injected. The reaction mixture was heated to 90 °C and allowed to react for 12 h before turning viscous. The resulting gel was diluted with CH_2Cl_2, purified from copper via an alumina plug and transferred to a 1.0 k MWCO Spectrum Labs dialysis bag and dialyzed against methanol. The purified solution was concentrated under vacuum to yield a white powder. From GPC: M_n = 4,900 $gmol^{-1}$, degree of polymerization ~ 20,

Đ ~ 1.05. ^{1}H NMR (400 MHz, $CDCl_3$): δ 7.20-6.12 (b, 80H), 4.55-4.05 (b, 40H), 3.01-2.47 (b, 60H), 2.31-1.10 (b, 265H). (Figure S13)

Synthesis of PMAS 4-arm Star, **9**

8 (1 equiv boc monomer) was dissolved in a 1:1 mixture of trifluoroacetic acid (1.5 equiv) and dry CH_2Cl_2 and stirred at room temperature for 2 h. The reaction mixture was then concentrated under vacuum and neutralized by slowly adding triethylamine (TEA; 3 equiv) and then stirring for 10 min. This solution was dissolved in CH_2Cl_2 and washed 1 x deionized water and 1 x brine before being dried over magnesium sulfate and concentrated under vacuum to yield a pale brown powder. The NMR has residual TEA and MeOH. ^{1}H NMR (400 MHz, $CDCl_3$): δ 7.23-6.23 (b, 80H), 3.80-3.50 (b, 40H), 2.50-2.22 (b, 60H), 1.59-1.12 (b, 58H). (Figure S14)

Synthesis of PMAS(Pep) 4-arm Star, **10**

This procedure was performed open to the atmosphere. **9** (1 equiv amine monomer) was dissolved in $CHCl_3$ in a scintillation vial charged with a stir bar. To the vial was added *N,N*-diisopropylethylamine (DIPEA) (3 equiv) followed by a solution of bis-1,2-(piperidino)-3-chlorocyclopropenium chloride (1.5 equiv) in chloroform. The reaction mixture was stirred at 65 °C for 6 h. The resulting solution was concentrated under vacuum, diluted with methanol, and transferred to a 3.5k MWCO Spectrum Labs dialysis bag and dialyzed against methanol. The dialyzed solution was finally concentrated under vacuum to yield a brown powder. The NMR has residual MeOH and H_2O. ^{1}H NMR (400 MHz, $CDCl_3$): δ 7.29-6.29 (b, 80H), 4.83-4.44 (b, 40H), 3.26-2.95 (b, 65H), 1.45-0.85 (b, 600H). (Figure S15)

Supplementary Tables and Figures

Table S1. Characterization of highest performing transfection agents and polyplexes at optimal transfection efficacy

Transfection agent	MM[a] (kDa)	Charge ratio[b]	D_H (nm)	ζ potential (mV)
PEI	25	50:1	490 ± 60	40 ± 10
PEI(Pep)	166	8:1	425 ± 100	65 ± 5
PEI(Mo)	164	20:1	400 ± 110	60 ± 6
PMAS(Pep)	53	5.5:1	140 ± 60	27 ± 8
PMAS(Mo)	53	5.5:1	215 ± 25	43 ± 6

[a] Molecular mass of transfection agent, calculated based on commercial 25 k linear PEI; for PMAS(R) materials, PMAS was measured by GPC calibrated using polystyrene standards of

narrow dispersity, then calculated for the corresponding TAC group. [b] Ratio of either N to phosphate anions (PEI) or TAC to phosphate anions (all others).

Table S2. Characterization of butyl- and isopropyl-derived transfection agents and polyplexes at optimal transfection efficacy.

Transfection agent	**MM[a] (kDa)**	**Charge ratio[b]**	**D_H (nm)**	**ζ potential (mV)**
PEI(Bu)	215	6:1	110 ± 40	45 ± 7
PEI(iP)	180	35:1	100 ± 40	58 ± 5
PMAS(Bu)	25	12:1	150 ± 50	31 ± 8
PMAS(iP)	21	5:1	160 ± 40	44 ± 6

[a] Molecular mass of transfection agent, calculated based on commercial 25 k linear PEI; for PMAS(R) materials, PMAS was measured by GPC calibrated using polystyrene standards of narrow dispersity, then calculated for the corresponding TAC group. [b] Ratio of TAC to phosphate anions.

Table S3. Polymer loading and pDNA weight ratios for gel electrophoresis and transfection experiments

Transfection [µg][a]	2.5	5	10	20	50	100
Gel [ng][b]	42	83	167	333	835	1665
Weight Ratio[c]	**0.83:1**	**1.66:1**	**3.33:1**	**6.66:1**	**16.7:1**	**33.3:1**

[a] Mass of polymer added for biocompatibility and transfection experiments. [b] Mass of polymer added for gel electrophoresis shift assay. [c] Weight ratio is given as polymer:pDNA.

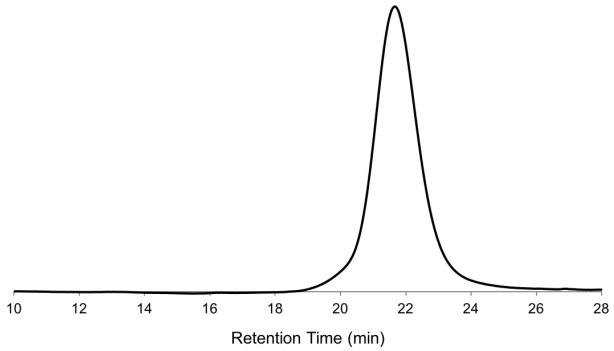

Figure S1. GPC trace of poly(methylaminostyrene), the parent polymer for all PMAS derived transfection reagents.

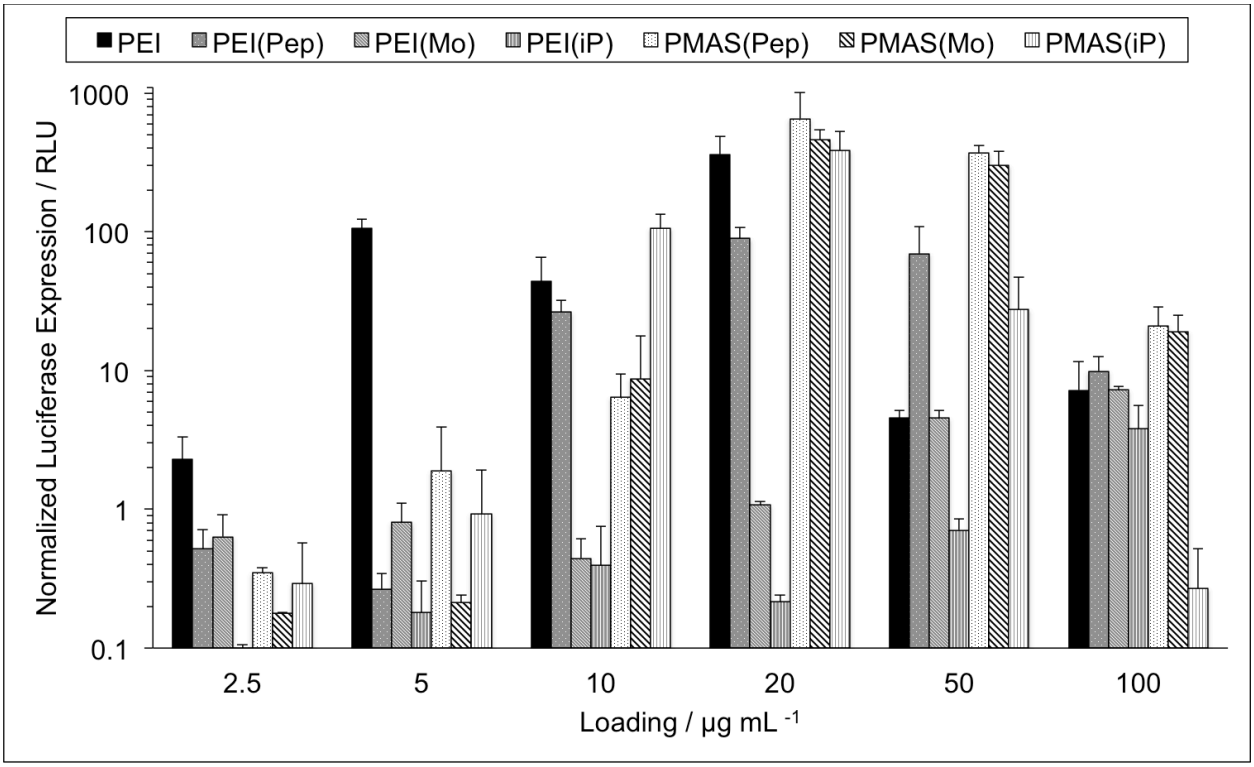

Figure S2. Luciferase expression in HEK-293T cells transfected with pDNA containing the firefly luciferase reporter gene using TAC polymers and 25 k linear PEI. Luciferase expression is measured after 48 h incubation with specified polymer loadings (all with pDNA loadings of 3 µg mL^{-1}) and normalized by cell count. Error bars show the standard deviation of triplicate measurements.

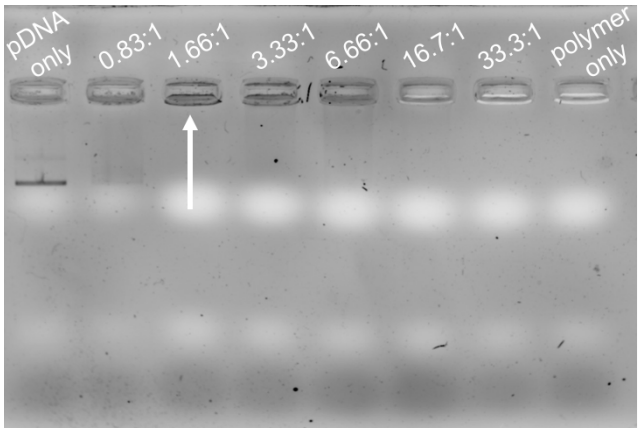

Figure S3. Gel electrophoresis shift assay of pDNA polyplexes formed with PMAS(Bu) at the indicated polymer:pDNA weight ratios. All pDNA is bound in polyplexes at a weight ratio of 1.66 PMAS(Bu): 1 pDNA.

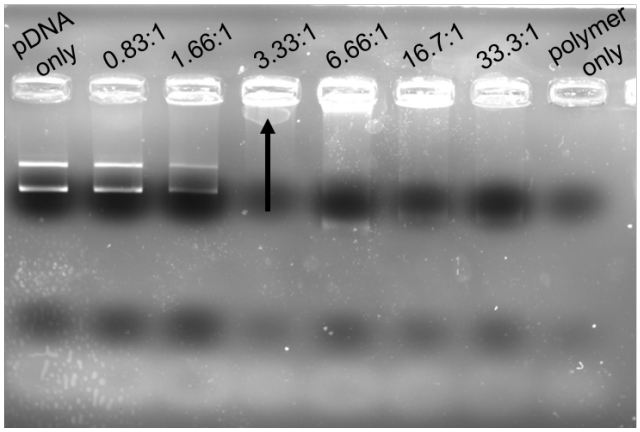

Figure S4. Gel electrophoresis shift assay of pDNA polyplexes formed with PEI(Bu) at the indicated polymer:pDNA weight ratios. All pDNA is bound in polyplexes at a weight ratio of 3.33 PEI(Bu): 1 pDNA.

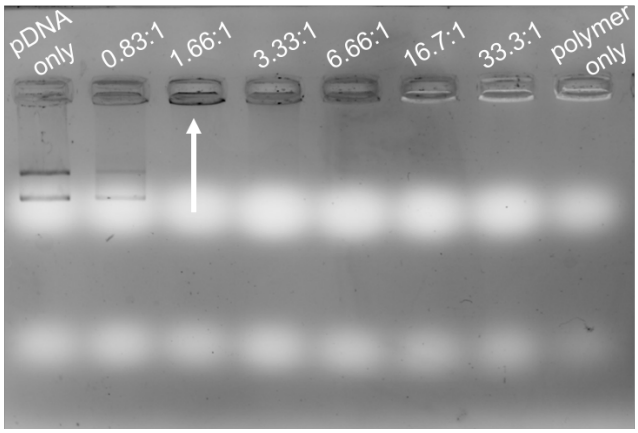

Figure S5. Gel electrophoresis shift assay of pDNA polyplexes formed with PMAS(iP) at the indicated polymer:pDNA weight ratios. All pDNA is bound in polyplexes at a weight ratio of 1.66 PMAS(iP): 1 pDNA.

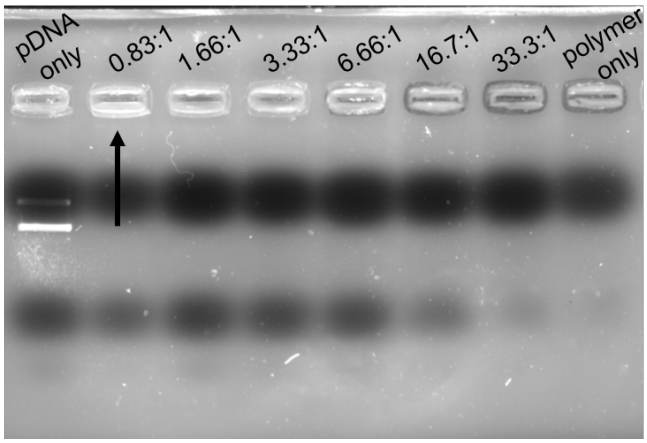

Figure S6. Gel electrophoresis shift assay of pDNA polyplexes formed with PEI(iP) at the indicated polymer:pDNA weight ratios. All pDNA is bound in polyplexes at a weight ratio of 0.83 PEI(iP): 1 pDNA.

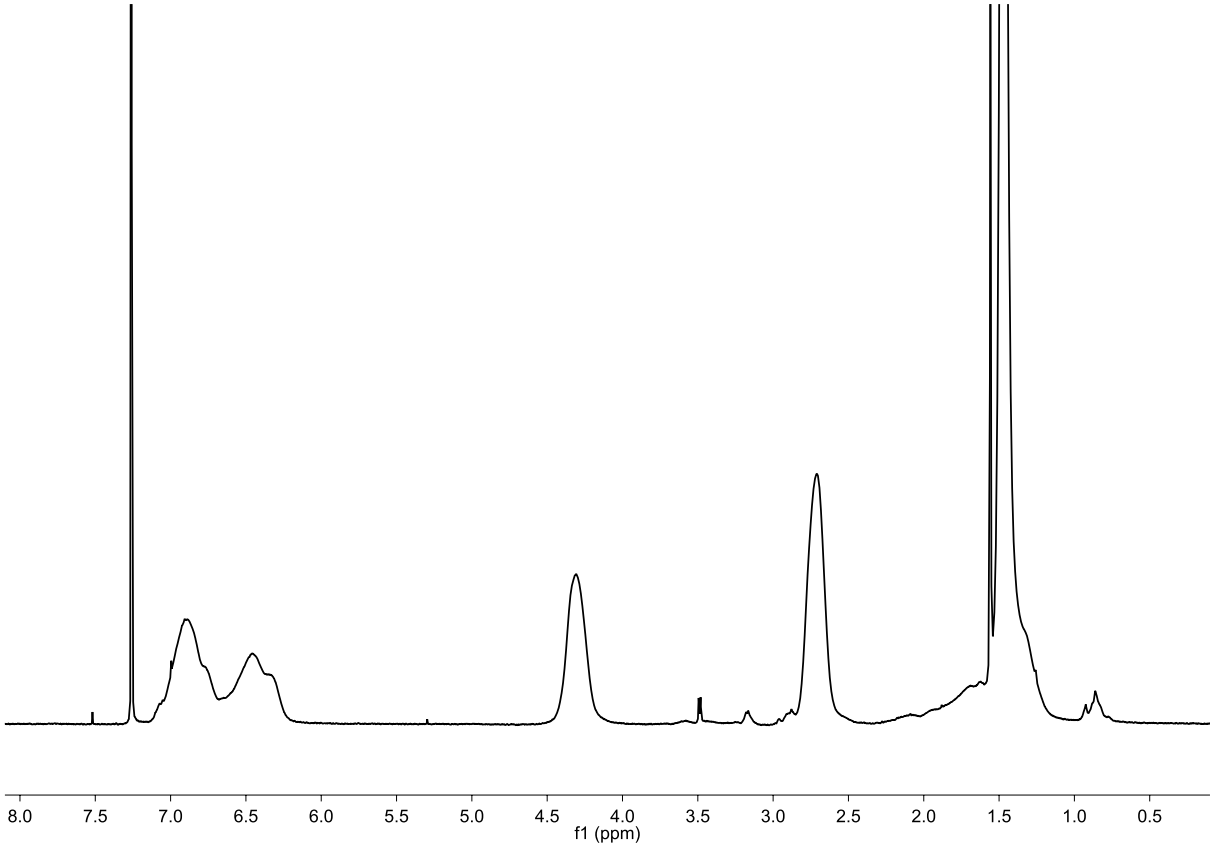

Figure S7. ^{1}H NMR spectrum of N_3-PBoc **3**

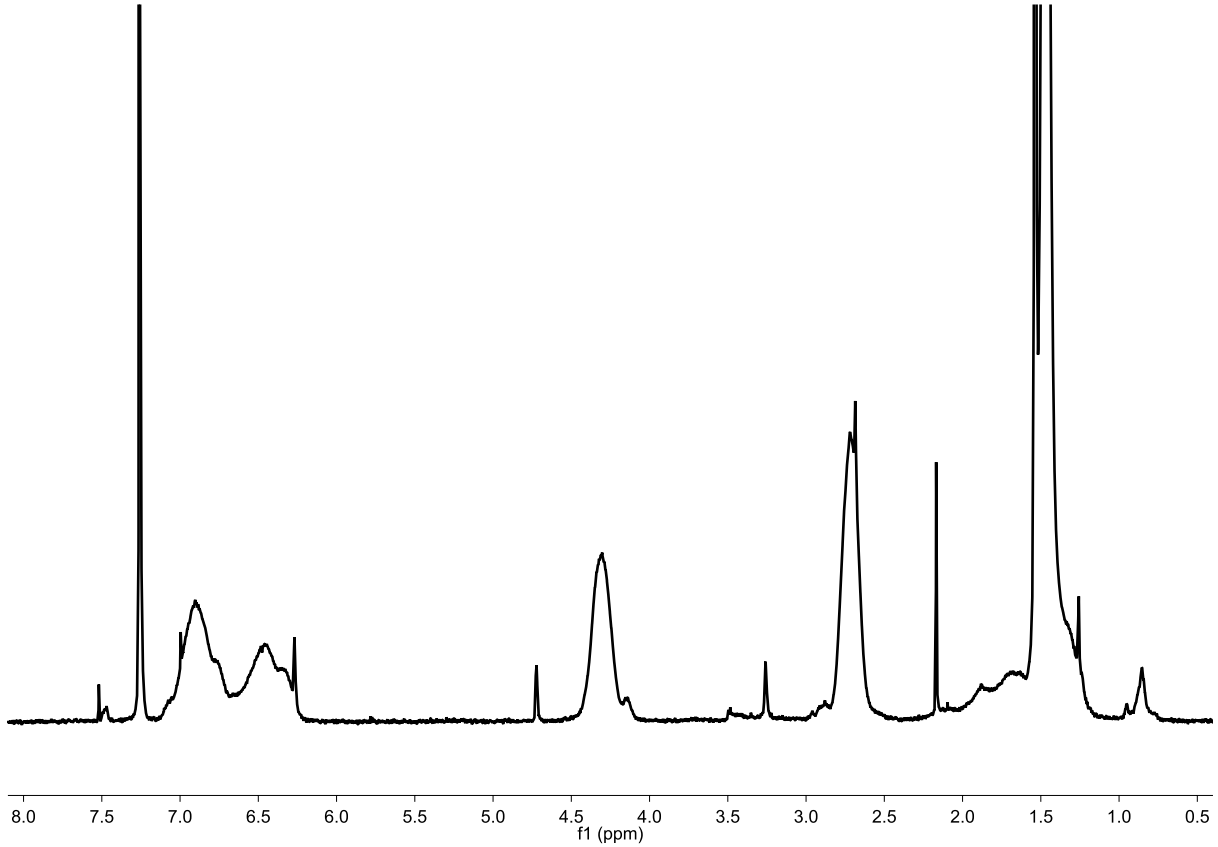

Figure S8. ^{1}H NMR spectrum of NB-PBoc **4**

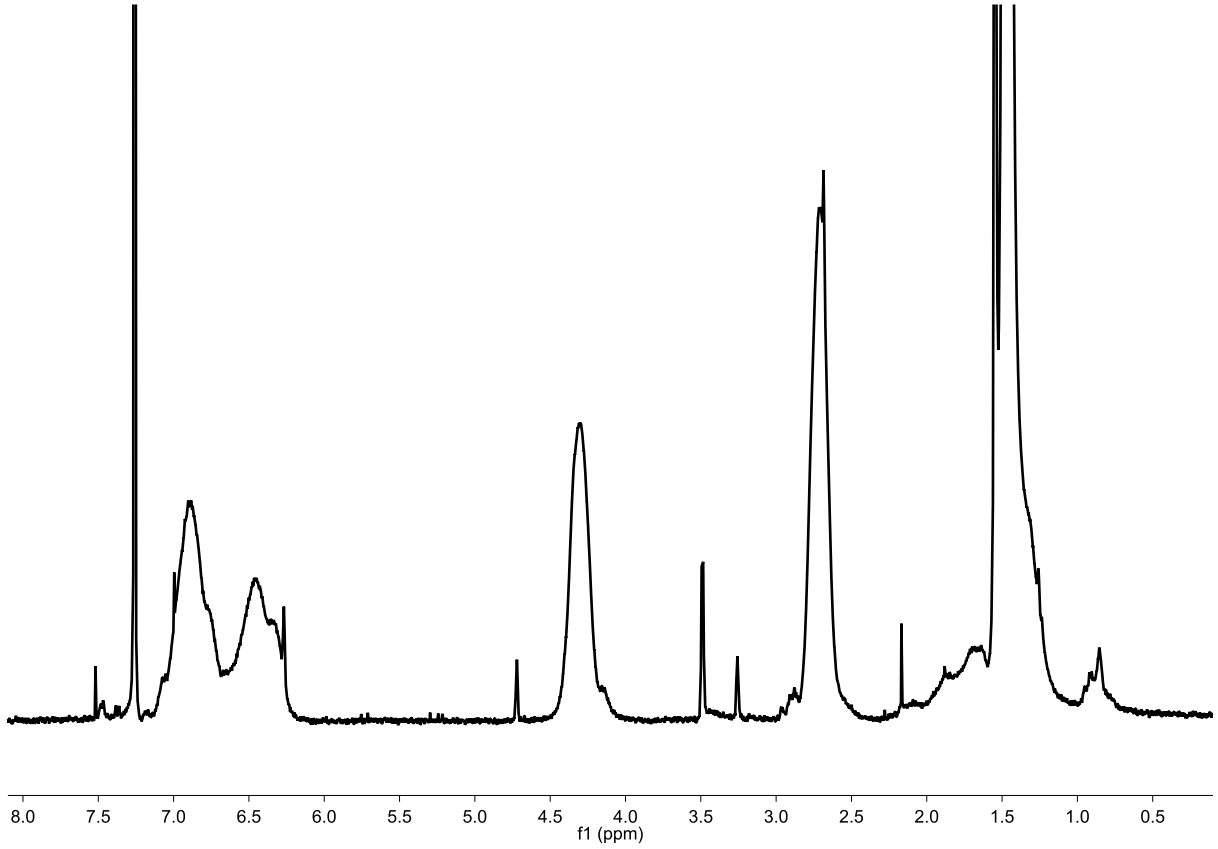

Figure S9. ^{1}H NMR spectrum of PBoc Brush **5**

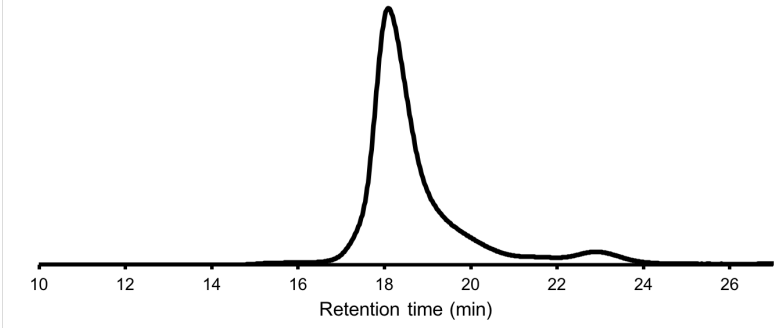

Figure S10. GPC trace of dialyzed PBoc Brush **5** showing both brush (18 min) and unreacted macromonomer (23 min) absorbances.

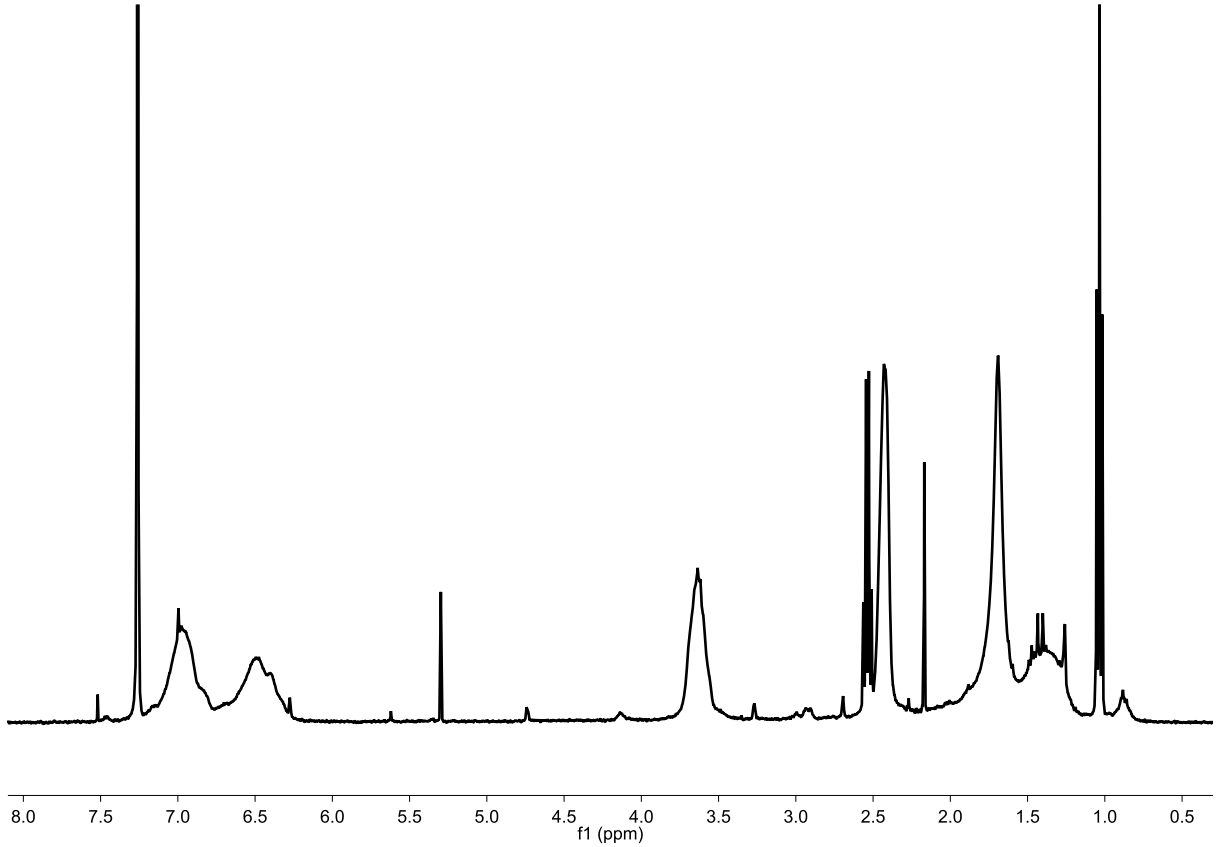

Figure S11. ^{1}H NMR spectrum of PMAS Brush **6**

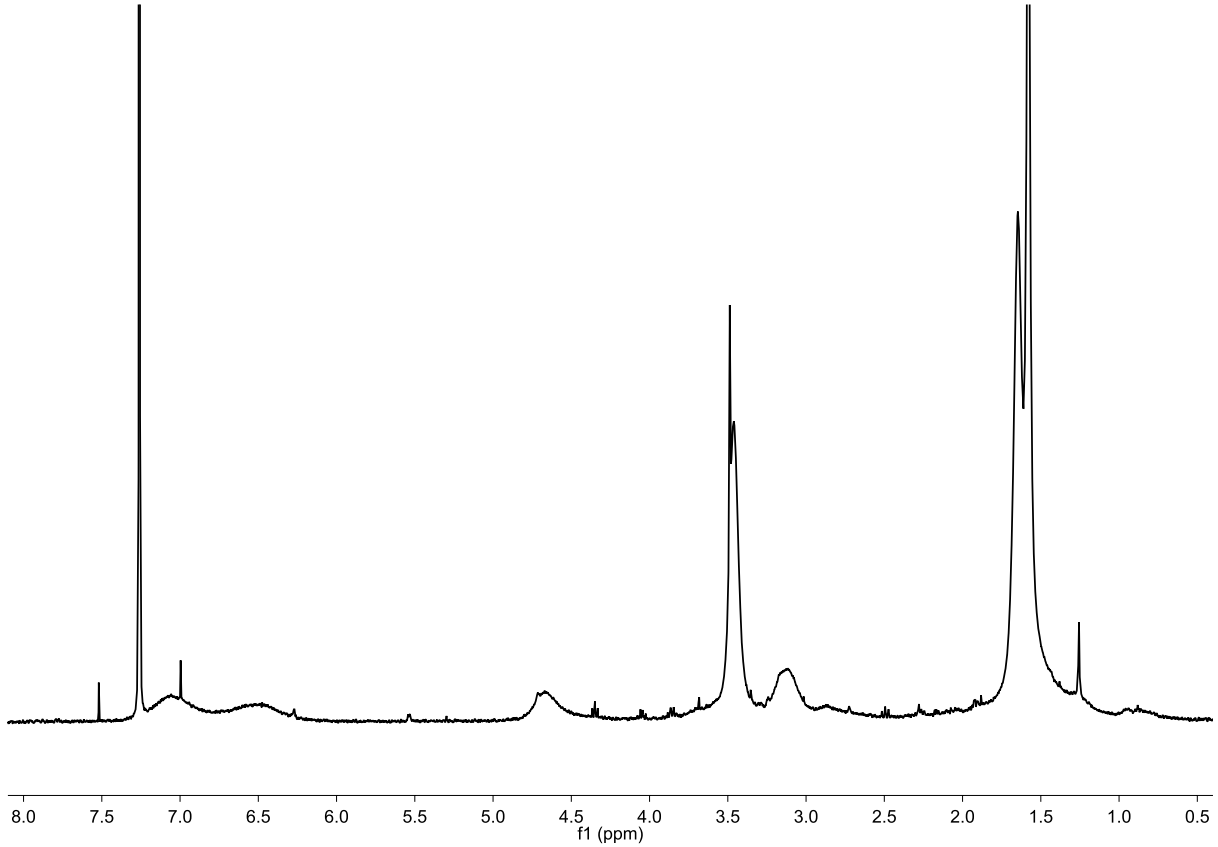

Figure S12. ^{1}H NMR spectrum of PMAS(Pep) Brush **7**

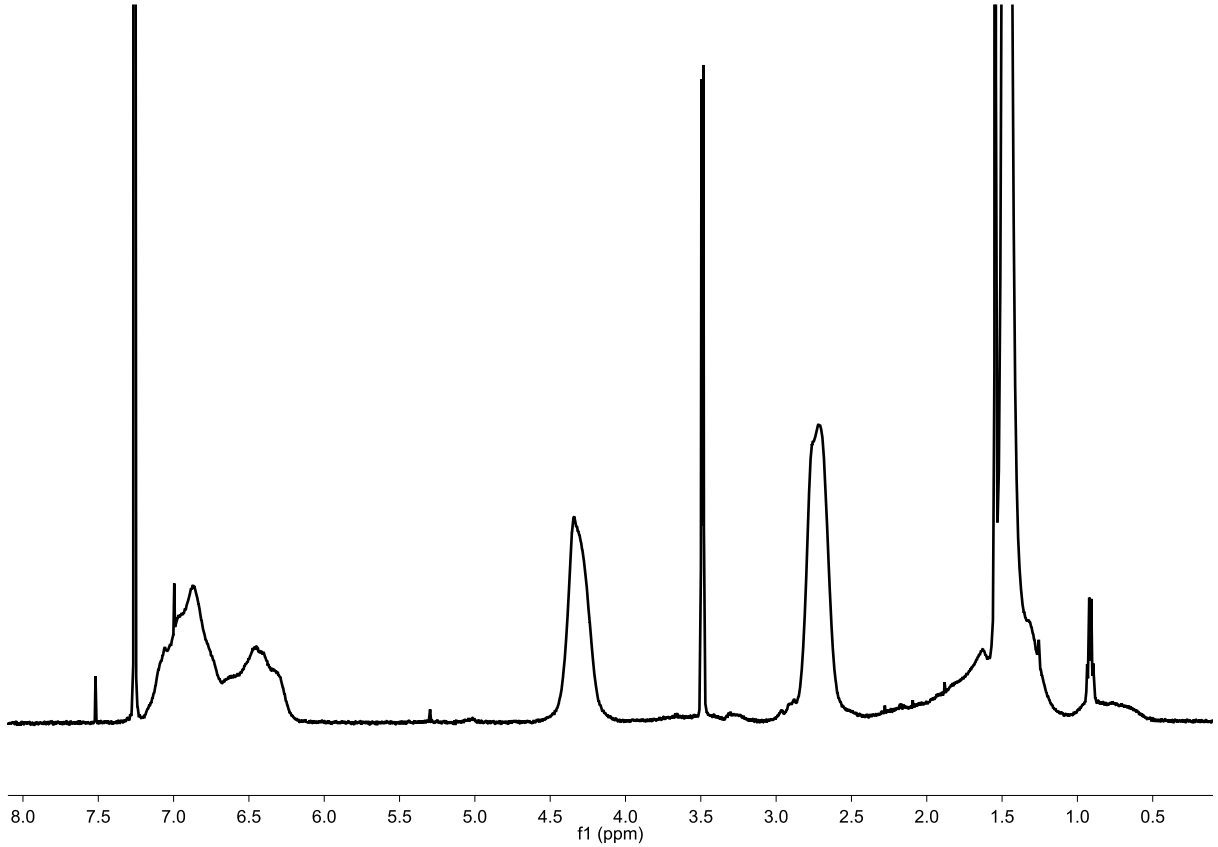

Figure S13. ^{1}H NMR spectrum of PBoc 4-arm Star **8**

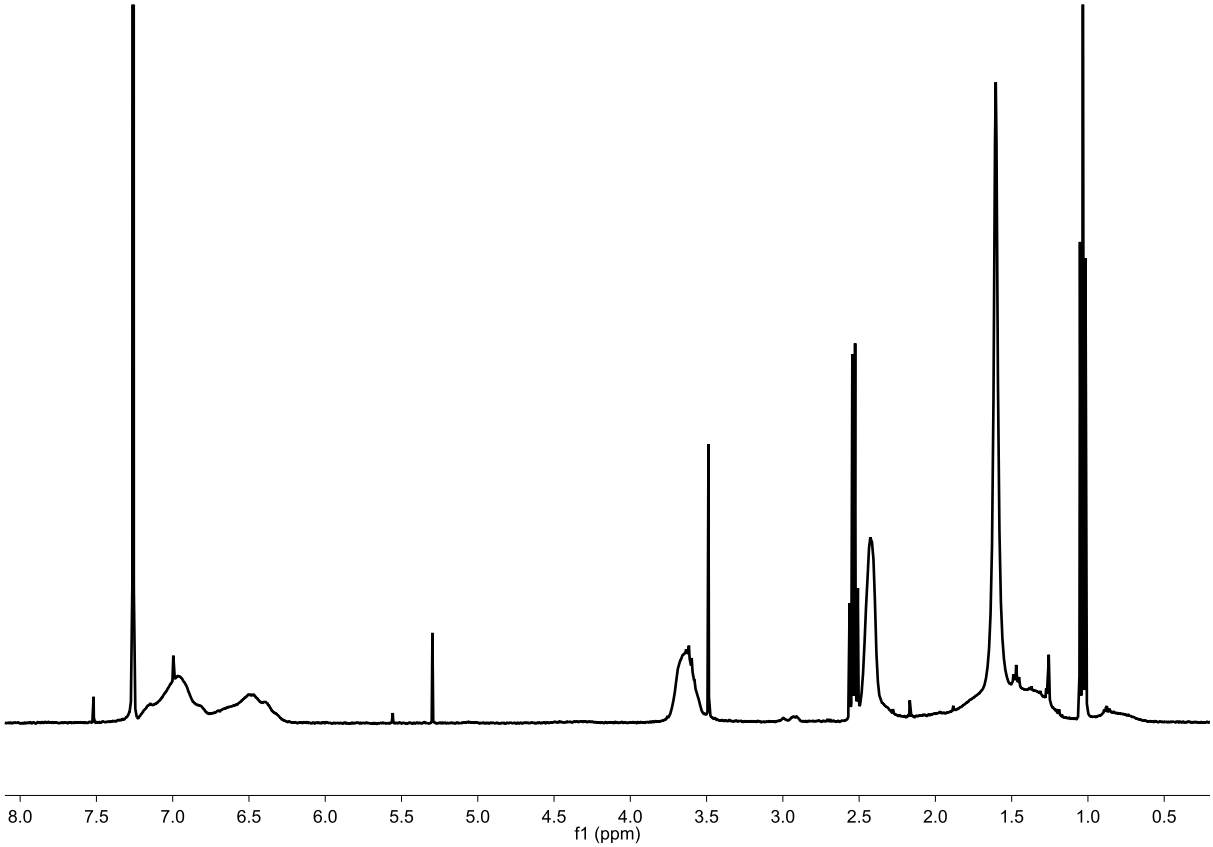

Figure S14. ^{1}H NMR spectrum of PMAS 4-arm Star **9**

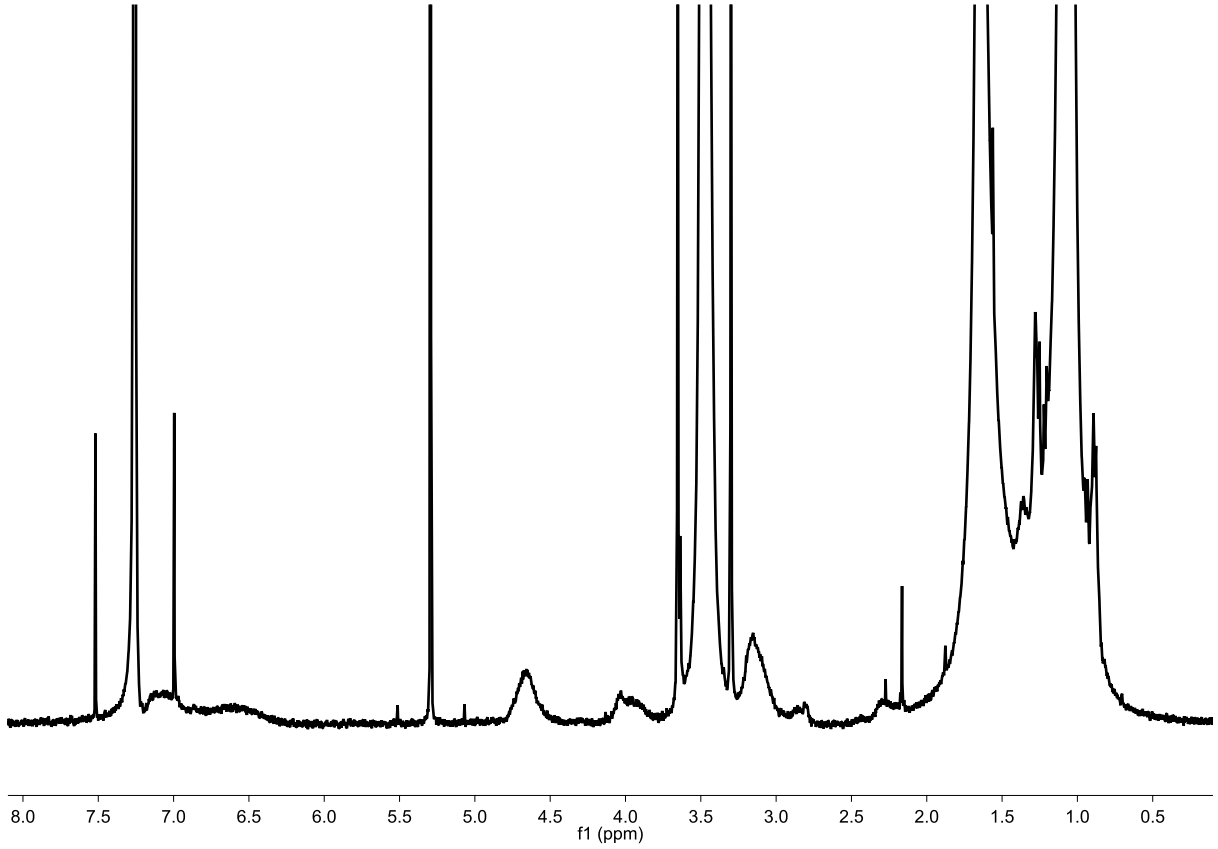

Figure S15. ^{1}H NMR spectrum of PMAS(Pep) 4-arm Star **10**

PART TWO:

BRINGING CYCLOPROPENIUM TO LIGHT

CYCLOPROPENIUM NANOPARTICLES FOR LIVE-CELL IMAGING

[This section is based on the publication *Chem. Commun.* **2017**, *53*, 6187]

Nanomaterials that offer precise localization and can be readily imaged have found great utility as contrast agents in biological and medical research.[1–3] In this part, a novel nanoparticle-based imaging strategy is introduced that couples biocompatible cyclopropenium nanoparticles and stimulated Raman scattering (SRS) microscopy. We thus transition from cyclopropenium as the functional moiety binding nucleic acids in a polymer, to cyclopropenium serving as the framework of a nanoparticle-based image contrast agent.

Recently, metal nanoparticles, quantum dots (Q-dots), and carbon-based materials have become attractive platforms for bioimaging.[4,5] Q-dots exhibit narrow light emission and high quantum yields that enable multiplexing, and metal nanoparticles offer precise shape tunability. However, these systems have been shown to be less than ideal in biological applications due to inherent limitations, including cytotoxicity from metal ion leaching, elaborate surface processing to maintain stability in fluctuating environments, and small scale syntheses with batch variability.[6,7] Alternatively, carbon-based materials such as graphene,[8] carbon nanotubes,[9] and nanodiamonds[10] have been developed as contrast agents in live-cell imaging, but they require precise control of chemical composition for reproducibility.[11]

Different from metal- or carbon-based materials, metal-free polymer nanoparticles have great potential in bioimaging and theranostics because of their modular chemical functionality.[12,13] Unfortunately, most polymeric nanoparticles rely on fluorescence reporting, and hence are limited by the intrinsic photophysics of fluorophores,[14] including self-quenching, broad emission, and photobleaching of organic dyes. Further compromising widespread use of polymer-based materials is the synthesis of complex architectures, such as those described in part one, including

bottle-brushes, star-shaped nanoparticles, and hollow nanomaterials.[12] Therefore, it is imperative to explore beyond conventional imaging agents and techniques. Developing a biocompatible platform of all-polymer nanoparticles that can be readily synthesized and optically imaged in live cells could significantly impact biotechnological and diagnostic applications.

Stimulated Raman scattering (SRS) is an emerging non-linear vibrational imaging technique that can overcome many limitations of fluorescence imaging and other metal-based nanoparticle imaging techniques.[15–18] Compared to conventional spontaneous Raman imaging, SRS provides 10^8 enhancement in excitation efficiency and over 1000-fold improvement in imaging speed through stimulated emission of vibrational transitions by an additional Stokes laser beam.[19,20] SRS is intrinsically free from photobleaching and blinking, and does not rely on metallic nanostructures for localized plasmonic enhancement such as in surface enhanced Raman scattering. In addition, the use of picosecond near-infrared lasers permits narrow-band detection of sharp vibrational peaks and deep tissue penetration with reduced phototoxicity. Vibrational labelling has recently been coupled with SRS microscopy as a powerful technique for bioorthogonal chemical imaging of small bio-molecules in live cells and tissues.[21–24] Thus far, SRS has been limited to small molecule probes, which must be custom-designed to be water-soluble, non-cytotoxic, and detectable under high dilution for live-cell imaging.

Functional synthetic latex nanoparticles represent a modular platform to generalize SRS imaging probes. Miniemulsion polymerization is a facile synthetic method that has been shown to reproducibly yield large-scale quantities of polymer nanoparticles with narrow size distribution.[25] Here, we show how the chemistry of the prototypical nanoparticle can be exploited to develop a new family of latexes for multiplexed live-cell imaging by SRS (**Figure 1**). Formation of the latex is enabled by a functional surfactant that is covalently incorporated through the hydrophobic

styrene moiety, while displaying the hydrophilic head group on the surface of the spherical nanoparticle.[26] The hydrophilic group is composed of the soft, highly delocalized trisaminocyclopropenium (TAC) cation that affords a positive surface charge and resistance to flocculation across a wide range of pH values.[27] Importantly, the hydrophobic polymer core is readily obtained through the radical polymerization of styrene and its derivatives. Introducing characteristic chemical bonds as vibrational tags onto the styrene monomer allows high labelling efficiency and enables SRS imaging with high sensitivity and specificity. We refer to this new family of polymer latexes as Raman-active polymer dots.

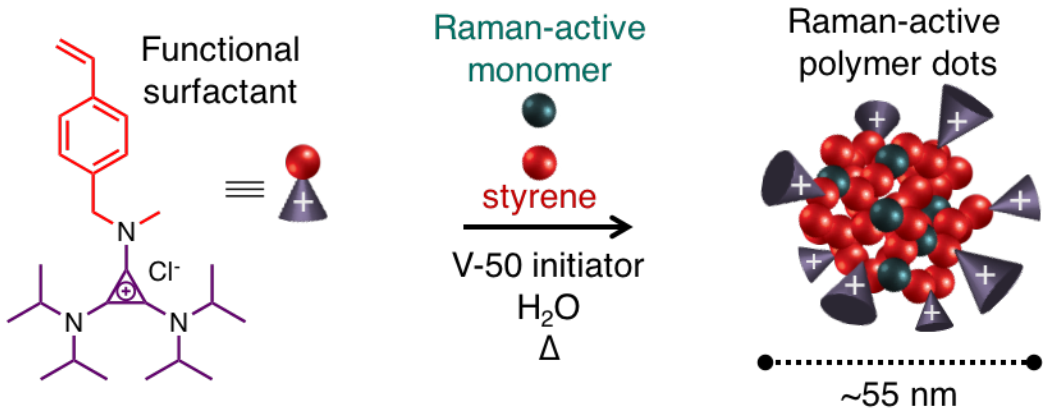

Figure 1. Schematic formulation of the latex: miniemulsion polymerization of Raman-active polymer dots.

A key attractive feature of the Raman-active polymer dots is their facile synthesis. The parent oil-in-water emulsion is obtained by adding a 95:5 *w*:*w* ratio of styrene monomer to TAC surfactant in water. A stable latex is obtained by radical polymerization using V-50, a thermally activated water-soluble initiator, and heating to 70 °C, followed by a 24 hour dialysis to remove unreacted monomer. The use of styrene provides a rich palette to decorate the aromatic unit with various vibrational tags for Raman imaging, without disturbing the size distribution of the latex. Using styrene derivatives with tiny vibrational labels to dope the emulsion furnished a library of Raman-active polymer dots (**Figure 2**). The uniform dot size can be varied from 30-100 nm by

changing the ratio of monomer to surfactant (**SI Table 1 and SI Figures 1-3**), with nearly 10^5 vibrational labels incorporated in each polymer dot.

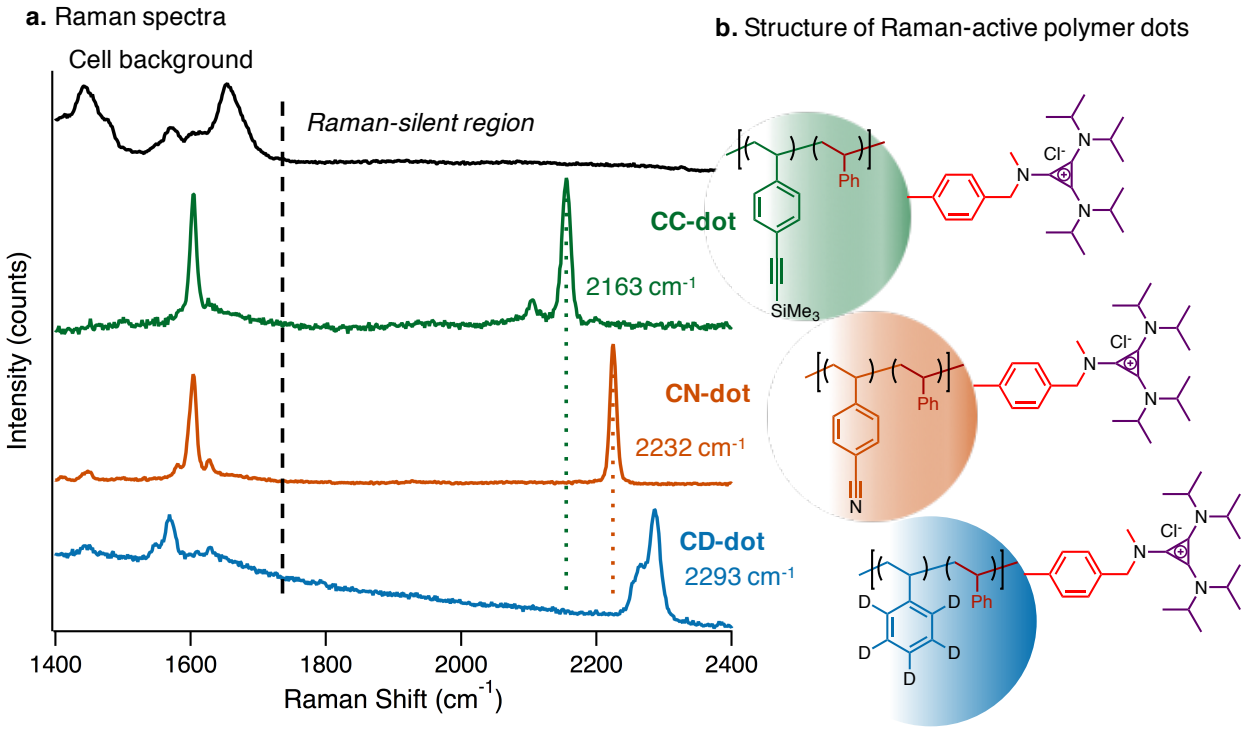

Figure 2. Spontaneous Raman spectra and structure of three distinct Raman-active polymer dots. (a) Spontaneous Raman spectra of nanoparticles with orthogonal vibrational modes of alkyne, nitrile, and carbon-deuterium bonds in the cell Raman-silent region (from 1740 to 2800 cm^{-1}). The intensity is scaled based on the peaks in the Raman-silent region. (b) Schematic structure of three Raman-active polymer dots with the core comprising styrene and styrenic derivatives and the surface coated with trisaminocyclopropenium (TAC) groups.

Alkyne, nitrile, and carbon-deuterium bonds (C-D) were chosen as bioorthogonal vibrational tags since they all exhibit characteristic and mutually resolvable peaks with narrow bandwidth (<2 nm) in the Raman region where cells possess minimal endogenous vibrations (referred to as the cell Raman-silent region, 1740-2800 cm^{-1}, **Figure 2** and **SI Figure 4**).[28] Both the alkyne and nitrile bonds were conjugated with the phenyl ring of styrene for enhanced Raman cross sections.[28] A trimethylsilane-protecting group was employed to further improve the alkyne signal strength while maintaining its frequency (2163 cm^{-1}, CC-dot) well separated from that of

the nitrile (2232 cm^{-1}, CN-dot).[29] Additionally, use of d_5-styrene fully separates the frequency (2293 cm^{-1}, CD-dot) from the nitrile vibration, compared to d_8-styrene that exhibits a broad spectrum due to the backbone C-D vibrations.[30]

We next studied the cellular behavior of Raman-active polymer dots as contrast agents in live-cell imaging. The latexes were synthesized without the use of any organic solvents or extra surface modification enabling their rapid application into cells. Live HeLa cells were separately incubated with CC-dots, CN-dots, or CD-dots, and we found that all Raman-active polymer dots efficiently entered the cells within 2 hours and accumulated mainly in vesicular structures near the cell nucleus (**Figure 3**). Imaging at the characteristic frequencies of alkyne (2163 cm^{-1}), nitrile (2232 cm^{-1}), and C-D (2293 cm^{-1}), cells incubated with the corresponding Raman-active nanoparticles show exclusive SRS signal with high signal to noise ratio (S/N >5, at 30 μs time constant) in the specific on-resonance channel (the colors in all images are pseudo-colors we assigned to each frequency). Thus, the three Raman-active polymer nanoparticles were found to be spectrally orthogonal in live cells with negligible cross-talk, allowing high fidelity multiplexed imaging without the need of spectral unmixing.

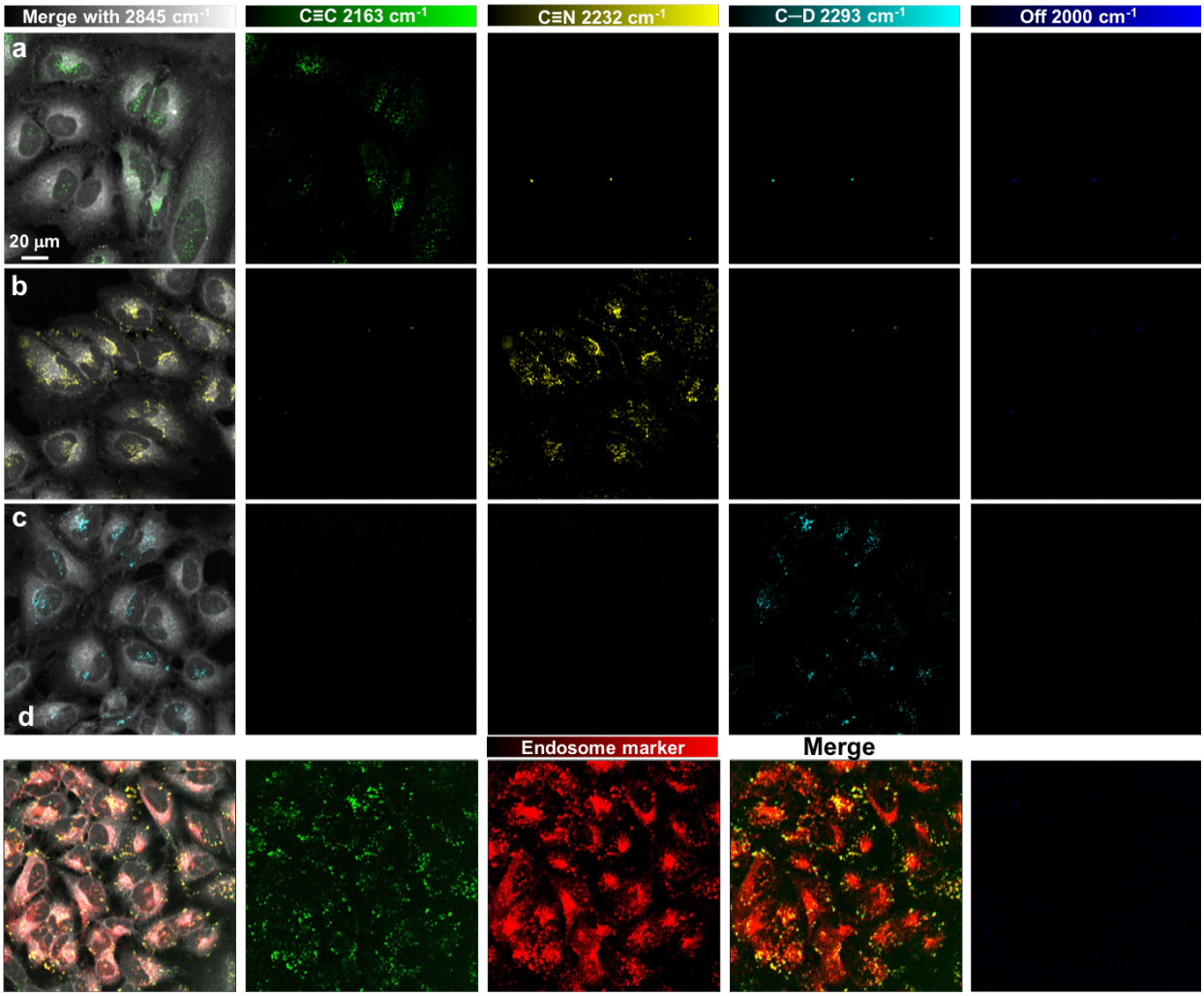

Figure 3. SRS imaging of Raman-active polymer dots entry in live HeLa cells. HeLa cells are incubated with the (a) CC-dot (b) CN-dot, and (c) CD-dot. Each Raman-active polymer dot shows its distinct frequency without cross-talk in cells. The images at 2845 cm^{-1} are lipid CH_2 channels showing cell morphology. (d) CC-dots highly co-localize with endosome marker in live HeLa cells, suggesting endocytic entry.

To determine the intracellular locations of polymer nanoparticles, the endosomes were co-stained in live HeLa cells with transferrin Texas Red conjugate. The correlative SRS and fluorescence imaging revealed high spatial co-localization between the Raman-active nanoparticle puncta in the SRS channel and the endosome marker in the fluorescence channel, suggesting the cellular entry of nanoparticles through endocytosis (**Figure 3d**).[31] Incubating HeLa cells with nanoparticles at 4 °C fully suppressed their cellular entry, further supporting the endocytic mechanism of entry (**SI Figure 5**).[31]

Time-dependent cellular entry kinetics were also characterized for all three Raman-active polymer dots. In as short as 1 hour, observable quantities of nanoparticles were found inside the cells, indicating fast entry kinetics,[2] likely due to the positive charge of cyclopropenium on the nanoparticle surface. This is in agreement with other studies showing positively-charged surfaces and nanoparticle sizes of ~50 nm to be ideal for rapid cellular uptake.[2] After 4 hours of incubation, significant amounts of nanoparticles are enriched in the endosomes surrounding the cell nucleus (**SI Figure 6**). Thus, the three Raman-active polymer dots were found to behave similarly with rapid entry via endocytosis within an hour, highlighting the fact that doping the styrene latexes with different vibrational labels does not introduce variability in their interaction with live cells.

Unlike fluorescent polymer nanoparticles that require electronic excitation, Raman scattering is based on chemical bond vibration, which is intrinsically free from photobleaching, blinking, and self-quenching. Thus, Raman-active polymer nanoparticles were expected to exhibit excellent photo-stability for long-term imaging. Indeed, by continuously imaging the nanoparticles in live HeLa cells for 100 frames (2.7 seconds per frame), we found minimal reduction in intensity (**Figure 4a**) and that the strong signal is stable, without bleaching or blinking, after nearly 300 seconds of continuous laser illumination, as shown quantitatively by the steady intensity time traces at three dense areas of puncta (**Figure 4b,c**). Compared to other imaging contrast agents which typically show fluorescence intermittency or rapid decay, Raman-active polymer dots display high photo-stability under SRS microscopy and are exceptionally well suited for tracking applications in live cells for long periods of time.

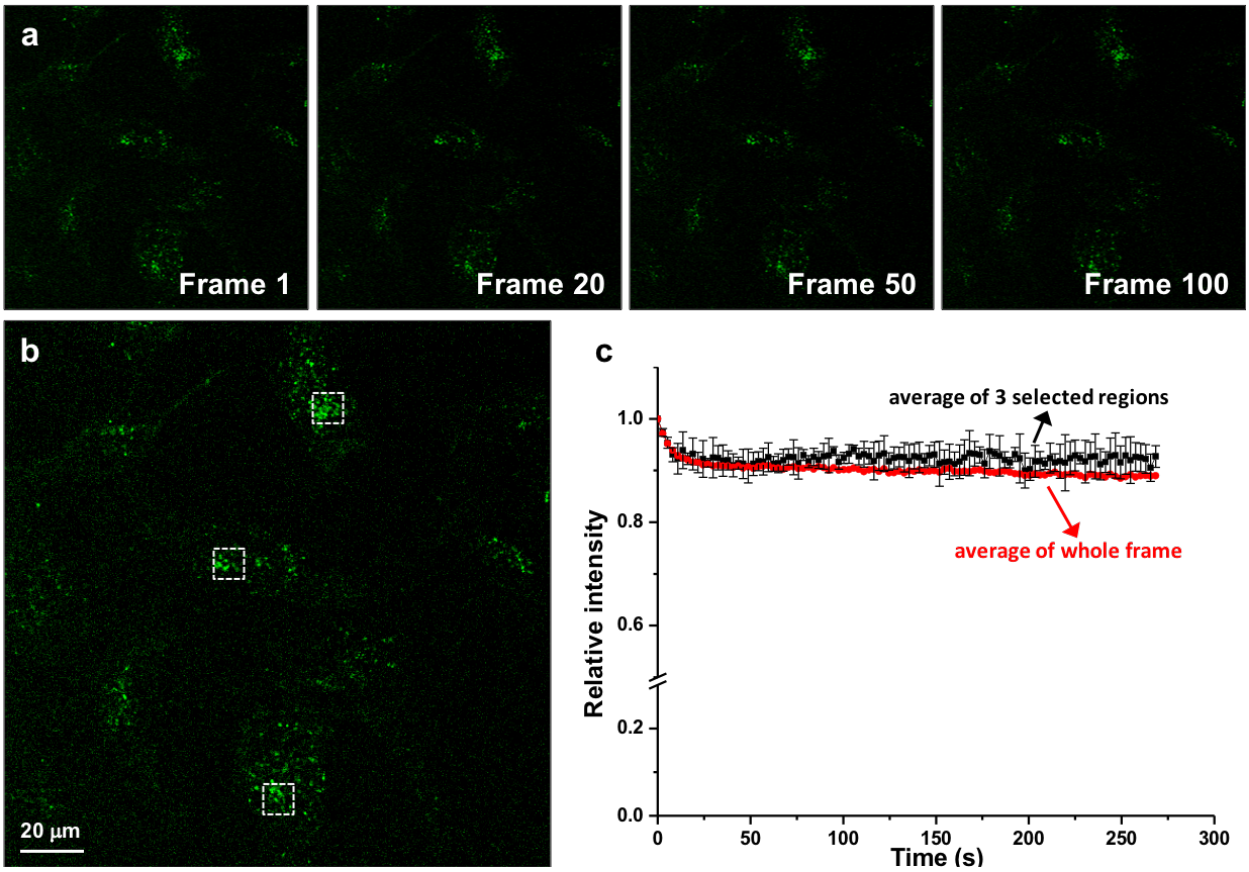

Figure 4. High photo-stability of Raman-active polymer dots in live cells. (a) SRS imaging of CC-dots in HeLa cells. Representative frames (1, 20, 50, and 100) are shown to display little change in intensity. (b,c) Intensity quantification of SRS images of Raman-active polymer dots in HeLa cells. Steady intensity traces of both the whole frame and 3 selected regions (white boxes) demonstrate high photo-stability of Raman-active polymer dots after 100 continuous frames.

To demonstrate the broad applicability of Raman-active polymer dots in live-cell imaging, we tested their cellular entry capacity and biocompatibility in five cell lines. In addition to HeLa, two other cancerous cell lines were evaluated (human breast cancer cells MCF-7 and human fibrosarcoma cells HT1080), as well as two non-cancerous cell lines (monkey kidney fibroblast-like cells COS-7 and mouse embryonic fibroblasts MEF). Incubated with the alkyne-labelled polymer dots, all four additional cell lines were efficiently labelled within 2 hours with strong accumulation of the Raman-active dots inside the cells (**SI Figure 7**). Furthermore, cytotoxicity assays showed all five cell lines (COS-7, MEF, MCF-7, HT1080, and HeLa) have greater than 85% (some even more than 95%) viability with all three Raman-active dots after 48 hour culture

(**SI Figure 8**). The biocompatible chemical composition of our organic nanoparticles should be responsible for such negligible cytotoxicity. By contrast, Q-dots without surface coating display acute toxicity at similar loadings.[32] These data demonstrate that Raman-active polymer dots exhibit minimal toxicity in all cell lines tested and would be widely applicable as imaging agents across a broad range of cells.

The ability to quickly identify cell type in a multicomponent system will allow fast readout of information in many applications such as cell screening or monitoring long-term spatial migration. As the three-color Raman-active polymer dots exhibit high detection orthogonality and biocompatibility across multiple cell lines, we employed them for multiplexed live-cell sorting in co-culture by SRS microscopy. Each cell type was "color-coded" by incubation with one specific Raman-active polymer dot (alkyne for COS-7, nitrile for MEF, and C-D for HeLa cells) after which the three cell types were mixed and cultured together.

After co-culture of 4 and 24 hours, cells could be unambiguously identified by their polymer dot labelling (**Figure 5**). In both cases, cells were indistinguishable by simple morphology inspection or by label-free SRS imaging of the lipid CH_2 vibration (2845 cm^{-1}). However, by imaging through the unique frequencies of alkyne, nitrile, and C-D, every cell in the frame can be rapidly and singularly identified by the color-coding of the Raman-active polymer dots. By merging all three channels together with the lipid CH_2 image, not only the identity of the cell type, but also the spatial location of each cell in a co-culture can be clearly mapped out. This demonstrates multi-color Raman-active polymer dots as promising live-cell multiplexed imaging agents.

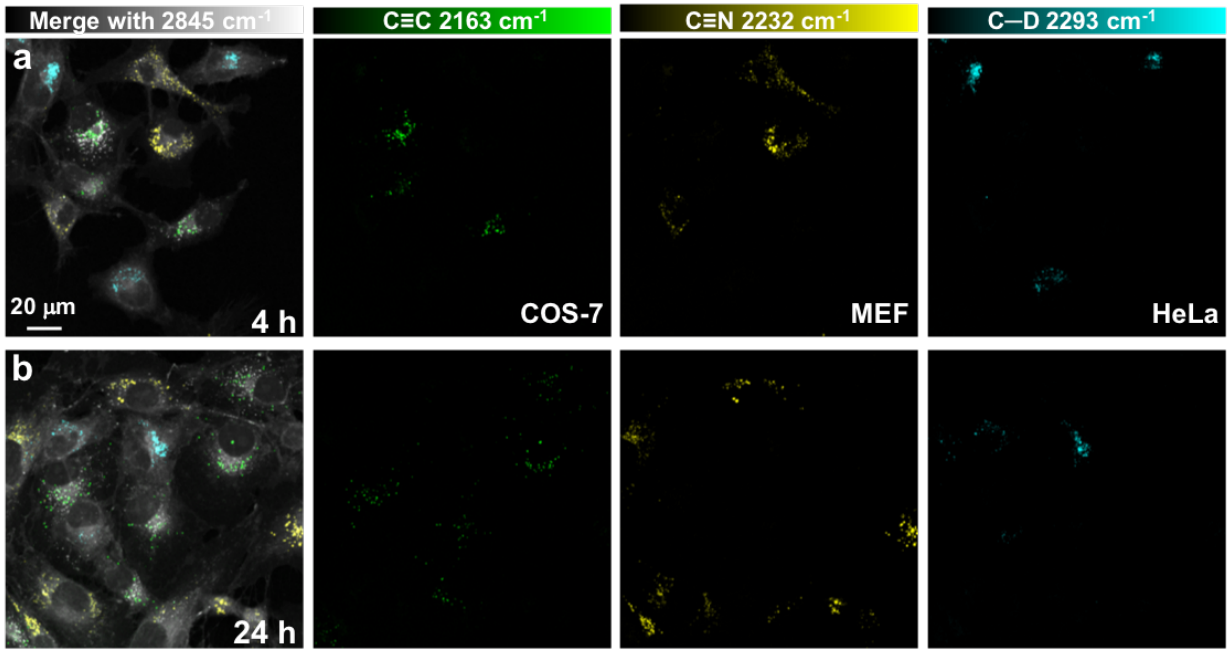

Figure 5. Multiplexed live-cell sorting in co-culture of three cell lines. Each cell line is color-coded with specific Raman-active polymer dots (CC-dot for COS-7, CN-dot for MEF, and CD-dot for HeLa) before being mixed in the co-culture. Cell types are unambiguously identified by 3-color polymer dots with multiplexed SRS imaging after 4 hours (a) and 24 hours (b).

We thus have developed a new strategy to image organic polymeric nanoparticles via stimulated Raman scattering that is free from the use of fluorescent dyes or metals. Characteristic chemical bonds of minimal size and orthogonal vibrational modes with narrow bandwidth were rationally designed and incorporated into organic polymer nanoparticles in a robust one-step synthesis. The nanoparticles were shown to have rapid cellular entry kinetics and high biocompatibility across a broad range of cell lines. We achieved near-infrared multi-color SRS imaging of these materials in live cells demonstrating high sensitivity, specificity, and photo-stability. We further applied this technology in multiplexed live-cell sorting with unambiguous identification of cell types in co-culture with fast readout. The multiplexing capability can be further expanded by precisely tuning the vibrational frequencies of the alkyne and nitrile through isotope editing,[33] and efforts to target these nanoparticles towards specific cell types are discussed in the next section. Addressing the previous issues of cytotoxicity, photo-stability, and synthetic

robustness for nanoparticle-based imaging reagents, we anticipate that multiplexed Raman-active polymer dots coupled with SRS microscopy will be an important technology in nanoparticle-based live-cell imaging for biotechnology and theranostic applications.

DESIGN OF TARGETABLE NANOPARTICLES FOR PRECISION TREATMENT

Advances in nanomedicine and diagnostics rely on the specific targeting of nanoparticles to cells and tissues of interest. Nanomaterials that can carry both therapeutic and imaging agents for diagnostic and treatment applications are of the highest interest for theranostic purposes. As most organic nanoparticles do not have sufficient contrast for long-term imaging they have predominantly been relegated to strictly therapeutic delivery agents.[34,35] However, our Raman-active polymer dots overcome this limitation as they possess an intrinsic contrast mechanism based on specific molecular vibrations positioning them as a promising theranostic platform.

Whereas in the previous section our Raman-active polymer dots were artificially targeted through incubation with a specific cell line before mixing, we sought a platform where our materials could be endowed with precise targeting moieties. Currently available theranostic technologies are mostly reliant on passive targeting of disease sites, such as the enhanced permeability and retention effect, where nanoparticles slowly accumulate over time in the leaky vasculature of tumor tissue. This mode of targeting is limited to cancerous and inflammatory tissue and the key parameter is circulation time. As such, nanoparticles are engineered to have stealth surface modifications and appropriate size to prevent non-specific binding and excretion.[36,37] Instead, we desired a modular platform for active targeting, where disease- and cell-specific targeting ligands could be functionalized onto the nanoparticle surface. The dominant targeting ligands are antibodies and other proteins that have high specificity for antigens or cell-membrane based receptors. Molecular-level recognition of diseased tissues has the potential to reduce non-specific off-target effects by promoting precise accumulation at the diseased site.[34,35,38,39] Thus, active targeting where we could functionalize specific proteins onto the surface of nanoparticles was our next goal in the development of Raman-active polymer dots.

We first endeavored to modulate our prototypical nanoparticle synthesis. Just as styrene provided a platform to decorate the aromatic unit with various vibrational tags for Raman imaging, we hoped to exploit the chemistry of the cyclopropenium cation to install functional handles. As cyclopropenium formed the hydrophilic component of our surfactant, tuning the amino substituents would lead to surface-level modifications on the nanoparticle. We specifically studied functional groups that could be employed downstream in robust click chemistry to targeting ligands, namely, azido, propargyl, and allyl moieties (**Figure 6**). Azides or alkynes could be specifically linked with the corresponding functional group on a targeting ligand via CuAAC click chemistry. Similarly, allyl groups could be employed in precise thiol-ene coupling with reactive cysteine residues in a protein.[40,41]

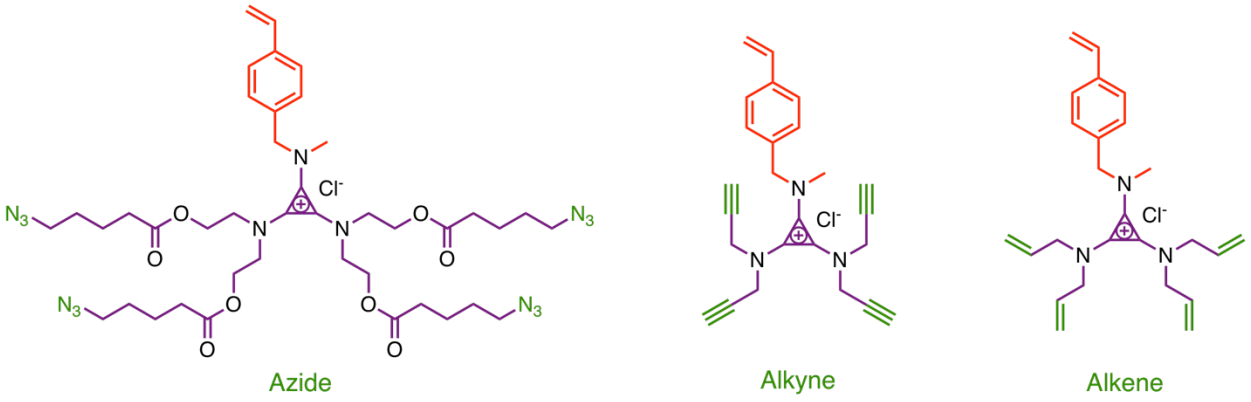

Figure 6. Attempted molecular structures for targeted nanoparticles include incorporation of azide, alkyne, or alkene functional groups.

Unfortunately, none of these proposed structures yielded stable nanoparticles. Neither the azido nor propargyl amines were able to be transformed into a corresponding BACCl derivative necessary for functionalization onto the methylaminostyrene polymerizable group (**Figure 7a,b**). We suspect this was due to off-target effects during the harsh hydrolysis conditions necessary to form the cyclopropenone. Thus, for these derivatives we were unable to synthesize a polymerizable monomer. In the case of the allyl derivative, the functionalization onto cyclopropenium and methylaminostyrene was smooth, but we were never able to isolate stable well-defined

nanoparticles (**Figure 7c**). This can most likely be attributed to the high degree of crosslinking available in these monomers, with five vinyl groups present per monomer. These unsuccessful synthetic efforts thus established a limit to the modularity of cyclopropenium chemistry and suggested that a different approach was necessary for the design of targetable Raman-active polymer dots.

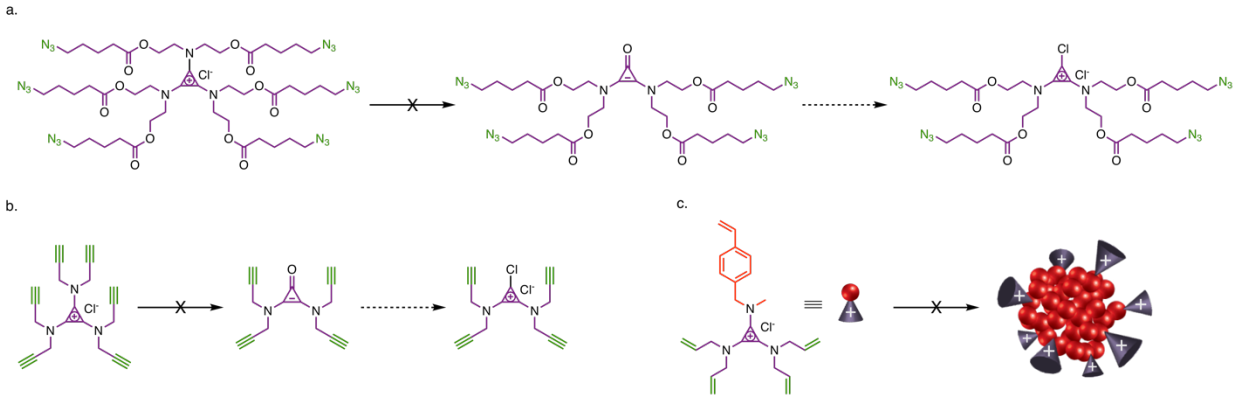

Figure 7. Unsuccessful synthetic efforts in the design of functional cyclopropenium derivatives. Azido (a) and propargyl (b) amines could not be transformed into the necessary cyclopropenone nor bisaminocyclopropenium chloride derivatives. Polymerization of allyl amines (c) did not yield stable nanoparticles.

We were ultimately able to synthesize targetable nanoparticles through a reengineering of the nanoparticle design. Rather than employing our polymerizable monomer as the surfactant, we designed an amphiphilic block copolymer comprising styrene and cyclopropenium-based blocks. Utilizing a block copolymer framework permitted chain-end functionalization with a functional handle of interest. We selected an NHS ester moiety due to its specific reactivity with primary amines, commonly found either on the N-terminus of proteins or in lysine residues, to afford stable amide bonds.[40] Rationally designing the block copolymer such that the NHS ester was on the hydrophilic (i.e. cyclopropenium) end, ensured it would be present on the nanoparticle surface (**Figure 8**). Treating this end-functionalized block copolymer as a surfactant for miniemulsion polymerizations permits the incorporation of fluorescent dyes or tiny vibrational labels as co-

monomers. Subsequent functionalization with a protein of interest affords a surface-decorated nanoparticle comprising cyclopropenium with imaging modalities in the hydrophobic core.

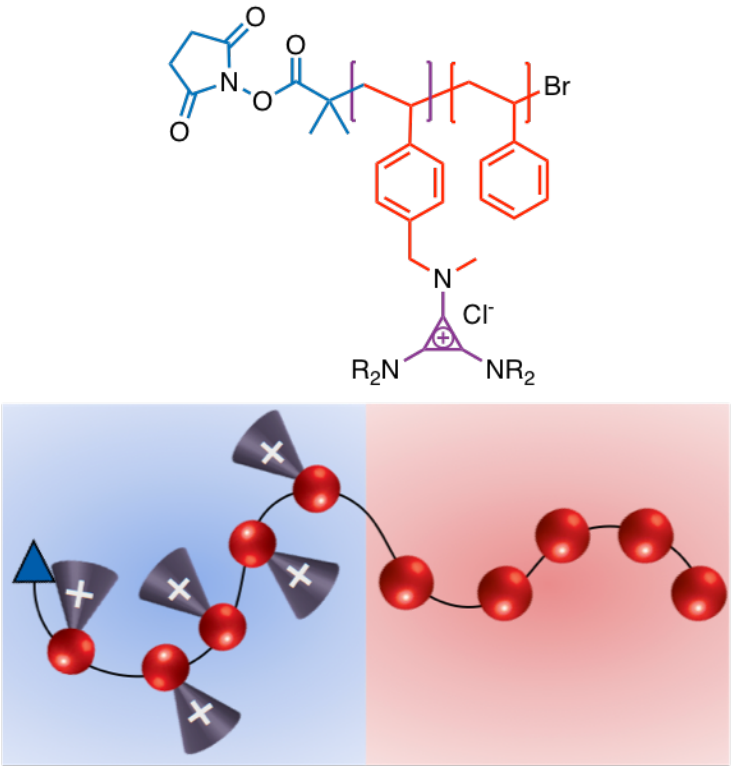

Figure 8. Chemical structure and graphical representation of NHS ester terminated block copolymer employed as surfactant for targetable nanoparticles.

We prepared this NHS ester-terminated block copolymer as a variant of our established post-polymerization functionalization chemistry described in the introduction (**Figure 9 and SI Figures 9-12**). Starting with a heterofunctional NHS ester ATRP initiator, we polymerized an N-Boc protected methylaminostyrene monomer, which yields polymers with controllable molecular mass and narrow dispersity. This homopolymer was then employed as a macroinitiator for the polymerization of styrene. Though the Boc-protected monomer is deactivating, slowing the rate of styrene polymerization, the order of these reactions is essential. The NHS ester ends up on the Boc-terminus, which we derivatize to form the hydrophilic cyclopropenium. This functionalization is accomplished in two steps: the Boc group is deprotected to yield the free secondary amine and

then this amine is quantitatively converted to a cyclopropenium ring through addition of a BACCl salt. We chose to use the piperidine derivative (BAC(Pep)) due to its high biocompatibility as demonstrated in part one. This functionalized block copolymer, denoted NHS-PMAS(Pep)-PS, was then employed in the standard nanoparticle reaction to afford nanoparticles with a styrenic core and cyclopropenium-based corona with pendent NHS ester moieties. Modulating the emulsion polymerization to incorporate either fluorescent dyes or vibrational labels afforded NHS-ester coated nanoparticles that could be imaged by either fluorescence or SRS microscopy (**SI Table 2**).

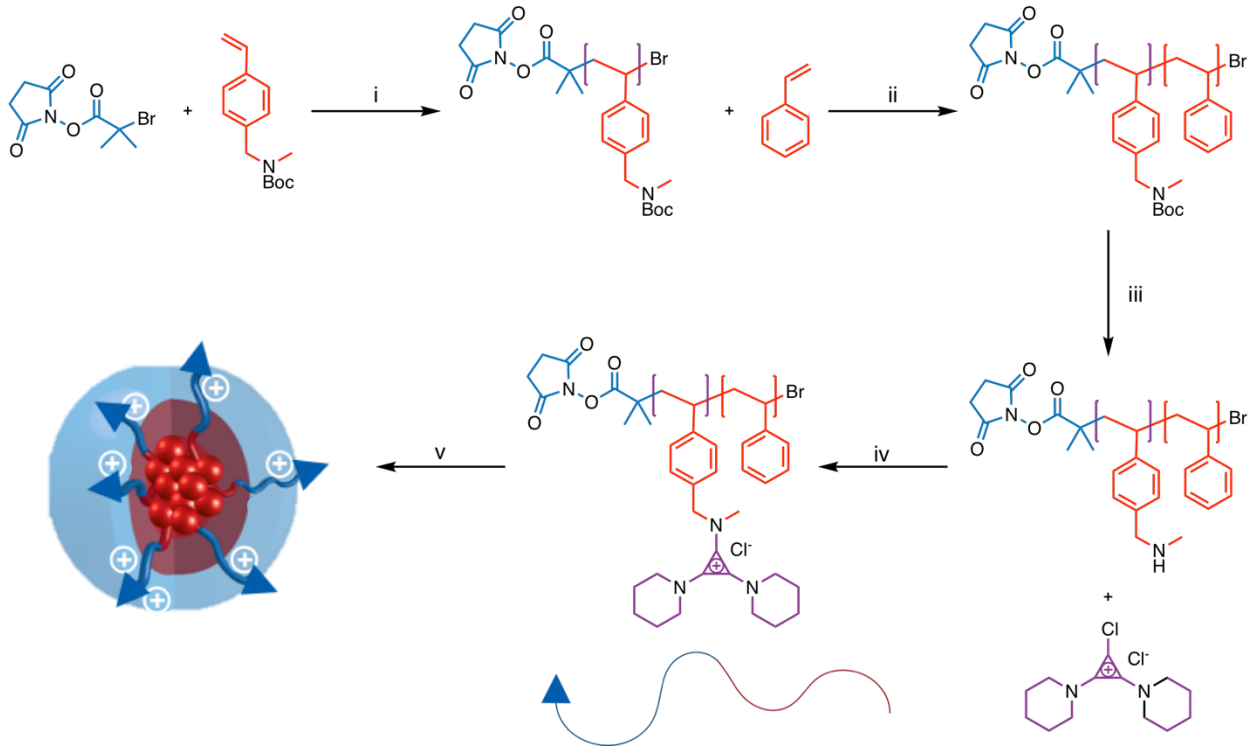

Figure 9. Synthetic scheme for targetable nanoparticles. (i) CuBr, TPMA, Anisole, 90 °C, 4 h; (ii) CuBr, PMDETA, Anisole, 100 °C, 24 h; (iii) 1. TMSCl, MeOH/CH_2Cl_2, 0 °C 2. NaOH; (iv) $CHCl_3$, DIPEA, 65 °C, 3 h; (v) Styrene, V-50, H_2O, 70 °C, 16-24 h.

Interested in exploiting the unique chemistry of these nanoparticles for theranostic applications, we initiated a collaboration with Prof. Valerio Dorrello, an expert in bioengineering. As of this writing this collaboration is ongoing with only preliminary results as we seek internal

or federal funding. Our ultimate goal is to employ targetable Raman-active polymer dots as a platform to specifically target and remove diseased lung tissue.

Hundreds of millions of people suffer from chronic respiratory diseases worldwide, and in the United States, end-stage lung disease is the third leading cause of death.[42] Lung transplantation, which is the only definitive treatment, remains limited by a severe shortage of donor organs.[43] Due to the extreme complexity of the lung with its 3D architecture, diversity in cell composition, and highly specialized matrix, prior attempts to bioengineer a functional lung have been largely unsuccessful.[44,45] We imagine that early intervention via targeted cell therapy could promote lung repair and regeneration, slow disease progression, and ultimately avoid the need for transplant.

A challenging paradigm shift in both lung disease and regenerative medicine will be to remove only defective cells, while preserving healthy cells and the surrounding lung vasculature and architecture. In particular, the dysfunction or injury of alveolar type II (ATII) epithelial cells, which are responsible for the production and recycling of pulmonary surfactant, has been implicated in multiple acute and chronic lung diseases.[46–48] Compared to previous attempts involving full decellularization of the lung, targeting damaged ATII cells exclusively has posed unsurmountable hurdles.[44,45,47] Developing innovative precisely targeted therapies of ATII cells is thus of high import.

Our theranostic approach involves decorating Raman-active polymer dots with two distinct proteins for both precision targeting and treatment. Lung surfactant protein A is specifically produced and recycled by ATII cells,[49] thus we envision it can serve as a targeting ligand for these cells. For treatment, we chose *Pseudomonas aeruginosa* exotoxin as a well-established toxin that can exert cytotoxic effects in cells.[50] Binding SP-A to PE through Raman-active polymer dots will

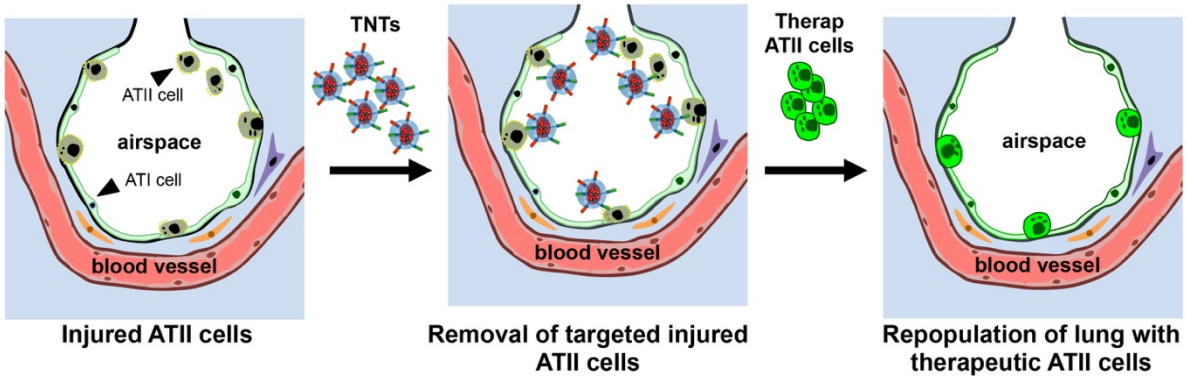

Figure 10. Theranostic approach for the targeting and treatment of end-stage lung disease. Targeting ligand-nanoparticle-toxin (TNT) conjugates will specifically target and destroy injured ATII epithelial cells . The void left by deceased ATII cells can then be repopulated by healthy exogenous ATII cells to re-establish alveolar homeostasis.

furnish a targeted, toxic, trackable molecule. This theranostic **t**argeting ligand-**n**anoparticle-**t**oxin (TNT) can specifically trigger apoptosis of ATII cells, leaving a void that could then be repopulated by healthy lung progenitors affording long-lasting repair and regeneration (**Figure 10**). This strategy thus provides sustained recovery while current treatments are only supportive.

At this point, we have established the foundation for this work, demonstrating the conjugation of a model fluorescent bovine serum albumin (BSA) protein to our targetable Raman-active polymer dots. The nanoparticles and fluorescent BSA were covalently linked via rapid reaction of the NHS ester moiety with primary amines on the protein, and then purified by ultracentrifugation. As we could calculate the number of nanoparticles in solution by,

$$N_p = \frac{6m}{\pi \rho d^3}$$

where m is the mass of particles, ρ is the density of the polymer (assumed to be 1.045 for styrene), and d is the diameter of the particles, but were unable to calculate the exact number of polymer chains per nanoparticle, we performed the reaction with high excess of protein to ensure reaction (ca. 10^4). The obtained protein-nanoparticle conjugate was characterized by fluorimetry and dynamic light scattering demonstrating a stable signal and discrete size (**SI Figures 13-14**).

This control experiment suggests the high potential for targetable Raman-active polymer dots as theranostic platforms.

We thus have begun to expand upon the applications of Raman-active polymer dots as both a targetable and therapeutic system. Synthesis of an end-functionalized amphiphilic block copolymer enabled the incorporation of an NHS ester group into the nanoparticle synthesis. With the block copolymer as a functional surfactant, the emulsion polymerization again could be modulated to include either fluorescent dyes or vibrational labels. The resulting NHS-ester coated nanoparticles could then be imaged accordingly by either fluorescence or SRS microscopy. We also have established that these nanoparticles can be conjugated with proteins, highlighting their future potential as a theranostic material for the precise treatment of lung diseases. Furthermore, due to the modularity of our approach, we expect that these targetable, trackable nanoparticles could be expanded to other cell types according to the disease and even extended to drug delivery.

REFERENCES

(1) Salata, O. V. *J. Nanobiotechnol.* **2004**, *2*, 3.
(2) Wolfbeis, O. S. *Chem. Soc. Rev.* **2015**, *44*, 4743–4768.
(3) Welch, M. J.; Hawker, C. J.; Wooley, K. L. *J. Nucl. Med.* **2009**, *50* (11), 1743–1746.
(4) Michalet, X.; Pinaud, F. F.; Bentolila, L. A.; Tsay, J. M.; Doose, S.; Li, J. J.; Sundaresan, G.; Wu, A. M.; Gambhir, S. S.; Weiss, S. *Science* **2005**, *307*, 538–545.
(5) Lane, L. A.; Qian, X.; Nie, S. *Chem. Rev.* **2015**, *115* (19), 10489–10529.
(6) Zhu, Z.; Yeh, Y.; Tang, R.; Yan, B.; Tamayo, J.; Vachet, R. W.; Rotello, V. M. *Nat. Chem.* **2011**, *3* (12), 963–968.
(7) Bogart, L. K.; Pourroy, G.; Murphy, C. J.; Puntes, V.; Pellegrino, T.; Rosenblum, D.; Peer, D.; Lévy, R. *ACS Nano* **2014**, *8* (4), 3107–3122.
(8) Sun, X.; Liu, Z.; Welsher, K.; Robinson, J. T.; Goodwin, A.; Zaric, S.; Dai, H. *Nano Res.* **2008**, *1* (3), 203–212.
(9) Liu, Z.; Li, X.; Tabakman, S. M.; Jiang, K.; Fan, S.; Dai, H. *J. Am. Chem. Soc.* **2008**, *130* (41), 13540–13541.
(10) Pope, I.; Payne, L.; Zoriniants, G.; Thomas, E.; Williams, O.; Watson, P.; Langbein, W.; Borri, P. *Nat. Nanotechnol.* **2014**, *9* (11), 940–946.
(11) Hong, G.; Diao, S.; Antaris, A. L.; Dai, H. *Chem. Rev.* **2015**, *115* (19), 10816–10906.
(12) Elsabahy, M.; Heo, G. S.; Lim, S.-M.; Sun, G.; Wooley, K. L. *Chem. Rev.* **2015**, *115* (19), 10967–11011.
(13) Wu, C.; Chiu, D. T. *Angew. Chem. Int. Ed.* **2013**, *52* (11), 3086–3109.
(14) Reisch, A.; Klymchenko, A. S. *Small* **2016**, *12* (15), 1968–1992.
(15) Freudinger, C. W.; Min, W.; Saar, B. G.; Lu, S.; Holtom, G. R.; He, C.; Tsai, J. C.; Kang, J. X.; Xie, X. S. *Science* **2008**, *322*, 1857–1861.
(16) Cheng, J.-X.; Xie, X. S. *Science* **2015**, *350* (6264), aaa8870.
(17) Prince, R. C.; Frontiera, R. R.; Potma, E. O. *Chem. Rev.* **2017**, *117* (7), 5070–5094.
(18) Liao, C.-S.; Cheng, J.-X. *Annu. Rev. Anal. Chem.* **2016**, *9* (1), 69–93.
(19) Min, W.; Freudiger, C. W.; Lu, S.; Xie, X. S. *Annu. Rev. Phys. Chem.* **2011**, *62*, 507–530.
(20) Krafft, C.; Schie, I. W.; Meyer, T.; Schmitt, M.; Popp, J. *Chem. Soc. Rev.* **2016**, *45* (7), 1819–1849.
(21) Wei, L.; Hu, F.; Chen, Z.; Shen, Y.; Zhang, L.; Min, W. *Acc. Chem. Res.* **2016**, *49* (8), 1494–1502.
(22) Hong, S.; Chen, T.; Zhu, Y.; Li, A.; Huang, Y.; Chen, X. *Angew. Chem. Int. Ed.* **2014**, *53* (23), 5827–5831.
(23) Hu, F.; Lamprecht, M. R.; Wei, L.; Morrison, B.; Min, W. *Sci. Rep.* **2016**, *6*, 39660.
(24) Hu, F.; Chen, Z.; Zhang, L.; Shen, Y.; Wei, L.; Min, W. *Angew. Chem. Int. Ed.* **2015**, *54* (34), 9821–9825.
(25) Choi, Y. T.; El-Aasser, M. S.; Sudol, E. D.; Vanderhoff, J. W. *J. Polym. Sci. Part A Polym. Chem.* **1985**, *23* (12), 2973–2987.
(26) Jiang, Y.; Freyer, J. L.; Cotanda, P.; Brucks, S. D.; Killops, K. L.; Bandar, J. S.; Torsitano, C.; Balsara, N. P.; Lambert, T. H.; Campos, L. M. *Nat. Commun.* **2015**, *6*, 5950.
(27) Killops, K. L.; Brucks, S. D.; Rutkowski, K. L.; Freyer, J. L.; Jiang, Y.; Valdes, E. R.; Campos, L. M. *Macromolecules* **2015**, *48* (8), 2519–2525.
(28) Yamakoshi, H.; Dodo, K.; Palonpon, A. F.; Fujita, K.; Kawata, S.; Sodeoka, M. *J. Am. Chem. Soc.* **2012**, *134* (51), 20681–20689.
(29) Fleischmann, S.; Komber, H.; Voit, B. *Macromolecules* **2008**, *41* (14), 5255–5264.
(30) Condirston, D. A.; Laposa, J. D. *J. Mol. Spectrosc.* **1976**, *63* (3), 466–477.
(31) Jaiswal, J. K.; Mattoussi, H.; Mauro, J. M.; Simon, S. M. *Nat. Biotechnol.* **2003**, *21* (1), 47–51.
(32) Derfus, A. M.; Chan, W. C. W.; Bhatia, S. N. *Nano Lett.* **2004**, *4* (1), 11–18.
(33) Chen, Z.; Paley, D. W.; Wei, L.; Weisman, A. L.; Friesner, R. A.; Nuckolls, C.; Min, W. *J. Am. Chem. Soc.* **2014**, *136* (22), 8027–8033.

(34) Park, S.; Aalipour, A.; Vermesh, O.; Yu, J. H.; Gambhir, S. S. *Nat. Rev. Mater.* **2017**, *2*, 17014.
(35) Chen, G.; Roy, I.; Yang, C.; Prasad, P. N. *Chem. Rev.* **2016**, *116* (5), 2826–2885.
(36) Pelaz, B.; Alexiou, C.; Alvarez-Puebla, R. A.; Alves, F.; Andrews, A. M.; Ashraf, S.; Balogh, L. P.; Ballerini, L.; Bestetti, A.; Brendel, C.; Bosi, S.; Carril, M.; Chan, W. C. W.; Chen, C.; Chen, X.; Chen, X.; Cheng, Z.; Cui, D.; Du, J.; Dullin, C.; Escudero, A.; Feliu, N.; Gao, M.; George, M.; Gogotsi, Y.; Grünweller, A.; Gu, Z.; Halas, N. J.; Hampp, N.; Hartmann, R. K.; Hersam, M. C.; Hunziker, P.; Jian, J.; Jiang, X.; Jungebluth, P.; Kadhiresan, P.; Kataoka, K.; Khademhosseini, A.; Kopeček, J.; Kotov, N. A.; Krug, H. F.; Lee, D. S.; Lehr, C.-M.; Leong, K. W.; Liang, X.-J.; Lim, M. L.; Liz-Marzán, L. M.; Ma, X.; Macchiarini, P.; Meng, H.; Möhwald, H.; Mulvaney, P.; Nel, A. E.; Nie, S.; Nordlander, P.; Okano, T.; Oliveira, J.; Park, T. H.; Penner, R. M.; Prato, M.; Puntes, V.; Rotello, V. M.; Samarakoon, A.; Schaak, R. E.; Shen, Y.; Sjöqvist, S.; Skirtach, A. G.; Soliman, M. G.; Stevens, M. M.; Sung, H.-W.; Tang, B. Z.; Tietze, R.; Udugama, B. N.; VanEpps, J. S.; Well, T.; Weiss, P. S.; Willner, I.; Wu, Y.; Yang, L.; Yue, Z.; Zhang, Q.; Zhang, Q.; Zhang, X.-E.; Zhao, Y.; Zhou, X.; Parak, W. J. *ACS Nano* **2017**, *11* (3), 2313–2381.
(37) Elsabahy, M.; Wooley, K. L. *Chem. Soc. Rev.* **2012**, *41*, 2545–2561.
(38) Kamaly, N.; Xiao, Z.; Valencia, P. M.; Radovic-Moreno, A. F.; Farokhzad, O. C. *Chem. Soc. Rev.* **2012**, *41* (7), 2971–3010.
(39) Richards, D. A.; Maruani, A.; Chudasama, V. *Chem. Sci.* **2017**, *8*, 63–77.
(40) Blasco, E.; Sims, M. B.; Goldmann, A. S.; Sumerlin, B. S.; Barner-Kowollik, C. *Macromolecules* **2017**, *50* (14), 5215–5252.
(41) Iha, R. K.; Wooley, K. L.; Nyström, A. M.; Burke, D. J.; Kade, M. J.; Hawker, C. J. *Chem. Rev.* **2009**, *109* (11), 5620–5686.
(42) Organization, W. H. *Global surveillance, prevention and control of Chronic Respiratory Diseases*; 2007.
(43) Kotloff, R. M.; Thabut, G. *Am. J. Respir. Crit. Care Med.* **2011**, *184* (2), 159–171.
(44) Ott, H. C.; Clippinger, B.; Conrad, C.; Schuetz, C.; Pomerantseva, I.; Ikonomou, L.; Kotton, D.; Vacanti, J. P. *Nat. Med.* **2010**, *16* (8), 927–933.
(45) Petersen, T. H.; Calle, E. A.; Zhao, L.; Lee, E. J.; Gui, L.; Raredon, M. B.; Gavrilov, K.; Yi, T.; Zhuang, Z. W.; Breuer, C.; Herzog, E.; Niklason, L. E. *Science* **2010**, *329* (5991), 538–541.
(46) Mulugeta, S.; Nureki, S.-I.; Beers, M. F. *Am. J. Physiol. Lung Cell. Mol. Physiol.* **2015**, *309* (6), L507–L525.
(47) Beers, M. F.; Morrisey, E. E. *J. Clin. Invest.* **2011**, *121* (6), 2065–2073.
(48) Lopez-Rodriguez, E.; Gay-Jordi, G.; Mucci, A.; Lachmann, N.; Serrano-Mollar, A. *Cell Tissue Res.* **2017**, *367* (3), 721–735.
(49) Olmeda, B.; Martínez-Calle, M.; Pérez-Gil, J. *Ann. Anat.* **2017**, *209*, 78–92.
(50) Michalska, M.; Wolf, P. *Front. Microbiol.* **2015**, *6* (963).

SUPPORTING INFORMATION

Materials

All materials were purchased from Sigma-Aldrich and used without further purification, except as noted below. Dulbecco's Modified Eagle Medium (DMEM), fetal bovine serum (FBS), penicillin/streptomycin, human recombinant insulin, fluorescent FITC bovine serum albumin, and transferrin Texas Red conjugate were purchased from Invitrogen. Eagle's Minimum Essential Medium (EMEM) medium was purchased from ATCC. Spectrum Labs dialysis bags were purchased from VWR. Eluents for column chromatography were HPLC grade and purchased from Fisher Scientific. Deuterated solvents used for NMR spectroscopy were purchased from Thermo Fisher Scientific. Organic solutions were concentrated with a Buchi rotary evaporator. Styrene, d_5-styrene, and 4-cyanostyrene were passed over a column of neutral alumina to remove inhibitor prior to polymerization. 4-(trimethylsilylethynyl)styrene and the trisaminocyclopropenium monomer were synthesized according to previously reported procedures. [Ref. #26 and #29]

Cell culture

HeLa, Cos-7, and MEF cells were grown in DMEM culture medium with 10% *v*/*v* FBS and 1% *v*/*v* penicillin/streptomycin. HT1080 cells were grown in EMEM culture medium with 10% *v*/*v* FBS and 1% *v*/*v* penicillin/streptomycin. MCF-7 cells were grown in EMEM culture medium with 10% *v*/*v* FBS, 1% *v*/*v* penicillin/streptomycin and 0.01 mg/ml human recombinant insulin. All cultures were incubated in humidified tissue incubators at 37 °C and 5% CO_2.

Dynamic light scattering

Nanoparticle size and zeta potential were measured on a Malvern Zetasizer Nano ZS (Malvern, United Kingdom). For all measurements, nanoparticles were diluted 1:100 in Milli-Q water at neutral pH. The reported diameters are the average of three measurements, where each measurement comprises at least 10 acquisitions. The zeta potential was calculated according to the Smoluchowski approximation.

SRS microscopy

A custom-modified integrated laser source (picoEMERALD, Applied Physics & Electronics, Inc.), is used to produce a Stokes beam (1064 nm, 6 ps) with intensity modulated sinusoidally at 8 MHz and a pump beam (tunable from 720 to 990 nm, 5–6 ps) both at 80 MHz repetition rate. Two beams are spatially and temporally overlapped before coupled into an inverted multiphoton laser-scanning microscope (FV1200MPE, Olympus) with optimized near-IR throughput. Lasers are focused onto the cell samples through a 25× water objective (XLPlan N, 1.05 N.A. MP, Olympus) and collected with an oil condenser lens (1.4 N.A., Olympus) after the sample. The Stokes beam is blocked with a high O.D. bandpass filter (890/220 CARS, Chroma Technology)

and only the pump beam is collected with a large area Si photodiode (FDS1010, Thorlabs) reverse-biased at a 64 DC voltage. The output photocurrent is electronically filtered (KR 2724, KR electronics), terminated with 50 Ω, and demodulated using a radio frequency lock-in amplifier (SR844, Stanford Research Systems) to extract the stimulated Raman loss signal with near shot-noise-limited sensitivity. The output signal of the lock-in amplifier at each pixel is sent to the analog interface box (FV10-ANALOG, Olympus) of the microscope and images are generated using Fluoview software (Olympus). The imaging experiments are all performed with 40 mW pump beam and 66 mW modulated Stokes beam (measured after the objective) at all frequencies. All images except those in the photo-stability test are acquired with 30 μs time constant from the lock-in amplifier and 100 μs pixel dwell time with ~27 s per frame (512 × 512 pixels). In photo-stability test with continuous imaging of 100 frames, 3 μs time constant using a fast lock-in amplifier (HF2LI, Zurich instrument) and 8 μs pixel dwell time are used for collecting 100 frames with 2.7 s per frame (512 × 512 pixels).

Spontaneous Raman spectroscopy

The spontaneous Raman spectra were collected on a confocal Raman microscope (Xplora, Horiba Jobin Yvon) at room temperature. A 27 mW (after the objective), 532-nm diode laser was used to excite the nanoparticle solutions through a 50 × air objective (MPlan N, 0.75 N.A., Olympus). The total data acquisition time for each sample was 10 s using the LabSpec 6 software.

Live-cell SRS imaging

For all SRS imaging experiments, cells are first seeded on glass coverslips in 24-well plates in ~0.5 mL culture medium for 2 days at 37 °C and 5% CO_2 before experiments.

For multicolor experiments, HeLa cells are incubated with ~1 nM alkyne, nitrile or deuterium labelled polymer dots (500-1500× dilution from stock solution) for 2 h before imaging.

For endosome co-localization experiment, HeLa cells are incubated with ~1 nM alkyne labelled polymer nanoparticles and 25 μg/ml transferrin Texas Red conjugate for 1 h before imaging.

For low-temperature cellular entry experiment, HeLa cells are incubated with ~1 nM alkyne labelled polymer dots at 4 °C for 2 h before imaging.

For time-dependent cellular entry experiments, HeLa cells are separately incubated with ~1 nM alkyne, nitrile and deuterium labelled polymer dots for 1, 2 and 4 h before imaging.

For photo-stability experiment, HeLa cells are incubated with ~1 nM alkyne labelled polymer dots for 2 h before continuous imaging of 100 frames.

For imaging experiments in multiple cells lines, all cells (COS-7, MEF, MCF-7 and HT1080) are incubated with ~1 nM alkyne labelled polymer dots for 2 h before imaging.

For multiplexed cell-type sorting experiments, COS-7, MEF and HeLa cells are specifically incubated with ~1 nM alkyne, nitrile and deuterium labelled polymer dots for 2.5 h. Then cells are trypsinized, mixed and seeded on coverslips in co-culture for 4 h and 24 h before imaging.

After all incubations, cells are washed with PBS solution for three times and the glass coverslips are taken out to assemble into imaging chambers filled with PBS for live-cell SRS imaging.

Cell viability

All cell lines are incubated with ~1nM alkyne, nitrile, and deuterium labelled polymer dots for 4 h. This media was then removed and replaced with fresh media and the cells were allowed to grow in the presence of internalized nanoparticles for two days. Trypan blue dye exclusion cell counting was then performed in triplicate with an automated cell counter (ViCell, Beckman-Coulter). Cell viability under experimental conditions is the viable cell count reported as a percentage relative to untreated cells.

Imaging processing

All images are acquired with FluoView scanning software, assigned color and analyzed by ImageJ.

Fluorimetry

Fluorescence emission spectra were obtained on a Horiba Fluoromax-4.

NMR Spectroscopy

^{1}H NMR spectra were recorded on a Bruker Avance III 400 MHz spectrometer. Standard abbreviations indicating multiplicity were used as follows: s (singlet), d (doublet), t (triplet), q (quartet), m (multiplet), b (broad).

Synthesis

Raman-active nanoparticle synthesis and purification

Nanoparticles were synthesized following a general procedure that was scaled accordingly using the indicated weight percentages for each monomer: TAC, styrene, and where applicable, 4-(trimethylsilylethynyl)styrene, 4-cyanostyrene, and d_5-styrene. To the mixture of monomers was added 2,2-azobis(2-methylpropionamidine) dihydrochloride (V-50) and deionized water such that there was 10 wt% monomers. The mixture was vortexed for 30 s and then added to a two-neck flask fitted with a condenser and stir bar. The solution was sparged with Ar for 15 min and then stirred at 70 °C for 16-24 h. The reaction was then cooled, transferred to a 1k MWCO Spectrum Labs dialysis bag and dialyzed against methanol for 24 h to remove unreacted monomer. The resulting solution was then diluted 1:1 in water to make the nanoparticle stock solution. (Table S1)

Procedures for the synthesis of tris-1,2,3-(diazidoamino)-cyclopropenium chloride, 2

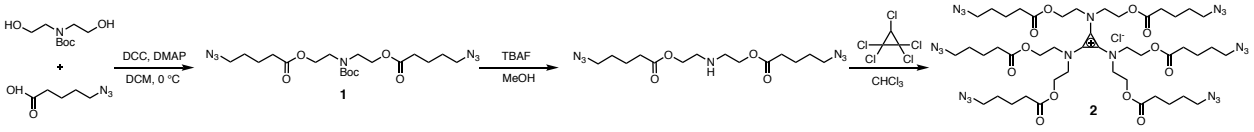

Synthesis of **1**

Boc-protected diethanolamine (1 equiv), 5-azidopentanoic acid (3 equiv), and 4-dimethylaminopyridine (DMAP; 1 equiv) were dissolved in DCM and cooled in an ice bath. *N,N'*-dicyclohexylcarbodiimide (DCC; 3 equiv) was dissolved in a 2M solution of DMF and added dropwise to the solution. The reaction was left to stir overnight and then the white precipitate was filtered off. The solution was diluted with DCM and washed 3 x $NaHSO_4$ (aq), 3 x $NaHCO_3$ (aq), and 1 x brine, and then dried with Na_2SO_4 and concentrated. The crude product was purified by column chromatography in 20:80 EtOAc:Hexanes to afford the title compound as a pale brown oil (85% Yield). ^{1}H NMR (400 MHz, $CDCl_3$): δ 4.20 (t, 4H), 3.41 (t, 4H), 2.35 (t, 4H), 1.93 (m, 4H), 1.8 (m, 4H), 1.65 (b 4H), 1.45 (s, 9H). MS (ESI): Calculated $[M+H]^+$: 456.25; Observed: 456.2570.

Synthesis of **2**

1 (1 equiv) was dissolved in methanol and sparged with Ar for 15 min in an ice bath. Tetrabutylammonium fluoride (TBAF; 5 equiv) was then added, and the solution was left to stir for 12 h under Ar. The solution was then concentrated under vacuum and redissolved in a minimal amount of chloroform and pentachlorocyclopropane (0.15 equiv) was slowly added under Ar. After 12 h this solution was concentrated under vacuum to a pale brown oil. ^{1}H NMR (400 MHz, $CDCl_3$): δ 4.44 (t, 12H), 3.23 (t, 12H), 2.35 (t, 4H), 1.71-1.56 (b, 24H), 1.41 (t, 12 H) MS (ESI): Calculated $[M+H]^+$: 1099.11; Observed: 1099.1250.

Synthesis of tris-1,2,3-(diapropargylamino)-cyclopropenium chloride, 3

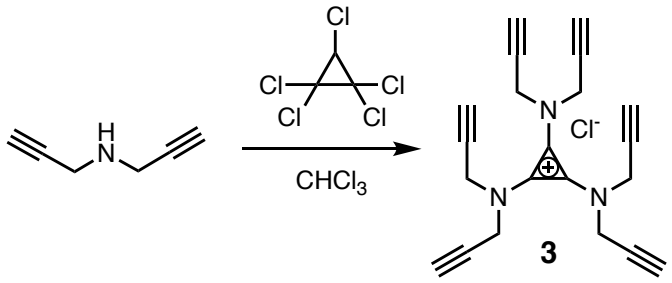

Dipropargylamine (7.5 equiv) was slowly added to a solution of pentachlorocyclopropane (1.0 equiv) in $CHCl_3$ (1M) in a round bottom flask immersed in an ice bath. The solution turned dark red and after stirring overnight was concentrated under vacuum to yield a crude red-brown solid. This solid was redissolved in CH_2Cl_2 and then washed 3 x 1M HCl, 1 x deionized water and 1 x brine before being dried over $MgSO_4$ and concentrated to afford the title compound. ^{1}H NMR

(400 MHz, $CDCl_3$): δ 3.52 (d, 12H), 2.22 (t, 6H). MS (ESI): Calculated $[M+H]^+$: 347.85; Observed: 348.82.

Procedures for the synthesis of NHS ester containing block copolymers

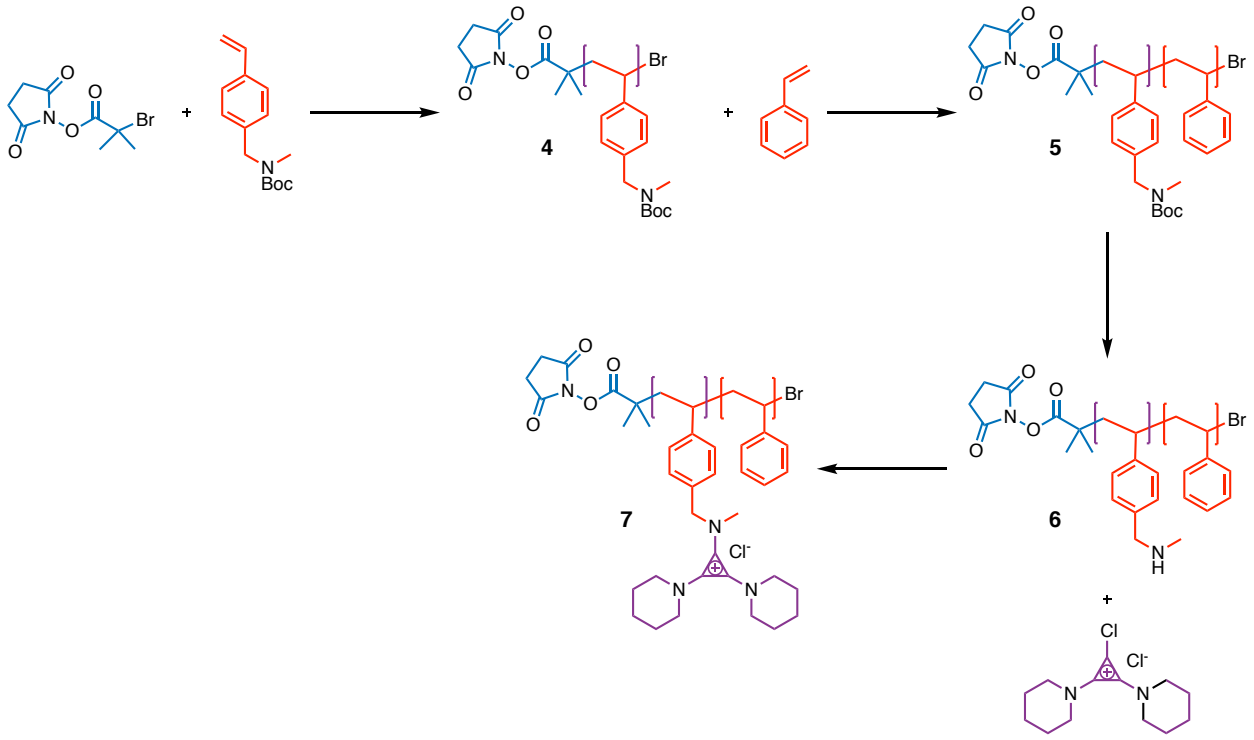

Synthesis of NHS-PBoc, **4**

Copper (I) bromide (0.5 equiv) and tris(2-pyridylmethyl)amine (TPMA; 0.5 equiv) were added to a dry Schlenk flask equipped with a stir bar and deoxygenated via three vacuum-argon cycles. Degassed *tert*-butyl methyl(4-vinylbenzyl)carbamate (100 equiv) was then added and allowed to stir for ten minutes to form copper complex. The mixture was then subjected to three freeze-pump-thaw cycles. The Schlenk flask was closed under argon and a degassed solution of 2-bromoisobutanoic acid *N*-hydroxysuccinmide ester (1 equiv) dissolved in anisole was injected. The reaction mixture was heated to 90 °C and allowed to react for 4 h before turning viscous. The resulting gel was diluted with THF, purified from copper via an alumina plug and transferred to a 3.5 k MWCO Spectrum Labs dialysis bag and dialyzed against methanol. The purified solution was concentrated under vacuum to yield a white powder. From GPC: M_n = 9,500 $gmol^{-1}$, degree of polymerization ~ 40, Đ ~ 1.10. ^1H NMR (400 MHz, $CDCl_3$): δ 7.12-6.18 (b, 160H), 4.55-4.03 (b, 80H), 2.99-2.40 (b, 120H), 1.75-1.15 (b, 500H). (Figure S9)

Synthesis of NHS-PBoc-PS, **5**

Copper (I) bromide (0.5 equiv) was added to a dry Schlenk equipped with a stir bar and deoxygenated via three vacuum-argon cycles. Degassed *N,N,N',N'',N''*-pentamethyldiethylenetriamine (PMDETA) (0.7 equiv) was added to the flask and was allowed

to stir for 10 minutes. Degassed styrene (100 equiv) was then added to the mixture and subjected to three freeze-pump-thaw cycles. The Schlenk flask was closed under argon and a degassed solution of **4** (1 equiv) in anisole (0.5 mL) was injected. The mixture was heated to 100 °C and allowed to react for 24 h. The resulting solution was diluted with THF, passed over an alumina plug, and transferred to a 3.5 k MWCO Spectrum Labs dialysis bag and dialyzed against methanol. The purified solution was concentrated under vacuum to yield an off-white powder. GPC and ^{1}H NMR indicate polymer contains ~40 units Boc-protected monomer and ~20 units styrene, Đ ~ 1.15. ^{1}H NMR (400 MHz, $CDCl_3$): δ 7.21-6.11 (b, 240H), 4.55-3.97 (b, 80H), 3.01-2.40 (b, 120H), 1.77-1.14 (b, 540H). (Figure S10)

Synthesis of NHS-PMAS-PS, **6**

5 (1 equiv Boc monomer) was dissolved in a 3:1 dichloromethane:methanol solution in a round bottom flask under argon. The flask was put on an ice bath and trimethylsilane chloride (TMSCl; 7 equiv) was added. The reaction was allowed to stir to room temperature with a gas outlet, and then concentrated under vacuum to yield an off-white powder. The powder was redissolved in methanol and 0.5 M NaOH was added dropwise, with stirring, until the polymer precipitated from solution. The suspension was centrifuged and the supernatant decanted. The polymer was washed twice more with deionized water and collected by centrifugation. The resulting polymer was dried under vacuum. ^{1}H NMR (400 MHz, CD_2Cl_2): δ 7.28-6.28 (b, 240H), 3.80-3.42 (b, 80H), 2.53-2.16 (b, 120H), 1.60-1.20 (b, 200H). (Figure S11)

Synthesis of NHS-PMAS(Pep)-PS, **7**

This procedure was performed open to the atmosphere. **6** (1 equiv amine monomer) was dissolved in chloroform in a scintillation vial charged with a stir bar. To the vial was added *N,N*-diisopropylethylamine (DIPEA; 3 equiv) followed by a solution of bis-1,2-(piperidino)-3-chlorocyclopropenium chloride (1.5 equiv) in chloroform. The reaction mixture was stirred at 65 °C for 6 h. The resulting solution was concentrated under vacuum, diluted with methanol, and transferred to a 3.5k MWCO Spectrum Labs dialysis bag and dialyzed against methanol. The dialyzed solution was finally concentrated under vacuum to yield a brown powder. ^{1}H NMR (400 MHz, $CDCl_3$): δ 7.20-6.04 (b, 240H), 4.96-4.27 (b, 80H), 3.68-3.24 (b, 340H), 3.20-2.90 (b, 120H), 1.90-1.37 (b, 1200 H). (Figure S12)

Targetable nanoparticle synthesis and purification

Nanoparticles were synthesized following a general procedure using 5 wt% NHS-PMAS(Pep)-PS (**7**) and a scaled amount of styrene based on if fluorophores or vibrational labels were incorporated. In the absence of an imaging modality 95 wt% styrene was used. For fluorescent nanoparticles, 2 wt% fluorescein methacrylate was incorporated with 93 wt% styrene. For alkyne-labelled nanoparticles, 47.5 wt% styrene was added with 47.5 wt% 4-(trimethylsilylethynyl)styrene. Finally, in the case of C-D labelled nanoparticles, 95 wt% d_5-styrene was used. In each case, to the mixture of monomers was added 2,2-azobis(2-

methylpropionamidine) dihydrochloride (V-50) and deionized water such that there was 10 wt% monomers. The mixture was vortexed for 2 min and then added to a two-neck flask fitted with a condenser and stir bar. The solution was sparged with Ar for 20 min and then stirred at 70 °C for 8-24 h. The reaction was then cooled, transferred to a 1k MWCO Spectrum Labs dialysis bag and dialyzed against methanol for 24 h to remove unreacted monomer. The resulting solution was then diluted 1:1 in water to make the nanoparticle stock solution. (Table S2)

Conjugation of targetable nanoparticle with fluorescent bovine serum albumin

Nanoparticles were diluted 100,000X in MilliQ water to give a concentration of 10^{10} nanoparticles mL^{-1}. Fluorescent BSA (2 mg, 0.02 μmol) was dissolved and diluted in phosphate buffer such that there were 10^{14} BSA molecules mL^{-1}. An equal volume of the nanoparticle solution was added to the BSA solution and then stirred overnight. This reaction was quenched with 1 drop of tetraethyleneglycol monoamine to minimize crosslinking. The protein-polymer conjugate was purified by 5 rounds of centrifugation at 5000 rpm, each time removing the supernatant and then redispersing in fresh MilliQ water.

Supplementary Tables and Figures

Table S1. Raman-active nanoparticles synthesis and characterization

Raman-active nanoparticle	TAC wt[a]%	Styrene wt%	Raman-labelled styrene wt%	D_H (nm)	ζ potential (mV)
Alkyne	5	47.5	47.5	55 ± 9	35 ± 5
Nitrile	5	70	25	60 ± 10	20 ± 10
Carbon-Deuterium	5	-	95	50 ± 7	35 ± 10

[a]All weight percentages determined by monomer feed

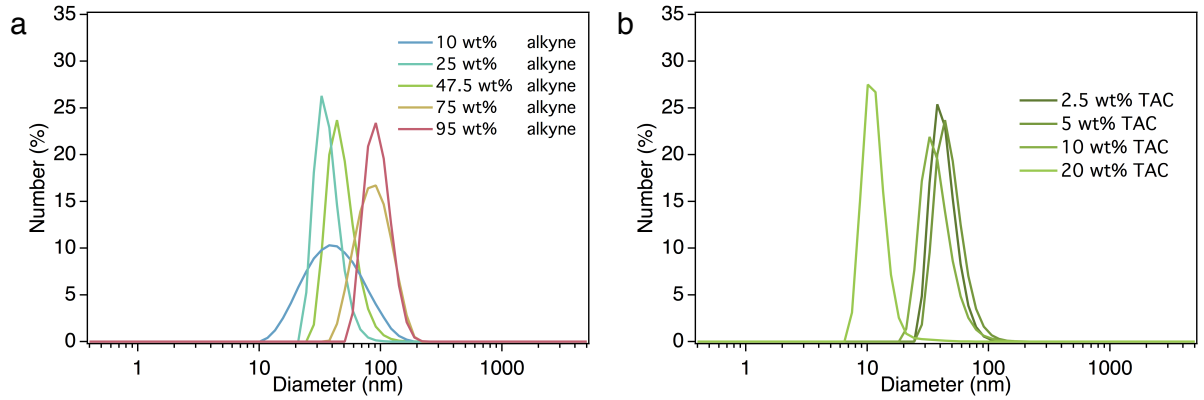

Figure S1. DLS data of alkyne labelled nanoparticles with varying loadings of alkyne monomer (a) and trisaminocyclopropenium monomer (b).

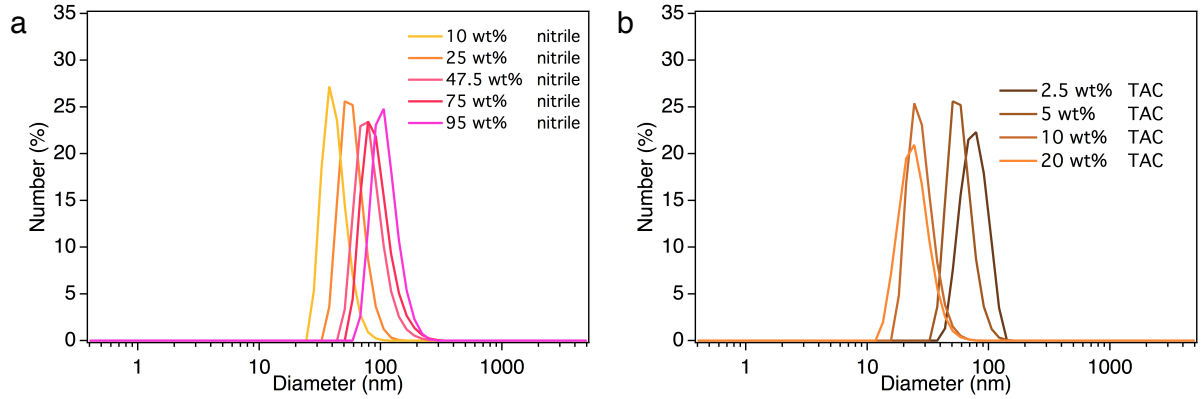

Figure S2. DLS data of nitrile labelled nanoparticles with varying loadings of nitrile monomer (a) and trisaminocyclopropenium monomer (b).

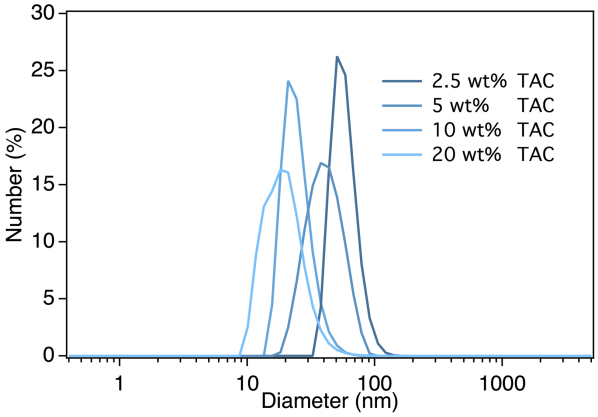

Figure S3. DLS data of deuterium labelled nanoparticles with varying loadings of trisaminocyclopropenium monomer.

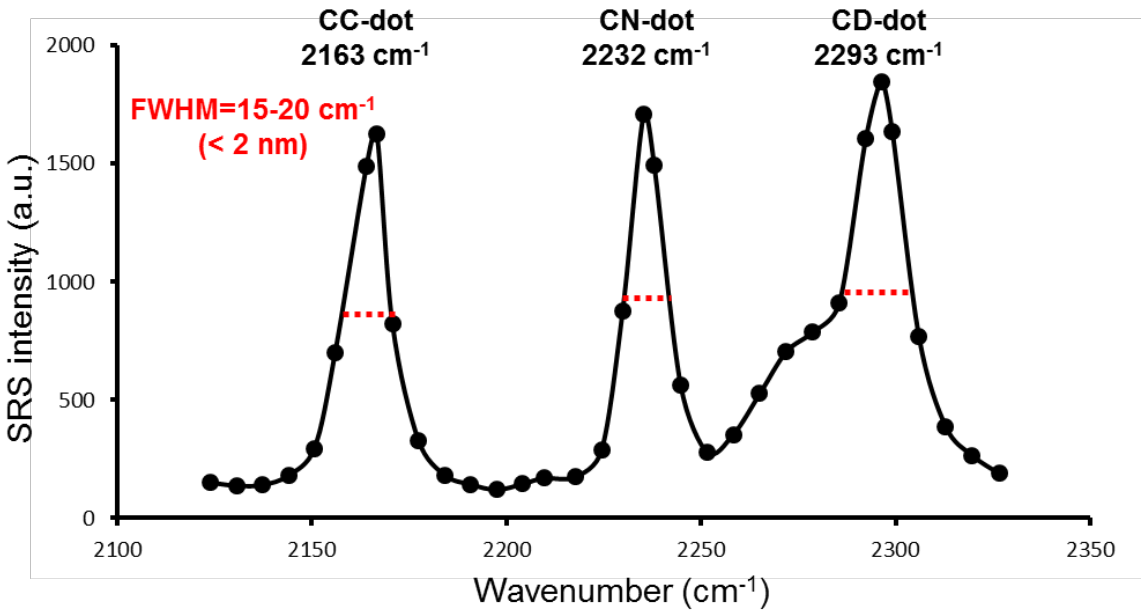

Figure S4. SRS spectrum of Raman-active polymer dots mixture. Three Raman-active polymer dots (CC-dots, CN-dots and CD-dots) show spectrally orthogonal Raman peaks with narrow bandwidth (FWHM=15-20 cm^{-1}, <2 nm) under SRS microscopy. SRS sweeping step size is 0.5 nm.

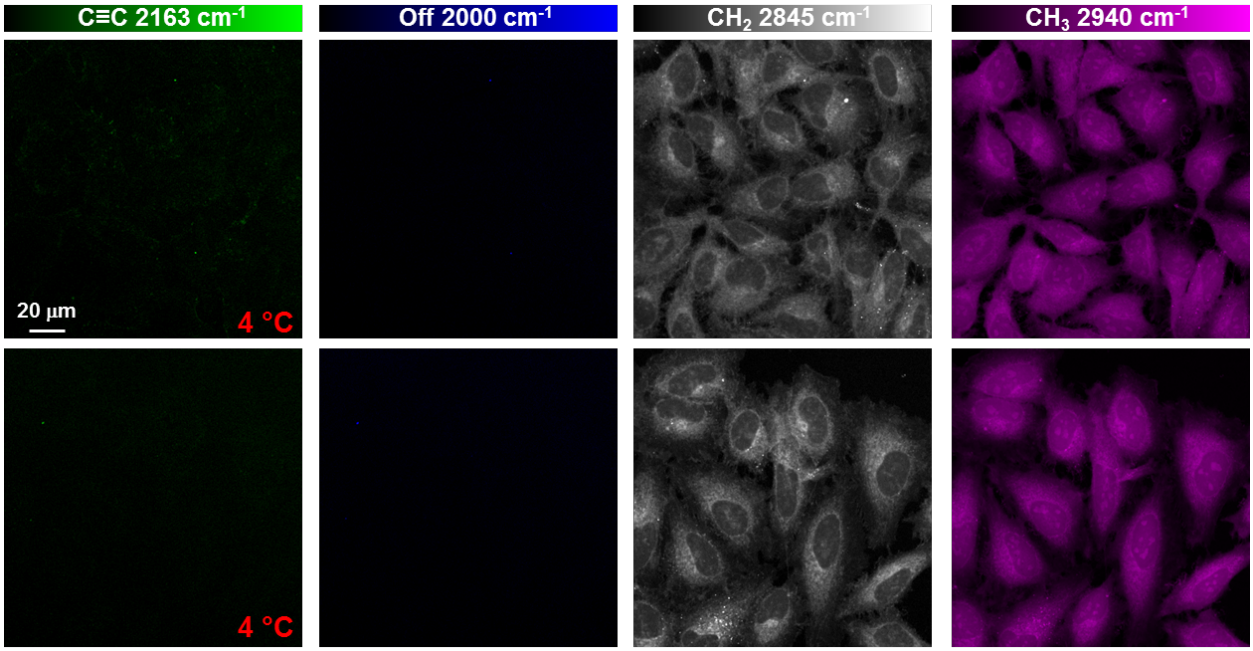

Figure S5. Low-temperature entry inhibition of Raman-active polymer nanoparticles in live HeLa cells. HeLa cells are incubated with alkyne labelled polymer nanoparticles for 2 hours at 4 °C with suppressed endocytosis and nanoparticle entry.

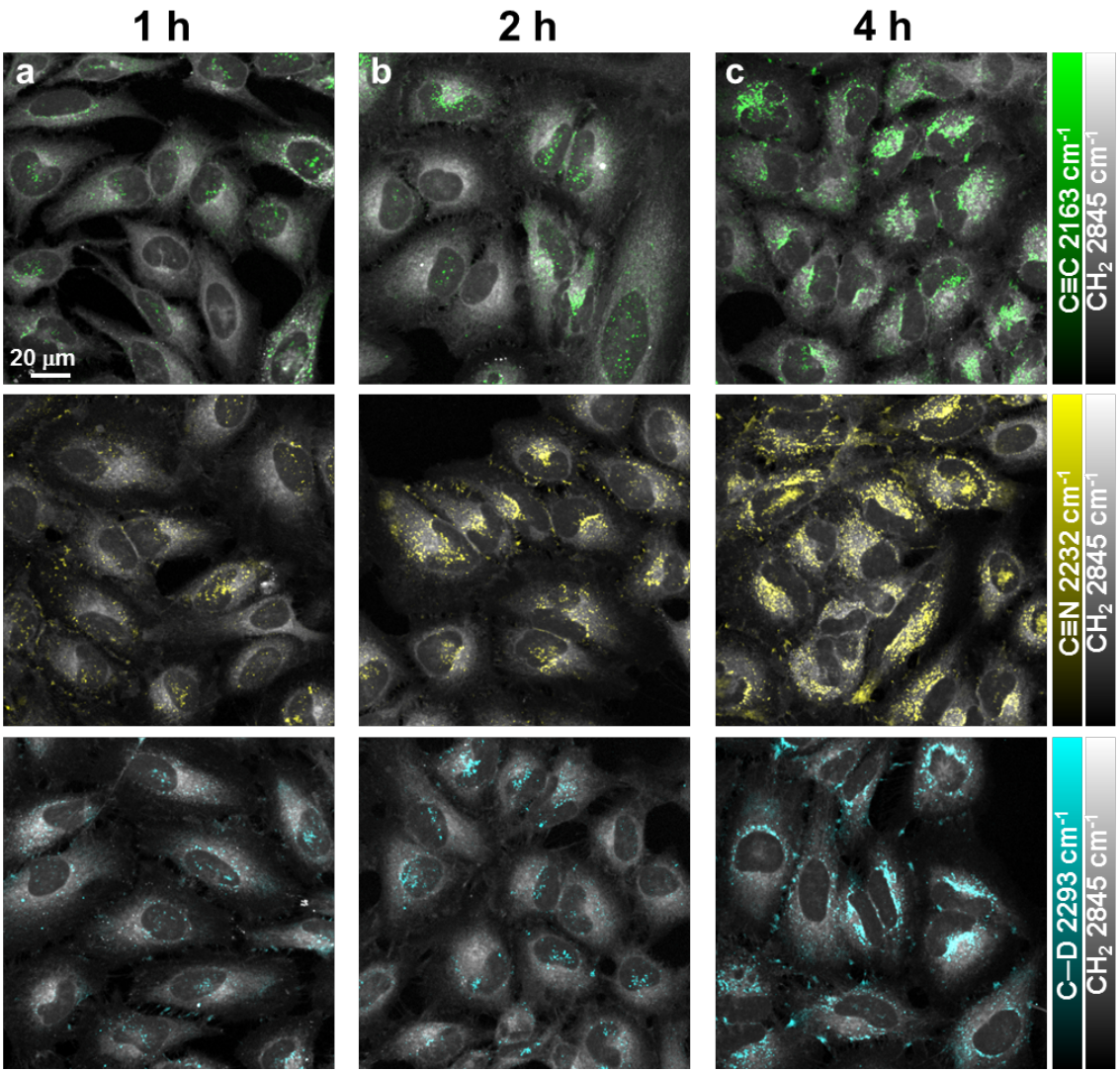

Figure S6. Time-dependent entry kinetics of Raman-active polymer nanoparticles in live HeLa cells. Cells are incubated with alkyne, nitrile and deuterium labelled polymer nanoparticles for various time of 1 h (a), 2 h (b) and 4 h (c). Rapid cellular entry is observed in 1 h for all three polymer nanoparticles.

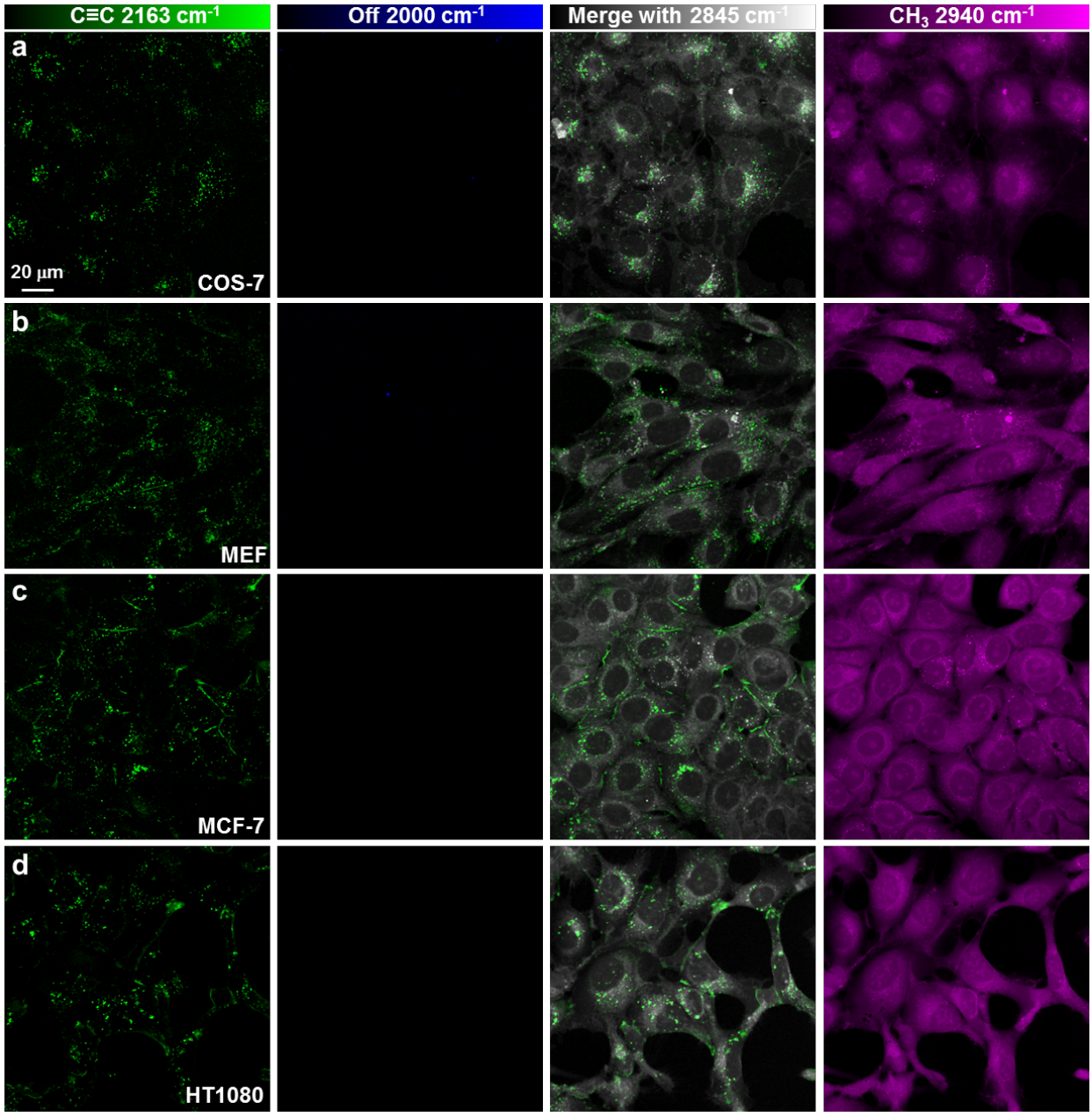

Figure S7. SRS imaging of Raman-active polymer dots in multiple cell lines. COS-7 (a), MEF (b), MCF-7 (c) and HT1080 (d) cells are incubated with alkyne labelled polymer dots for 2 hours. Both non-cancerous and cancerous cell lines are efficiently labelled by Raman-active nanoparticles.

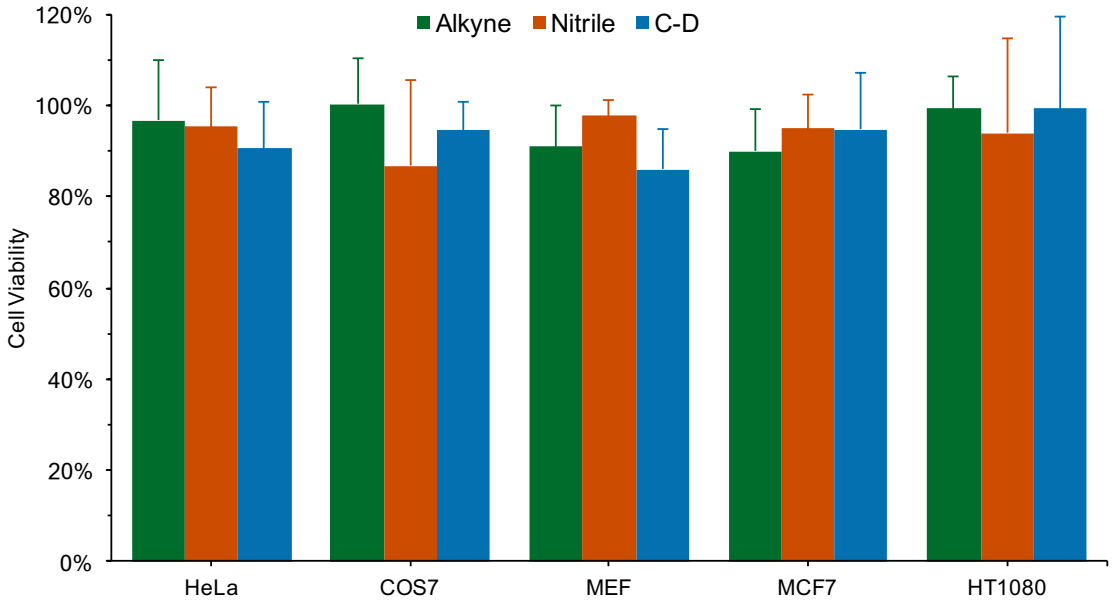

Figure S8. Viability assay of multiple cell lines incubated with alkyne (green), nitrile (orange), and deuterium (cyan) labelled polymer nanoparticles. All cells are incubated with nanoparticles for four hours before exchanging with fresh media and allowing the cells to grow for two days. All five tested cell lines shows greater than 85% viability after 48 h with the three Raman-active polymer nanoparticles. Cell viability is calculated as a percentage relative to control with error bars representing standard deviation of triplicate measurements.

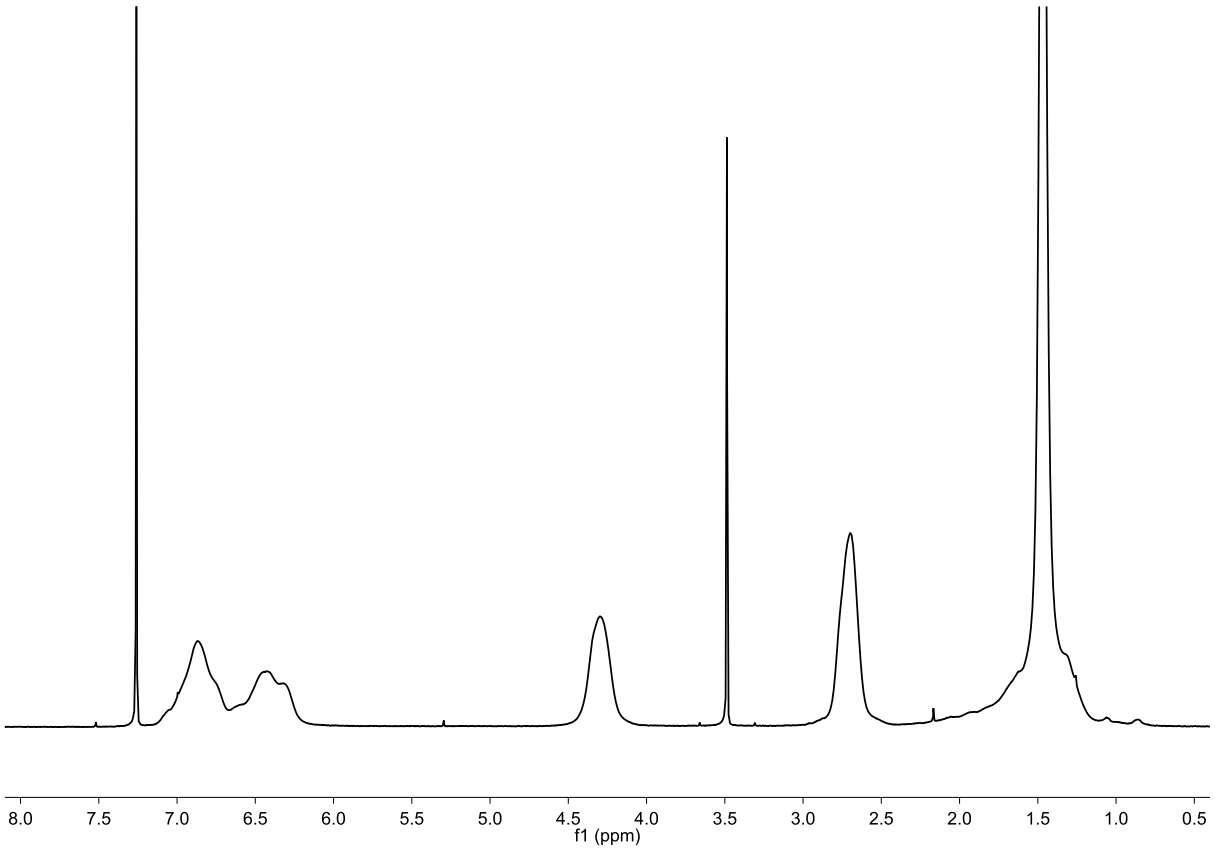

Figure S9. ^{1}H NMR spectrum of NHS-PBoc **4**

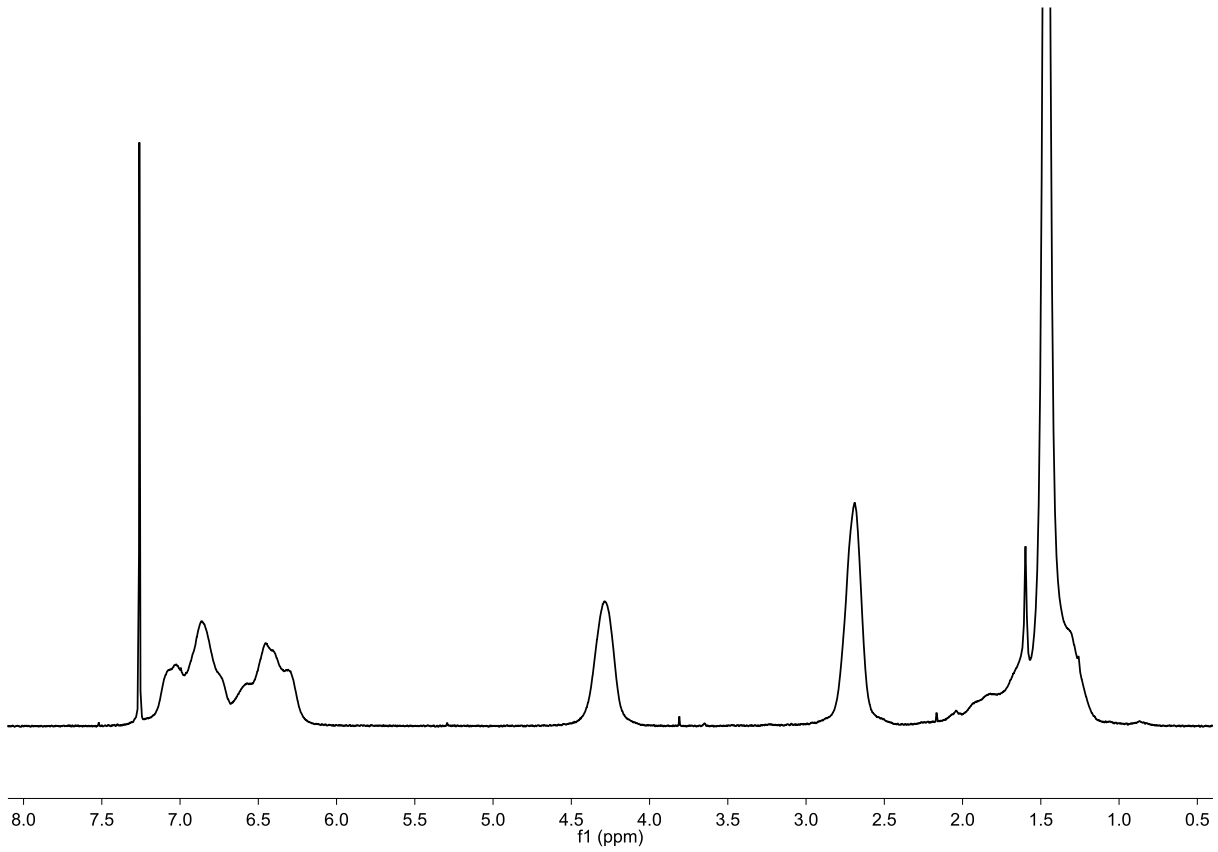

Figure S10. ^{1}H NMR spectrum of NHS-PBoc-PS **5**

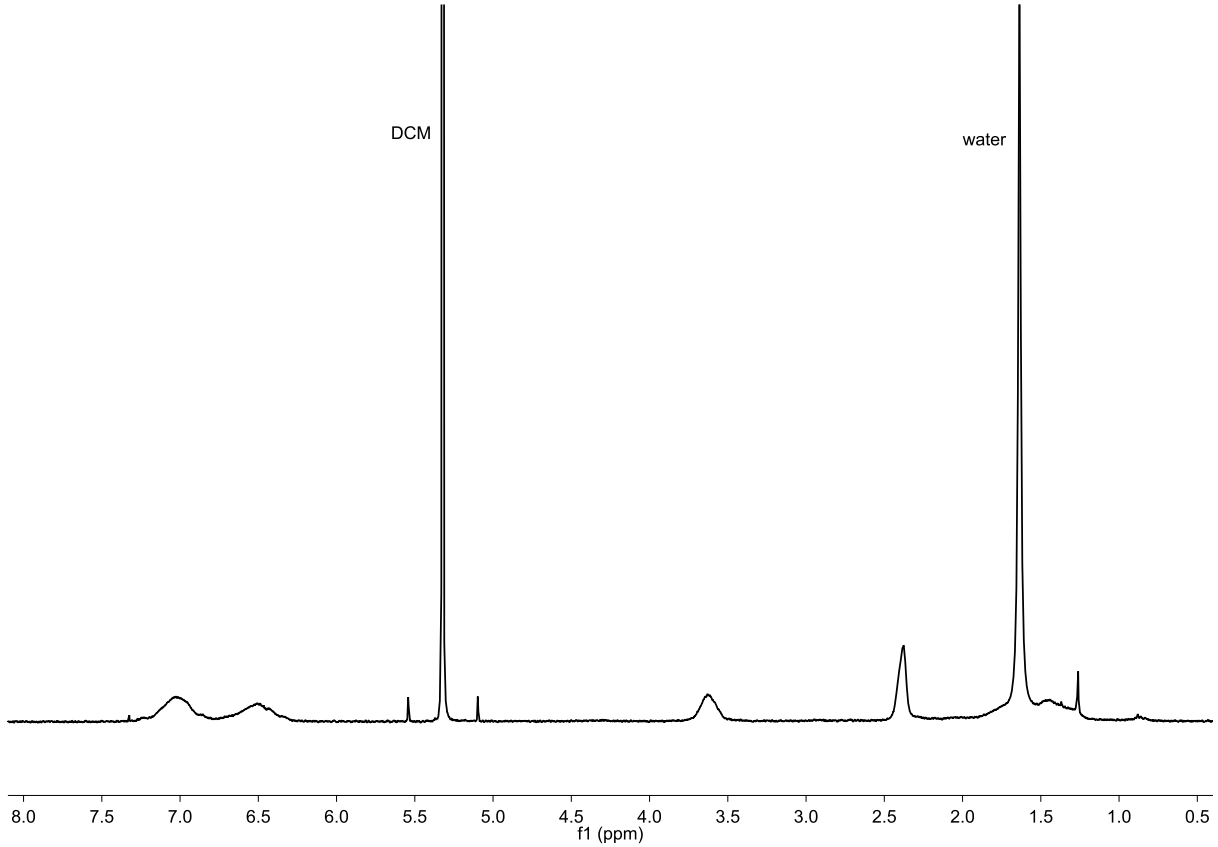

Figure S11. ^{1}H NMR spectrum of NHS-PMAS-PS **6**

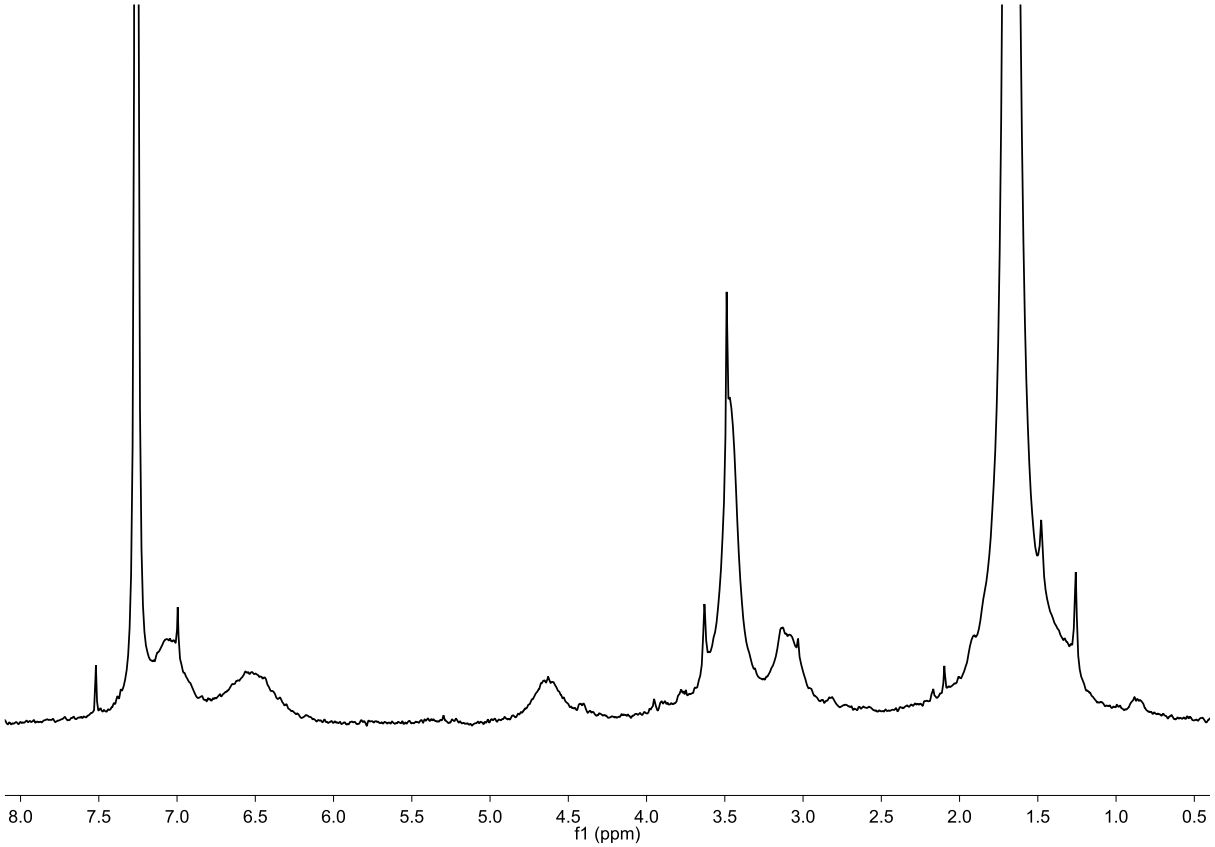

Figure S12. ^{1}H NMR spectrum of NHS-PMAS(Pep)-PS **7**

Table S2. Targetable nanoparticles characterization

Imaging functionality	**D_H (nm)**	**ζ potential (mV)**
Styrene only	60 ± 11	22 ± 10
Alkyne	160 ± 70	25 ± 8
Carbon-Deuterium	92 ± 10	16 ± 5
Fluorescein	80 ± 5	45 ± 7

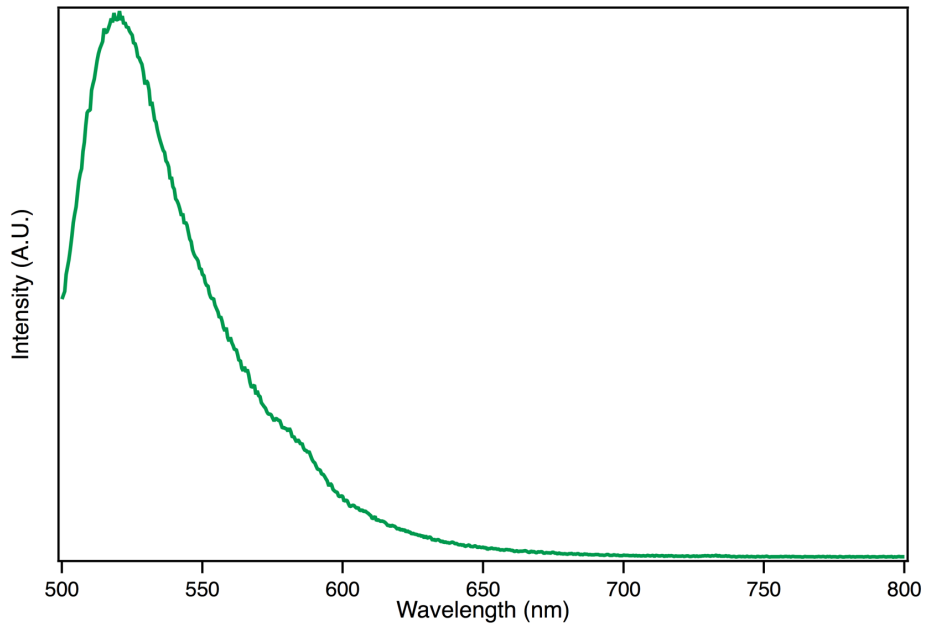

Figure S13. Fluorescence emission spectra for alkyne labelled targetable nanoparticles conjugated with fluorescent bovine serum albumin (λ_{max} 488).

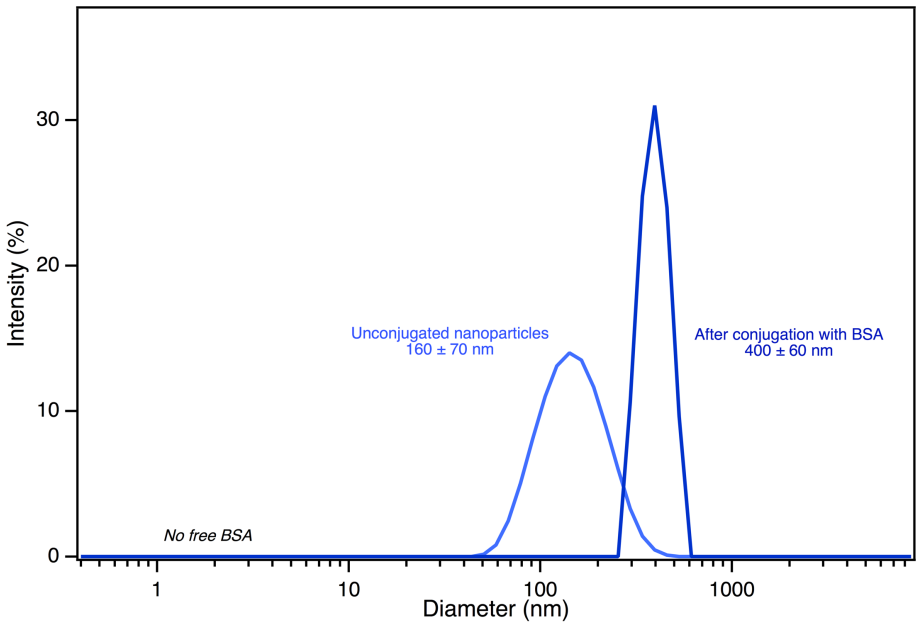

Figure S14. DLS data of alkyne labelled targetable nanoparticles before and after conjugation with fluorescent bovine serum albumin (BSA).

PART THREE:

BRINGING CYCLOPROPENIUM BACK TO POLYMERS

CYCLOPROPENIUM AS A CATIONIC CROSSLINKER

In this final part, we describe a novel role for cyclopropenium in polymer chemistry. Previously, we incorporated cyclopropenium directly – functionalizing at the building block level – to explore structure-property relationships as either the backbone or amino substituents were modulated. Here, we show how we can exploit the robust reaction of cyclopropenium precursors and secondary amines to generate cyclopropenium in situ. Reacting precursors with secondary amine-containing polymers generates cyclopropenium as a polymer crosslinker.

Chemical crosslinking reactions covalently bonding two or more molecules are ubiquitous across macromolecules to confer stability and endow functionality.[1] Crosslinking of biopolymers has been shown to enhance mechanical properties and improve stability, while nanoparticles require crosslinkers to maintain their shape and size.[2,3] Rationally designing crosslinkers represents one of the most promising avenues to install functionality into synthetic polymers.[4,5] Disulfides, which are cleaved to thiols in low pH or reducing environments, can endow a polymer with stimuli-responsive biodegradable behavior[6,7] and thermally reversible crosslinkers, such as those formed from Diels-Alder cycloadditions, can promote self-healing.[8–10] Polymers such as poly(ethylenimine) (PEI), are widely derivatized via functional crosslinkers to optimize performance.[11] Especially in biotechnological applications, where stability, biocompatibility, and precise targeting will drive clinical acceptance, the design of novel macromolecular crosslinkers is highly desirable.[2,3]

Polycationic PEI nanoparticles have been synthesized by crosslinking with diiodoalkanes, followed by N-alkylation.[12,13] These nanoparticles displayed high stability to a variety of external stimuli and possessed a marked antibacterial effect due to the repeating quaternary ammonium cation along the polymer backbone. However, in addition to the two-step synthesis these

nanoparticles required a multi-step purification. Here, we present a facile one-step crosslinking of secondary amine-containing polymers, such as PEI, to form cyclopropenium-crosslinked cationic nanoparticles that does not require purification.

The cyclopropenium cation possesses unique structural and electronic properties that have motivated its incorporation into small molecules for a range of applications including organocatalysis[14,15] and redox flow batteries[16,17]. As the smallest Hückel aromatic ring, it possesses an unusually high degree of stability for a carbocation[18], and when substituted with three amino groups, the cation is both stable and isolable.[19,20] In fact, the trisaminocyclopropenium cation is even stable in strongly alkaline aqueous solutions, motivating its utility as a membrane in alkaline fuel cells.[21,22] However, in spite of these multifaceted efforts with small molecules, cyclopropenium has only recently been incorporated into polymeric structures.[23]

We have previously demonstrated that secondary amine-containing polymers can be readily functionalized with a bisaminocyclopropenium chloride derivative (BACCl), yielding cyclopropenium functionality at the monomer level (**Figure 1a**).[24] While a large variety of BACCl salts of different functionalities can be prepared, they are typically highly reactive species and

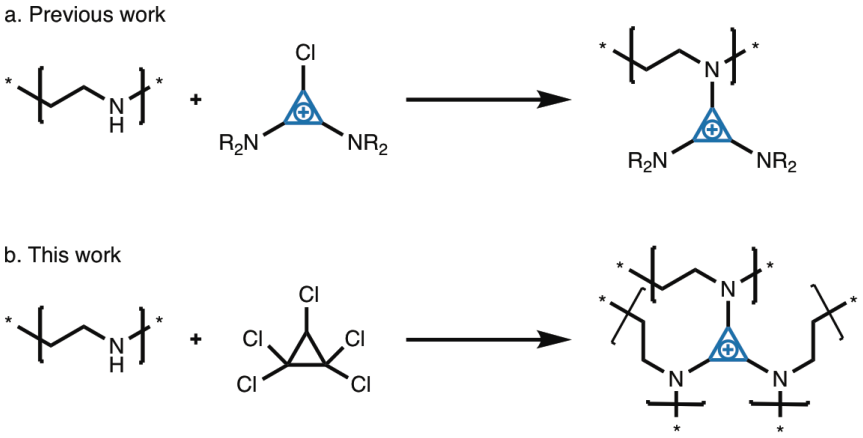

Figure 1. Synthesis of cyclopropenium-containing polymers. Cyclopropenium can be functionalized at the monomer level with reactive bisaminocyclopropenium chloride derivatives (a) or generated as a crosslinker in situ by reaction with a stable precursor (b).

must be generated immediately before use. Here we show that by instead employing a stable cyclopropenium precursor, namely, pentachlorocyclopropane or tetrachlorocyclopropene, we can generate the cation in situ.

Reaction of a secondary amine-containing polymer, such as PEI, with either pentachlorocyclopropane or tetrachlorocyclopropene furnishes cyclopropenium as a crosslink between three amino groups (**Figure 1b**). The reaction takes place rapidly open to air as the temperature rises from 0 °C to room temperature, affording a polymer crosslinked by trisaminocyclopropenium rings. This crosslinker provides a highly pH-stable cation, and when dispersed in aqueous media, these crosslinked polymers form stable nanoparticle aggregates with highly positive charge. We believe this strategy will enable the incorporation of the cyclopropenium cation into novel classes of advanced materials.

We chose poly(ethylenimine) (PEI) as the polymer to crosslink with cyclopropenium as it is readily commercially available and the simplest secondary amine-containing polymer. We selected two different sizes of linear PEI (L-PEI; 25 kDa and 10 kDa) to compare the effects of crosslinking on different molecular weight. Either pentachlorocyclopropane or tetrachlorocyclopropene was added dropwise to a solution of L-PEI in chloroform at different ratios corresponding to 30, 10, and 5 mol% crosslinker. As cyclopropenium is capable of crosslinking three amines, this corresponds to 90%, 30%, and 15% crosslinking, respectively. In all cases, the crosslinked polymer immediately precipitated, indicating reduced solubility and successful crosslinking of the parent polymer. Indeed, after the crosslinking reaction the polymers were insoluble in all common organic solvents.

We confirmed the presence of an aromatic cyclopropenium ring in the crosslinked polymers with a combination of ^{13}C NMR and FT-IR spectroscopy. While parent L-PEI only

shows two ^{13}C signals corresponding to its backbone carbons, the crosslinked polymer has an additional signal at 170 ppm indicative of the aromatic carbons of cyclopropenium (**Figure 2a**). Note, that this is significantly farther downfield than the carbons of pentachlorocyclopropane and tetrachlorocyclopropene which have carbons at 75 ppm and 125 ppm, respectively.[25] As the crosslinked polymers were insoluble in all organic solvents, we dispersed them in CD_3OD for

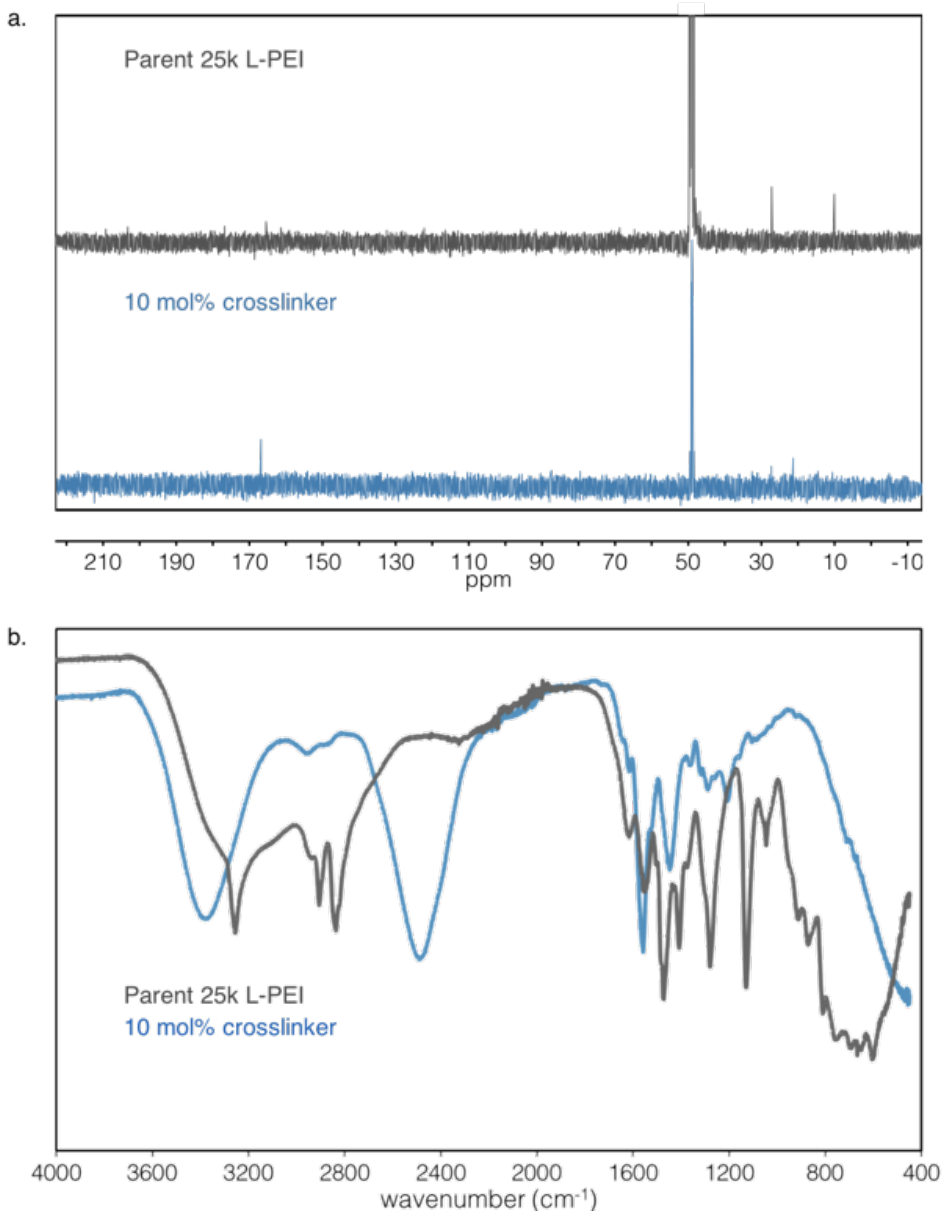

Figure 2. ^{13}C NMR (a) and FT-IR (b) spectra of parent linear PEI compared to those of a crosslinked polymer. The appearance of aromatic carbon peaks (a) and disappearance of secondary amine absorbances (b) suggests in situ formation of the cyclopropenium cation and crosslinking with secondary amines.

these measurements. The presence of cyclopropenium in the crosslinked materials is further evidenced by FT-IR spectroscopy which shows attenuation of the secondary amine absorbances at ~2900 cm^{-1} (**Figure 2b**). These data suggest that the insoluble materials comprise aromatic cyclopropenium rings.

We next evaluated the thermal stability of these materials. Crosslinking of 25k L-PEI led to increased stability at lower temperatures, most likely owing to a lower degree of water, but we found that the decomposition temperatures are only slightly increased (**Figure 3a**). Similarly, the less hygroscopic 10k L-PEI shows an unchanged thermal degradation profile relative to its crosslinked derivatives (**Figure 3b**). Surprisingly, the percentage of crosslinker did not seem to affect the thermal stability in either case, with all crosslinked materials yielding a thermal decomposition of 300 °C. Additionally, there was no T_g evident in any of the crosslinked materials (**SI Figure 1**). Thus, while cyclopropenium-mediated crosslinking of PEI chains dramatically changes solubility, thermal stability only slightly increases.

Though they do not have high processability in the solid state, the crosslinked PEI polymers can be dispersed as stable nanoparticles in aqueous media and exhibit a permanent positive charge, characteristic of the cyclopropenium moiety. We used dynamic light scattering to determine the hydrodynamic diameter (D_H) and zeta potential (ζ) of all crosslinked polymers (**Table 1**). All measured particles show a size ca. 200 nm with a highly positive surface charge. The trisaminocyclopropenium cation, stabilized both by aromaticity and resonance, is uniquely a permanent positive charge, stable across a wide pH range. To test whether our high zeta potentials were due to the cyclopropenium crosslinker or protonated secondary amines on the

PEI backbone, we basified our materials with 1M NaOH and remeasured their surface potential. Indeed, all L-PEI crosslinked materials maintained a positive zeta potential even in strongly

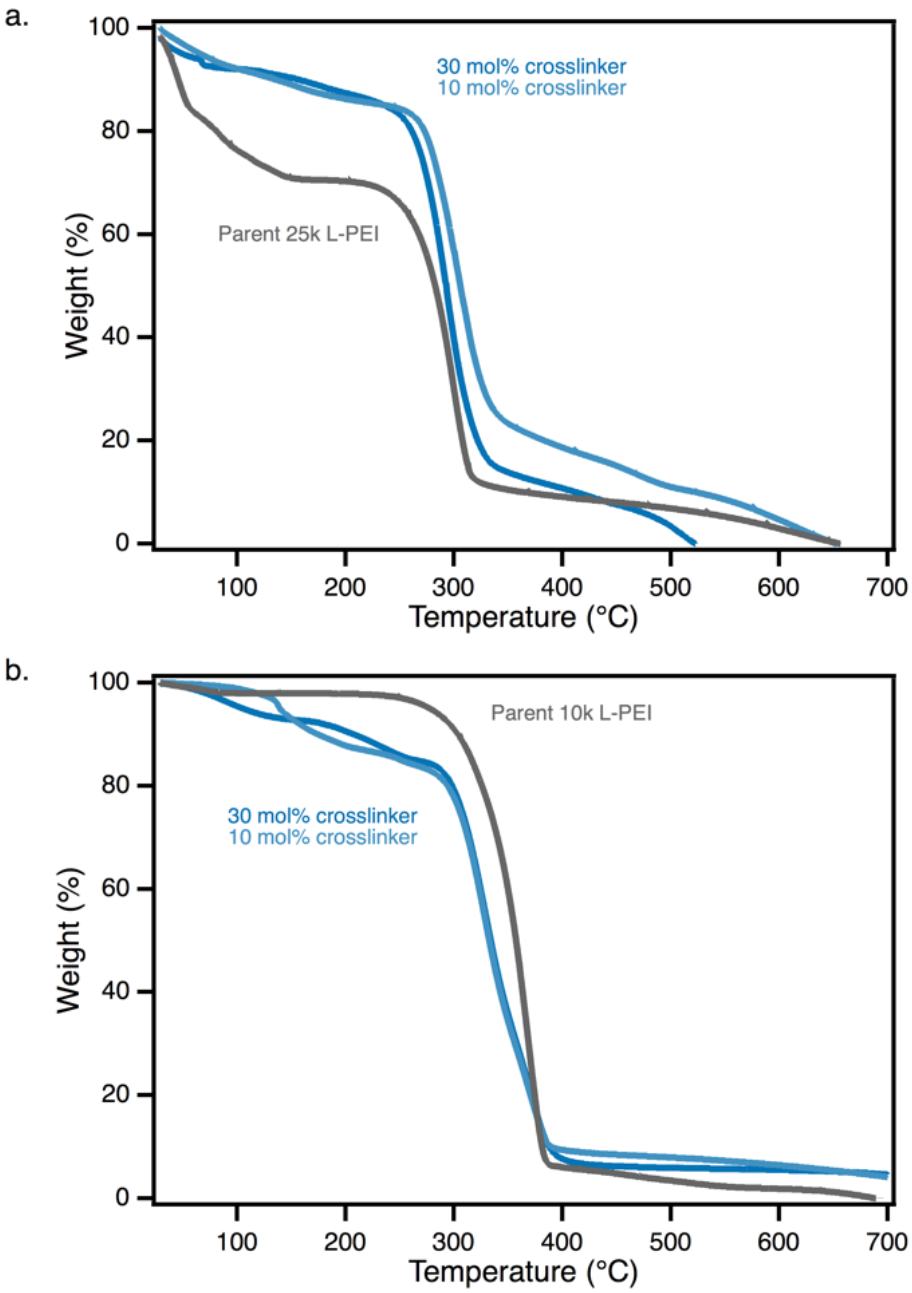

Figure 3. Thermal gravimetric analysis of crosslinked polymers. Cyclopropenium crosslinking of 25k L-PEI (a) and 10k L-PEI (b) minimally changes thermal decomposition temperature. There is no change in thermal decomposition with increased crosslinking density.

basic conditions. Thus, the stable cationic charge characteristic of the L-PEI crosslinked materials derives from pH-stable cyclopropenium units.

MW	Mol% Crosslinker	D_H (nm)	ζ Potential (mV)	ζ Potential at pH 14 (mV)
L-PEI 25k	30%	145 ± 10	45 ± 4	4 ± 1
	10%	179 ± 3	43 ± 6	3 ± 1
	5%	203 ± 9	27 ± 5	9 ± 2
L-PEI 10k	30%	105 ± 3	25 ± 6	2 ± 0.5
	10%	82 ± 6	20 ± 4	2 ± 0.5
	5%	90 ± 3	22 ± 6	4 ± 2

Table 1. Size and surface charge of crosslinked L-PEI nanoparticles.

In order to confirm the size and shape of these nanoparticles, we performed transmission electron microscopy (TEM). The TEM measurements corroborated our DLS results: these crosslinked PEI polymers form nanoparticles in solution, approximately 200 nm in diameter (**Figure 4**). Furthermore, TEM revealed that these nanoparticles are spherical, which represents the first time PEI has been crosslinked into nanoparticles in one step, at ambient temperature, without purification.

Finally, to explore the modularity of this synthetic strategy, we performed the cyclopropenium-mediated crosslinking on two additional polymers containing secondary amines, namely branched PEI (B-PEI) and poly(methylaminostyrene) (PMAS). While all the secondary amines in PEI are found in the main chain, PMAS contains pendent secondary amines, and B-PEI is composed of approximately 25% primary amines and 25% tertiary amines.[11] For B-PEI, we were only able to isolate nanoparticles when the crosslinking was performed with 30 mol% pentachlorocyclopropane (**SI Figure 2)**. Furthermore, the B-PEI crosslinked materials showed a marked decrease in surface charge, suggesting a higher degree of unreacted amines that would be

neutrally charged at basic pH (**SI Table 1)**. As primary amines can ring open pentachlorocyclopropane to an allyl cation rather than form cyclopropenium,[28] these data may be a result of a lower degree of cyclopropenium crosslinkers. For PMAS, we found that crosslinking with cyclopropenium led to insoluble polymers that could not be dissolved nor dispersed in any solvent. While the reduced solubility suggested successful crosslinking and the materials demonstrated high thermal stability (**SI Figure 3**), we were unable to disperse these materials in

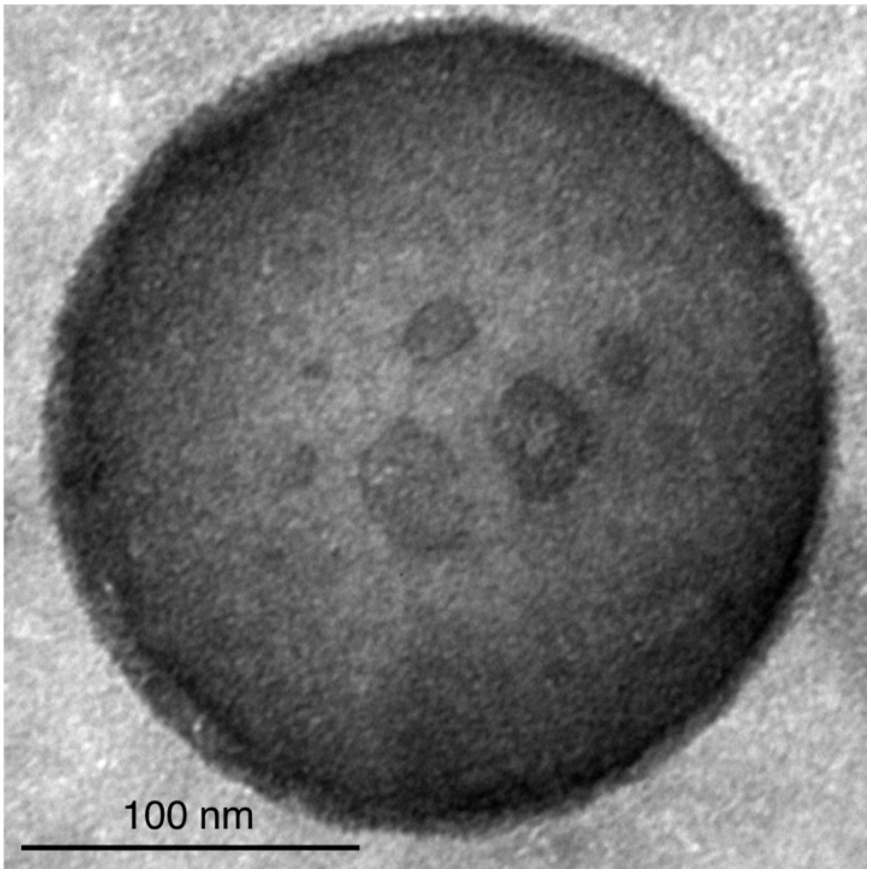

Figure 4. Transmission electron micrograph of cyclopropenium-crosslinked 25k L-PEI.

aqueous media to form nanoparticles. We hypothesize that this is due to the high hydrophobicity of the parent polymer. These results suggest it will be important for future cyclopropenium-mediated crosslinking work to avoid the presence of primary amines and limit hydrophobicity to ensure the synthesis of stable cationic crosslinked nanoparticles.

In conclusion, we have shown that polymers containing secondary amines can be rapidly crosslinked with cyclopropenium in one step, at ambient temperature, and without purification to form nanoparticles with high thermal stability and a permanent positive charge. The spherical nanoparticles are of discrete size and maintain their positive charge in strongly alkaline solutions due to their stable cyclopropenium linkages. The crosslinkers can be rapidly formed from the addition of either pentachlorocyclopropane or tetrachlorocyclopropene to a solution of any polymer containing secondary amines. This strategy will enable the synthesis of novel structures comprising cyclopropenium, permitting the incorporation of this smallest Hückel aromatic ring into fully conjugated materials. Furthermore, the planarity and C_3 symmetry of cyclopropenium suggests its potential utility in the synthesis of framework materials or other periodic structures.

REFERENCES

(1) Das, M.; Fox, C. F. *Ann. Rev. Biophys. Bioeng.* **1979**, *8*, 165–193.
(2) Reddy, N.; Reddy, R.; Jiang, Q. *Trends Biotechnol.* **2015**, *33* (6), 362–369.
(3) Wong, S. S.; Wong, L. *Enzym. Microb Technol* **1992**, *14* (11), 866–874.
(4) Langer, R.; Tirrell, D. A. *Nature* **2004**, *428*, 487–492.
(5) Elsabahy, M.; Heo, G. S.; Lim, S.-M.; Sun, G.; Wooley, K. L. *Chem. Rev.* **2015**, *115* (19), 10967–11011.
(6) Jung, B.; Theato, P. *Adv. Polym. Sci.* **2013**, *253*, 37–70.
(7) Grover, G. N.; Maynard, H. D. *Curr. Opin. Chem. Biol.* **2010**, *14* (6), 818–827.
(8) Iha, R. K.; Wooley, K. L.; Nyström, A. M.; Burke, D. J.; Kade, M. J.; Hawker, C. J. *Chem. Rev.* **2009**, *109* (11), 5620–5686.
(9) Chen, X.; Dam, M. a; Ono, K.; Mal, A.; Shen, H.; Nutt, S. R.; Sheran, K.; Wudl, F. *Science* **2002**, *295* (5560), 1698–1702.
(10) Fiore, G. L.; Rowan, S. J.; Weder, C. *Chem. Soc. Rev.* **2013**, *42* (17), 7278–7288.
(11) Jäger, M.; Schubert, S.; Ochrimenko, S.; Fischer, D.; Schubert, U. S. *Chem. Soc. Rev.* **2012**, *41* (13), 4755–4767.
(12) Beyth, N.; Yudovin-Farber, I.; Bahir, R.; Domb, A. J.; Weiss, E. I. *Biomaterials* **2006**, *27* (21), 3995–4002.
(13) Farah, S.; Khan, W.; Farber, I.; Kesler-Shvero, D.; Beyth, N.; Weiss, E. I.; Domb, A. J. *Polym. Adv. Technol.* **2013**, *24* (5), 446–452.
(14) Bandar, J. S.; Tanaset, A.; Lambert, T. H. *Chem. Eur. J.* **2015**, *21* (20), 7365–7368.
(15) Bandar, J. S.; Lambert, T. H. *J. Am. Chem. Soc.* **2012**, *134*, 5552–5555.
(16) Hendriks, K. H.; Robinson, S. G.; Braten, M. N.; Sevov, C. S.; Helms, B. A.; Sigman, M. S.; Minteer, S. D.; Sanford, M. S. *ACS Cent. Sci.* **2018**, *4* (2), 189–196.
(17) Montoto, E. C.; Cao, Y.; Hernández-Burgos, K.; Sevov, C. S.; Braten, M. N.; Helms, B. A.; Moore, J. S.; Rodríguez-López, J. *Macromolecules* **2018**, *51* (10), 3539–3546.
(18) Breslow, R. *J. Am. Chem. Soc.* **1957**, *79* (1), 5318.
(19) Yoshida, Z.; Tawara, Y. *J. Am. Chem. Soc.* **1971**, *93* (1962), 2573–2574.
(20) Bandar, J.; Lambert, T. *Synth.* **2013**, *45*, 2485–2498.
(21) Kerber, R. C.; Hsu, C.-M. *J. Am. Chem. Soc.* **1973**, *95* (10), 3239–3245.
(22) Sevov, C. S.; Samaroo, S. K.; Sanford, M. S. *Adv. Energy Mater.* **2017**, *7* (1602027).
(23) Jiang, Y.; Freyer, J. L.; Cotanda, P.; Brucks, S. D.; Killops, K. L.; Bandar, J. S.; Torsitano, C.; Balsara, N. P.; Lambert, T. H.; Campos, L. M. *Nat. Commun.* **2015**, *6*, 5950.
(24) Freyer, J. L.; Brucks, S. D.; Gobieski, G. S.; Russell, S. T.; Yozwiak, C. E.; Sun, M.; Chen, Z.; Jiang, Y.; Bandar, J. S.; Stockwell, B. R.; Lambert, T. H.; Campos, L. M. *Angew. Chem. Int. Ed.* **2016**, *55* (40), 12382–12386.
(25) Tobey, S. W.; West, R. *J. Am. Chem. Soc.* **1966**, *1965* (11), 2478–2481.
(26) Samal, S. K.; Dash, M.; Van Vlierberghe, S.; Kaplan, D. L.; Chiellini, E.; van Blitterswijk, C.; Moroni, L.; Dubruel, P. *Chem. Soc. Rev.* **2012**, *41* (21), 7147–7194.
(27) Zhou, J.; Liu, J.; Cheng, C. J.; Patel, T. R.; Weller, C. E.; Piepmeier, J. M.; Jiang, Z.; Saltzman, W. M. *Nat. Mater.* **2012**, *11*, 82–90.
(28) Taylor, M. J.; Surman, P. W.; Clark, G. R. *J. Chem. Soc., Chem. Commun.* **1994**, *375* (2), 2517–2518.

SUPPORTING INFORMATION

Materials

All materials were purchased from Sigma-Aldrich and were used without further purification except for pentachlorocyclopropane and poly(methylaminostyrene) which were synthesized according to previously reported procedures. [Refs. #24 and 25]

Characterization

^{13}C NMR spectra were recorded in MeOD on a Bruker Avance III 500 spectrometer. IR spectra were recorded on a Perkin Elmer Spectrum Two FT-IR spectrometer. Thermal gravimetric analysis was performed on a TA Instruments Q500 from 50 to 700 °C at a ramp rate of 5 °C min^{-1} under a nitrogen atmosphere. Differential scanning calorimetry was performed on a TA Instruments Q2000 fitted with a RCS90 refrigerated cooling system. DSC measurements were taken at a sampling rate of 10 °C min^{-1} in the temperature range of 0 °C to 200 °C.

Hydrodynamic diameter and zeta potential were measured on a Malvern Zetasizer Nano ZS. Crosslinked polymers were dispersed in H_2O and diluted to a concentration of 0.1 mg / mL. Tween 80 was added to the 25k L-PEI crosslinked polymers as a stabilizer so that the polymer solution contained a 1:100 *w*/*w* ratio of Tween 80:Polymer. For measurements at basic conditions, 1M NaOH was added dropwise to the polymer solution until a pH of 14 was achieved. The reported diameters are the average of three measurements, where each measurement comprises at least 10 acquisitions. The zeta potentials were calculated according to the Smoluchowski approximation.

Nanoparticles were analyzed on a Jeol (Jem-1400*Plus* equipped with Gatan Orius SC 600 camera) transmission electron microscopy using negative staining. Briefly, 5 µl of sample in water was placed on formvar/carbon coated copper grids (200 mesh, EMS), mixed with 5 µl of uranyl acetate (2%) for ~10 sec, excess mix of sample and stain was gently absorbed and grids were air-dried.

General Crosslinking Procedure

Pentachlorocyclopropane or tetrachlorocyclopropene (10-30 mol%) were added dropwise to a 0.5 mM solution of PEI in $CHCl_3$ at 0 °C. A white precipitate formed instantly and the reaction was left to stir for 3 h. The solid was then isolated via filtration and dried under vacuum.

Supplementary Tables and Figures

Table S1. Size and surface charge of crosslinked B-PEI nanoparticles

MW	Mol% Crosslinker	D_H (nm)	ζ Potential (mV)	ζ Potential at pH 14 (mV)
B-PEI 1.3k	30%	254 ± 4	27 ± 0.3	- 4.5 ± 2

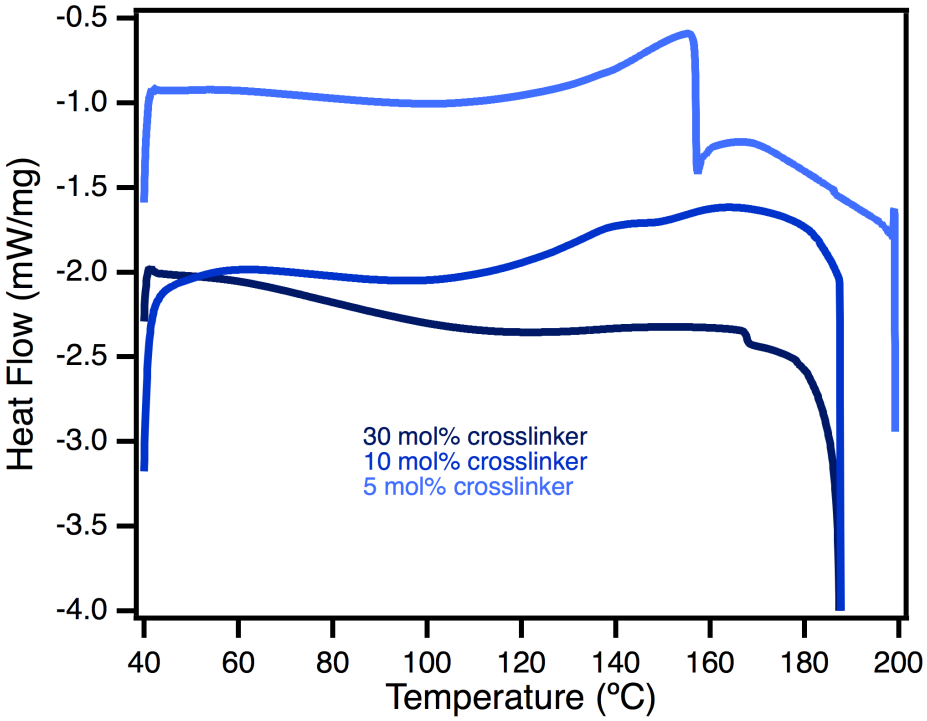

Figure S1. Differential scanning calorimetry of 10k L-PEI crosslinked polymers.

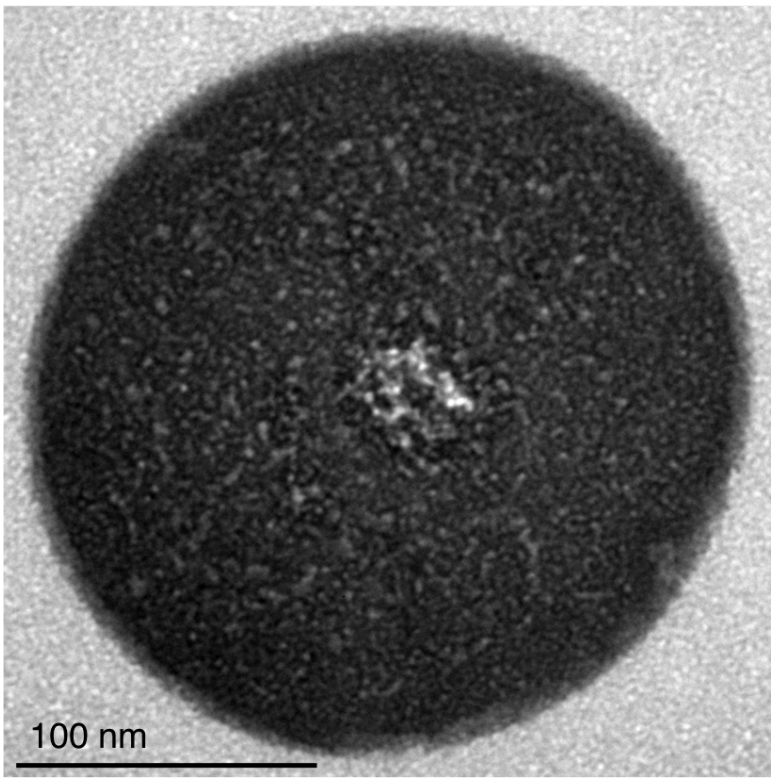

Figure S2. Transmission electron micrograph of cyclopropenium-crosslinked branched-PEI 1.3k

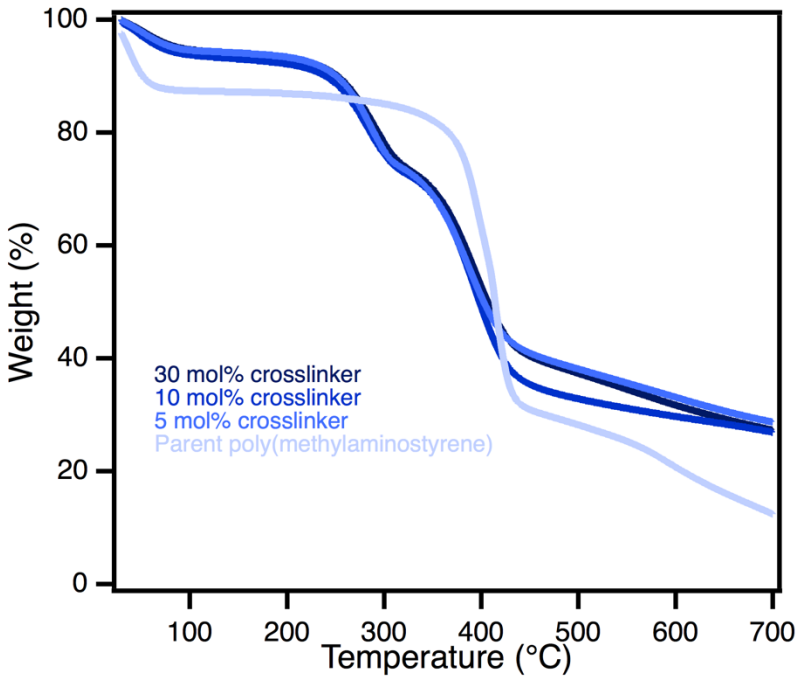

Figure S3. Thermal gravimetric analysis of poly(methylaminostyrene) crosslinked polymers. There is no change in thermal decomposition with increased crosslinking density.